

**Design and Analysis of Smart Microstrip Patch Antennas for 4G and 5G
Communication**



By

Maryam Rasool

(Registration No: 00000241084)

Thesis Supervisor: Dr. Farooq Ahmed Bhatti

Department of Electrical Engineering

Military College of Signals

National University of Sciences & Technology (NUST)

Islamabad, Pakistan

(2022)

Design and Analysis of Smart Microstrip Patch Antennas for 4G and 5G Communication



By

Maryam Rasool

(Registration No: 00000241084)

A thesis submitted to the National University of Sciences and Technology, Islamabad,

in partial fulfilment of the requirements for the degree of

**Doctor of Philosophy in
Electrical (Telecommunication) Engineering**

Thesis Supervisor: Dr. Farooq Ahmed Bhatti

Department of Electrical Engineering

Military College of Signals

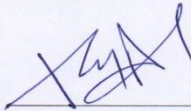
National University of Sciences & Technology (NUST)

Islamabad, Pakistan

(2022)

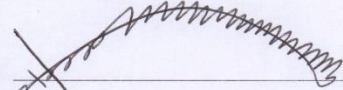
THESIS ACCEPTANCE CERTIFICATE

Certified that final copy of PhD Thesis written by **Ms. Maryam Rasool**. Registration No. **00000241084**, of **Military College of Signals** has been vetted by undersigned, found complete in all respects as per NUST Statutes / Regulations / PhD Policy, is free of plagiarism, errors, and mistakes and is accepted as partial fulfillment for award of PhD degree. It is further certified that necessary amendments as pointed out by GEC members and foreign/local evaluators of the scholar have also been suitably incorporated in the said thesis.

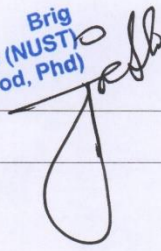
Signature:  _____

Name of Supervisor: Dr Farooq Ahmed Bhatti

Date: 8/9/22 _____

Signature (HOD):  _____

Date: 8-9-22 _____

Signature (Dean/Principal)  _____
Brig
Dean, MCS (NUST)
Asif Masood, Phd

Date: 8/9/22 _____



Form Ph.D-7
DOCTORAL PROGRAMME
OF STUDY
(Must be type written)

National University of Sciences & Technology REPORT OF DOCTORAL THESIS DEFENCE

Name: Maryam Rasool

NUST Regn No: 00000241084

School/College/Centre: Military College of Signals

Title: Design and Analysis of Smart Microstrip Patch Antennas for 4G and 5G Communication

DOCTORAL DEFENCE COMMITTEE

Doctoral Defence held on 8th Sep 2022

	QUALIFIED	NOT QUALIFIED	SIGNATURE
GEC Member-1: <u>Prof Dr Abdul Rauf</u>	<input checked="" type="checkbox"/>	<input type="checkbox"/>	
GEC Member-2: <u>Prof Dr Imran Rashid</u>	<input checked="" type="checkbox"/>	<input type="checkbox"/>	
GEC Member-3: <u>Prof Dr Adil Masood Siddiqui</u>	<input checked="" type="checkbox"/>	<input type="checkbox"/>	
GEC Member (External): <u>Asst Prof Dr Bilal Ijaz</u>	<input checked="" type="checkbox"/>	<input type="checkbox"/>	
Supervisor: <u>Assoc Prof Dr Farooq Ahmed Bhatti</u>	<input checked="" type="checkbox"/>	<input type="checkbox"/>	
External Evaluator-1: <u>Asst Prof Dr Laeeq Riaz</u> (Local Expert)	<input checked="" type="checkbox"/>	<input type="checkbox"/>	
External Evaluator-2: <u>Asst Prof Dr Saleem Shahid</u> (Local Expert)	<input checked="" type="checkbox"/>	<input type="checkbox"/>	
External Evaluator-3: <u>Assoc Prof Dr Mehmet Nuri Akinci</u> (Foreign Expert)	<input checked="" type="checkbox"/>	<input type="checkbox"/>	
External Evaluator-4: <u>Asst Prof Dr Agah Oktay Ertay</u> (Foreign Expert)	<input checked="" type="checkbox"/>	<input type="checkbox"/>	

FINAL RESULT OF THE DOCTORAL DEFENCE

(Appropriate box to be signed by HOD)

PASS
 FAIL

The student Maryam Rasool Regn No 00000241084 is accepted for Doctor of Philosophy Degree.

Dated: 8/9/22

Brig
 Asif Masood (NUST)
 Dean/Commandant/Principal/DG

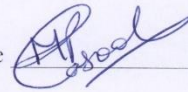
Distribution:
 01 x original copy each for PGP Dte, Exam Branch Main Office NUST and Student's dossier at the School/College/Centre.
 01 x photocopy each for HoD, Supervisor, Co-Supervisor (if appointed), sponsoring agency (if any) and 05 copies for insertion in Dissertation.
 Note: * Decision of External Evaluators (Foreign Experts) will be sought through video conference, if possible, on the same date and their decision will be intimated (on paper) to HQ NUST at a later date.

CERTIFICATE OF APPROVAL

This is to certify that research work presented in this thesis, titled “**Design and Analysis of Smart Microstrip Patch Antennas for 4G and 5G Communication**” was conducted by **Ms. Maryam Rasool** under the supervision of **Dr. Farooq Ahmed Bhatti**. No part of this thesis has been submitted anywhere else for any other degree. This thesis is submitted to the **Department of Electrical Engineering** in partial fulfillment of the requirements for the degree of Doctor of Philosophy in field of **Electrical (Telecommunication) Engineering, Department of Electrical Engineering, Military College of Signals, National University of Sciences and Technology, Islamabad.**

Student Name: **Maryam Rasool**

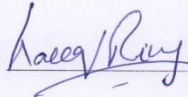
Signature



Examination Committee:

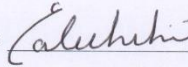
a. External Examiner 1: **Asst Prof Dr Laseeq Riaz**
(Assistant Professor, COMSATS University, Islamabad)

Signature



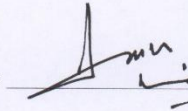
b. External Examiner 2: **Asst Prof Dr Saleem Shahid**
(Assistant Professor, Air University, Islamabad)

Signature



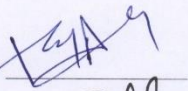
c. Internal Examiner 1: **Prof Dr Imran Rashid**
(Chief Instructor, Engineering Wing)

Signature



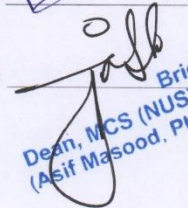
Supervisor: **Assoc Prof Dr Farooq Ahmed Bhatti**

Signature



Dean: **Prof Dr Asif Masood**

Signature



Brig
Dean, MCS (NUST)
(Asif Masood, Phd)

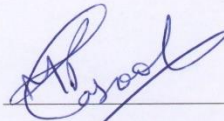
Author's Declaration

I, **Maryam Rasool**, hereby state that my PhD thesis titled “**Design and Analysis of Smart Microstrip Patch Antennas for 4G and 5G Communication**” is my own work and has not been submitted previously by me for taking any degree from National University of Sciences and Technology (NUST), Islamabad, or anywhere else in the country / world.

At any time if my statement is found to be incorrect even after my Graduation, the university has the right to withdraw my PhD degree.

Dated: 8-9-2022

Signature:



Name of Student:

(Maryam Rasool)

Plagiarism Undertaking

I solemnly declare that research work presented in the thesis titled "**Design and Analysis of Smart Microstrip Patch Antennas for 4G and 5G Communication**" is solely my research work with no significant contribution from any other person. Small contribution/help wherever taken has been duly acknowledged and that complete thesis has been written by me.

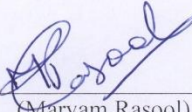
I understand the zero tolerance policy of the HEC and that of National University of Sciences and Technology (NUST), Islamabad, towards plagiarism. Therefore I, as an Author of the above titled thesis declare that no portion of my thesis has been plagiarized and any material used as reference is properly referred / cited.

I undertake that if I am found guilty of any formal plagiarism in the above titled thesis even after award of PhD degree, the University reserves the rights to withdraw / revoke my PhD degree and that HEC and the University has the right to publish my name on the HEC / University Website on which names of students are placed who submitted plagiarized thesis.

Date: 8-9-2022

Student/ Author Signature: _____

Name: _____


(Maryam Rasool)

DEDICATION

*This PhD thesis is dedicated to my maternal
grandmother, mother, maternal aunt,
honourable teachers, family and friends for their
love, endless support, guidance, and inspiration.*

ACKNOWLEDGEMENTS

Thanks to Almighty ALLAH for all the uncountable blessings.

I would like to express my sincere gratitude to my supervisor Dr Farooq Ahmed Bhatti for his support and guidance during my studies. His comments and fruitful suggestions helped me complete my dissertation in a timely fashion.

I would also like to thank my GEC committee members Dr Abdul Rauf, Dr Imran Rashid, Dr Adil Masood, and Dr Bilal Ijaz for their tremendous support and cooperation.

A special thanks also goes to Dr Adnan Iftikhar for helping me with my research publications.

Finally, I would like to express my gratitude to all my family members and friends, especially my maternal grandmother Ms Kaneez Akhtar, mother Ms Riffat Rasul and maternal aunt Ms Nighat Rasul, who have rendered valuable assistance to my PhD Studies and have kept me motivated throughout this journey.

ABSTRACT

Wireless mobile communication has seen evolution of technology from first generation (1G) to fifth generation (5G) networks in recent times. The proposed 5G technology relies upon two major frequency divisions, the sub 6 GHz band (frequencies lower than 6 GHz) and the mmWave band (24 GHz to 100 GHz). Initially 5G services are being offered in non-standalone mode along with 4G services however, later on standalone 5G networks will also be deployed. It is need of the hour to design smart and intelligent multiband antennas for the modern 4G and 5G wireless communication systems that can improve the overall performance of a communication network by reducing size, complexity, and cost of the antenna structure. This thesis presents three antenna designs that have been developed smartly and intelligently to meet the demands of modern wireless communication systems. All the developed antenna designs have been manufactured and tested for significant antenna performance parameters.

The first developed structure consists of a printed patch antenna design to achieve frequency and bandwidth reconfigurability. Two RF PIN diodes are simultaneously operated to achieve the multi-reconfigurability operation. The patch is inspired from a circular loop design. The antenna operates in dual band configuration at 3.42 and 8.02 GHz in the diodes 'OFF' state, whereas the antenna switches to triple band operation at 2.21, 4.85, and 10.19 GHz in the diodes 'ON' state. Moreover, the antenna also exhibits an increased bandwidth from 7.54 to 12 GHz in the diodes 'ON' state, as compared to a narrow bandwidth from 7.71 to 8.48 GHz in the diodes 'OFF' state. The implemented design exhibits measured gains of 3.06 dBi, 2.81 dBi, and 2.92 dBi at 2.21, 4.85, and 10.19 GHz in the PIN diodes 'ON' state, respectively, while in the PIN diodes 'OFF' state, at 3.42 GHz the gain is 3.03 dBi and at 8.02 GHz the gain is 3.37 dBi.

The second developed design is a quadband two element MIMO antenna based on a multi-slotted structure. The design demonstrates the applicability of proposed MIMO antenna for 4G and 5G systems. A simple de-coupler structure has been incorporated on the bottom side to reduce the mutual coupling at operating frequency bands of 2.5 GHz, 3.7 GHz, 4.3 GHz, and 5.5 GHz. Furthermore, it is also observed that the measured envelope correlation coefficient of the designed MIMO antenna is considerably lower than 0.05. Also, the design exhibits measured gains of 3.49 dBi, 2.97 dBi, 2.93 dBi, and 2.54 dBi at 2.5 GHz, 3.7 GHz, 4.3 GHz, and 5.5 GHz, respectively.

Finally, the third developed design is a compact multi-slotted antenna array structure. The antenna array is able to resonate at four distinct mmWave bands with centre frequencies of 30.58, 34.5, 38.3, and 49.3 GHz. Rogers RT Duroid 5880 with a relative permittivity of 2.2, loss tangent of 0.0009 and thickness of 0.5 mm has been used for fabrication of the array antenna. The proposed array structure exhibits measured gains of 7.98, 8.43, 9.93, and 9.87 dBi at 30.58, 34.5, 38.3, and 49.3 GHz respectively. The antenna array due to its compact size, simple design and quadband resonance can effectively find applications in the proposed future 5G mmWave bands.

TABLE OF CONTENTS

DEDICATION	i
ACKNOWLEDGEMENTS	ii
ABSTRACT	iii
TABLE OF CONTENTS	v
LIST OF FIGURES	viii
LIST OF TABLES	xi
LIST OF ACRONYMS	xii
LIST OF PUBLICATIONS	xiv
CHAPTER 1 INTRODUCTION.....	1
1.1 Background.....	1
1.2 Evolution of Mobile Communication Technology Generations – 1G to 5G.....	2
1.3 Significance of Antennas in Wireless Communication.....	7
1.4 Significance of Microstrip Patch Antennas in Wireless Communication	8
1.5 Thesis Motivation	9
1.6 Thesis Contributions.....	12
1.7 Thesis Organization.....	14
CHAPTER 2 LITERATURE REVIEW	17
2.1 Recent Trends in Microstrip Patch Antenna Design Technology.....	17
2.2 Review of Frequency Reconfigurable Microstrip Patch Antenna Design Technology.....	25
2.3 Review of Multiple Input Multiple Output (MIMO) Microstrip Patch Antenna Design Technology.....	29
2.4 Review of mmWave Microstrip Patch Antenna Design Technology.....	33

2.5 Summary.....36

**CHAPTER 3 ANTENNA DESIGN 1: A MULTI-RECONFIGURABLE ANTENNA
BASED ON CIRCULAR LOOP DESIGN.....38**

3.1 Introduction.....38

3.2 Design of Proposed Multi-Reconfigurable Antenna.....40

3.2.1 Antenna Design Evolution.....43

3.2.2 Parametric Analysis.....45

3.2.3 Integration of PIN Diodes in Final Antenna Design.....48

3.2.4 Investigation of Surface Current Distribution for Designed Antenna.....50

3.3 Significant Antenna Results and Analysis.....51

3.3.1 Reflection Coefficient Results.....53

3.3.2 Far Field Results.....56

3.3.3 Comparison with Related Literature.....59

3.4 Summary.....60

**CHAPTER 4 ANTENNA DESIGN 2: A QUADBAND MIMO ANTENNA BASED
ON A MULTI SLOTTED STRUCTURE.....62**

4.1 Introduction.....62

4.2 Detailed Design Development of Proposed Antenna Structure.....63

4.2.1 Development of Single Element Antenna.....64

4.2.2 Development of Two Element MIMO Antenna.....68

4.2.3 Investigation of Surface Current Distribution for Two Element MIMO
Antenna.....69

4.3 Important Antenna Results and Analysis.....71

4.3.1 Reflection Coefficient Results.....71

4.3.2 Mutual Coupling Results.....73

4.3.3 Radiation Characteristics.....74

4.3.4 Peak Gain and Radiation Efficiency Results.....74

4.4 MIMO Antenna Performance Results.....	78
4.4.1 Envelope Correlation Coefficient.....	78
4.4.2 Channel Capacity Loss.....	79
4.4.3 Total Active Reflection Coefficient.....	80
4.4.4 Diversity Gain.....	81
4.5 Comparison with Related Literature.....	82
4.6 Summary.....	83
CHAPTER 5 ANTENNA DESIGN 3: COMPACT MMWAVE MULTIBAND ANTENNA ARRAY.....	85
5.1 Introduction.....	85
5.2 Detailed Design of the Proposed Antenna Array.....	87
5.2.1 Antenna Design Evolution.....	88
5.2.2 Analysis of Current Distribution Plots.....	90
5.3 Significant Results and Analysis of the Proposed mmWave Antenna Array.....	91
5.3.1 Reflection Coefficient Results.....	92
5.3.2 Radiation Characteristics of the Proposed mmWave Antenna Array.....	93
5.3.3 mmWave Antenna Array Peak Gain Results.....	94
5.3.4 mmWave Antenna Array Radiation Efficiency Results.....	95
5.4 Comparison with Related Literature.....	96
5.5 Summary.....	97
CHAPTER 6 CONCLUSION AND FUTURE WORK.....	98
6.1 Conclusion.....	98
6.2 Future Work.....	100
REFERENCES.....	101

LIST OF FIGURES

Figure 1.1 Evolution of Mobile Communication Generations – 1G to 5G.....	6
Figure 1.2 A Typical Wireless Communication System.....	8
Figure 2.1 Antenna Geometry Presented in (a) [23] (b) [25].....	18
Figure 2.2 Antenna Geometry Presented in [28] (a) Top Side (b) Bottom Side.....	20
Figure 2.3 Antenna Geometry Presented in (a) [30] (b) [31].....	21
Figure 2.4 Antenna Geometry Presented in (a) [34] (b) [37].....	22
Figure 2.5 Antenna Geometry Presented in (a) [38] (b) [39].....	24
Figure 2.6 Antenna Geometry Presented in (a) [41] (b) [43].....	26
Figure 2.7 Antenna Geometry Presented in (a) [45] (b) [47].....	28
Figure 2.8 Antenna Geometry Presented in (a) [49] (b) [51].....	30
Figure 2.9 Antenna Geometry Presented in (a) [53] (b) [55].....	32
Figure 2.10 Antenna Geometry Presented in (a) [57] (b) [59].....	34
Figure 2.11 Antenna Geometry Presented in (a) [61] (b) [63].....	35
Figure 3.1 Final Design of Proposed Multi-Reconfigurable Antenna, Patch Structure (Left) and Modified Ground Structure (Right).....	41
Figure 3.2 Evolution Steps for Antenna Design (top and bottom): (A) Design A (B) Design B (C) Design C (D) Design D.....	43
Figure 3.3 Evolution Steps for Antenna Design (top and bottom): (A) Design A (B) Design B (C) Design C (D) Design D.....	44
Figure 3.4 Reflection Coefficient Results for Removed Arc Length Variation.....	45
Figure 3.5 Reflection Coefficient Results for Horizontal Strip Length Variation.....	46
Figure 3.6 Reflection Coefficient Results for Strip Width Variation.....	47

Figure 3.7 Reflection Coefficient Results for Partial Ground Length Variation.....	47
Figure 3.8 Marked Diode Positions on Antenna Radiating Patch.....	49
Figure 3.9 Surface Current Distribution (for patch and ground) in PIN diodes ‘OFF’ state at: (A) 3.42 GHz and (B) 8.02 GHz.....	51
Figure 3.10 Surface Current Distribution (for patch and ground) in PIN diodes ‘ON’ state at: (A) 2.21 GHz (B) 4.85 GHz (C) 8.02 GHz and (D) 10.19 GHz....	52
Figure 3.11 Fabricated Antenna Prototype.....	53
Figure 3.12 Simulated Reflection Coefficient Results for Four Possible Configurations of PIN Diodes.....	55
Figure 3.13 Simulated and Measured Reflection Coefficient Results for PIN Diodes ‘OFF’ and ‘ON’ States.....	55
Figure 3.14 Simulated and Measured Radiation Patterns for PIN Diodes ‘OFF’ State at (A) 3.42 GHz and (B) 8.02 GHz.....	57
Figure 3.15 Simulated and Measured Radiation Patterns for PIN Diodes ‘ON’ State at (A) 2.21 GHz (B) 4.85 GHz (C) 8.02 GHz and (D) 10.19 GHz.....	58
Figure 4.1 Complete Layout of Single Element Antenna (a) Top (b) Bottom.....	64
Figure 4.2 Detailed View of Multi-Slotted Rectangular Patch Loaded with L and I Shaped Slots.....	65
Figure 4.3 Design Evolution Steps.....	67
Figure 4.4 Magnitude Reflection Coefficient Results for Figure 4.3.....	67
Figure 4.5. Two Element MIMO Antenna Design (a) Top (b) Bottom.....	69
Figure 4.6 Surface Current Distribution for MIMO Antenna (Top and Bottom) (a) 2.5 GHz (b) 3.7 GHz (c) 4.3 GHz (d) 5.5 GHz.....	71
Figure 4.7 Magnitude Reflection Coefficient ($ S_{11} $ (dB)) Results of Proposed MIMO Antenna.....	72
Figure 4.8 Mutual Coupling ($ S_{21} $ (dB)) Results of Proposed MIMO Antenna.....	73

Figure 4.9 Radiation Pattern Plots (Simulated) of Proposed MIMO Antenna at (a) 2.5 GHz (b) 3.7 GHz (c) 4.3 GHz (d) 5.5 GHz.....	75
Figure 4.10 Radiation Pattern Plots (Measured) of Proposed MIMO Antenna at (a) 2.5 GHz (b) 3.7 GHz (c) 4.3 GHz (d) 5.5 GHz.....	76
Figure 4.11 Simulated (with and without decoupler) and Measured Peak Gain Results.....	77
Figure 4.12 Simulated (with and without decoupler) and Measured Radiation Efficiency Results.....	78
Figure 4.13 Simulated (with and without decoupler) and Measured ECC Results.....	79
Figure 4.14 Simulated (with and without decoupler) and Measured CCL Results.....	80
Figure 4.15 Simulated (with and without decoupler) and Measured TARC Results.....	81
Figure 4.16 Simulated (with and without decoupler) and Measured DG Results.....	82
Figure 5.1 Detailed Antenna Array Design (a) Top (b) Bottom.....	87
Figure 5.2 Antenna Design Evolution Steps (a) Design A (b) Design B (c) Design C (d) Design D.....	89
Figure 5.3 Reflection Coefficient Results ($ S_{11} $ dB) for Design Evolution Steps Shown in Figure 5.2.....	89
Figure 5.4 Single Element Surface Current Distribution at (a) 30.58 GHz (b) 34.5 GHz (c) 38.3 GHz (d) 49.3 GHz.....	91
Figure 5.5 Manufactured Antenna Array Top and Bottom View.....	91
Figure 5.6 Reflection Coefficient Results ($ S_{11} $ dB) Simulated and Measured.....	92
Figure 5.7 Simulated and Measured Radiation Pattern Plots at (a) 30.58 GHz, (b) 34.5 GHz, (c) 38.3 GHz, and (d) 49.3 GHz.....	94

LIST OF TABLES

Table 3.1 Detailed Dimensions of Multi-Reconfigurable Antenna.....	42
Table 3.2 Detailed Magnitude Reflection Coefficient Results.....	56
Table 3.3 Peak Gain (dBi) and Radiation Efficiency (%) Results.....	58
Table 3.4 Related Literature Comparison.....	59
Table 4.1 Dimensions Involved in Figures 4.1 and 4.2.....	65
Table 4.2 Dimensions Involved in Figure 4.5.....	69
Table 4.3 Comparison of Proposed MIMO Antenna with Related Literature.....	83
Table 5.1 Dimensions Involved in Figure 5.1.....	88
Table 5.2 In-depth Simulated and Measured Reflection Coefficient ($ S_{11} $ dB) Results.....	93
Table 5.3 Simulated and Measured Peak Gain Results for Proposed mmWave Antenna Array.....	95
Table 5.4 Simulated and Measured Peak Gain Results for Proposed mmWave Antenna Array.....	95
Table 5.5 Comparison of Proposed mmWave Antenna Array with Recent Literature....	96
Table 6.1 Summarized Comparison of Presented Antennas.....	98

LIST OF ACRONYMS

1G – First Generation

2G – Second Generation

3G – Third Generation

4G – Fourth Generation

5G – Fifth Generation

FDMA – Frequency Division Multiple Access

NMT – Nordic Mobile Telephone

NTT – Nippon Telephone and Telegraph Company

AMPS – Advanced Mobile Phone System

TACS – Total Access Communication System

ETACS – European Total Access Communication System

GSM – Global System for Mobile Communication

TDMA – Time Division Multiple Access

MMS – Multimedia Message Service

SMS – Short Message Service

CDMA – Code Division Multiple Access

GPRS – General Packet Radio Service

EDGE – Enhanced Data for GSM Evolution

UMTS – Universal Mobile Telecommunications Systems

HSDPA – High Speed Downlink Packet Access

HSUPA – High Speed Uplink Packet Access

HSPA+ – High Speed Packet Access Plus

LTE – Long Term Evolution

IP – Internet Protocol

OFDM – Orthogonal Frequency Division Multiplexing

MIMO – Multiple Input Multiple Output

mmWave – Millimetre Wave

NR – New Radio

IoT – Internet of Things

LIST OF PUBLICATIONS

The work in this thesis has been based upon following publications:

1. M. Rasool, A. Khan, F. Bhatti, B. Ijaz and A. Iftikhar, "A Compact Circular Loop Inspired Frequency and Bandwidth Reconfigurable Antenna for 4G, 5G, and X-Band Applications," *Radioengineering*, vol. 29, no. 3, pp. 471-478, 2020, doi: 10.13164/re.2020.0471.
2. M. Rasool, I. Rashid, A. Rauf, A. Masood, F. A. Bhatti and B. Ijaz, "A Multi-Slotted 2-Element Quadband MIMO Antenna for 4G and 5G Applications," *Journal of Electromagnetic Waves and Applications*, vol. 35, no. 15, pp. 2062-2077, 2021, doi: 10.1080/09205071.2021.1934565.
3. M. Rasool, Z. B. Tariq, B. Ijaz, A. Iftikhar and F. A. Bhatti, "A Compact Multi-slotted Quadband Antenna Array for 5G mmWave Applications," *2021 International Conference on Engineering and Emerging Technologies (ICEET)*, 2021, pp. 1-4, doi: 10.1109/ICEET53442.2021.9659776.

CHAPTER 1

INTRODUCTION

1.1 Background:

History is evident that human beings, in order to establish connectivity, have always strived to develop communication networks that can reliably transfer information over long distances. Communication networks based upon the involved transmission medium can be classified into two major categories: wired and wireless. Wired communication networks have certain advantages over the wireless networks in terms of speed and security etc, wireless networks however, support mobility, can offer greater coverage, access, and flexibility [1]. Earliest examples of wireless communication can be traced back to primitive human civilizations using light and smoke signals, drums, bells, pigeons etc to convey information from one point to another. Later on, these ancient forms of wireless communication were gradually replaced with technologically advanced inventions like radios, telegraphs, telephones, satellites etc [2].

Wireless communication networks have had a profound impact on human lives since past few decades. Life today has become completely dependent upon wirelessly connected devices. Technologies like mobile communication, WiFi, Bluetooth, and satellite communication etc have transformed the human lives completely and have turned the world into a well-connected global village. Wireless communication technology finds applications in almost every field of life today, like multimedia communication, security and surveillance systems, smart homes, teleconferencing, remote classrooms, remote hospitals, monitoring systems, detection and tracking systems, automated vehicles etc [3].

1.2 Evolution of Mobile Communication Technology Generations – 1G to 5G:

The wireless communication technology primarily came into being due to the existence and discovery of radio waves. The spectrum of radio waves ranges from 3 *kHz* to 300 *GHz* [4]. These waves practically allow connections “anywhere and anytime”. The advent of mobile wireless communications can be traced to radio telegraph transmissions by Marconi in 1899. Early applications involved voice transmission only and services were designed to predominantly cater for the military requirements. Radio telephones were commercially put to use in ships travelling through the Atlantic around 1929. Also, around late 1920s land mobile systems were made available and different government departments particularly the police in the US started using these services [5]. The BELL labs US launched the first commercial mobile phone service around 1946. A concept of frequency reuse was introduced by the BELL labs US known as the principle of cellular concept. The principle aimed at providing efficient coverage by exploiting the frequency reuse concept. Although frequency reuse concept originated in the US, the practical demonstration of this concept in a commercial mobile phone system was provided by the Nordic countries with the development of Nordic Mobile Telephone (NMT) in 1981, hence giving birth to cellular mobile communication [6]. Evolution of modern mobile communication technology is frequently described through the term “generation”, where each generation represents a significant and important breakthrough in the development and deployment of mobile communication networks.

The term First Generation (1G) is used to describe the earliest generation of cellular mobile phone technology. The initial incidents of formal deployment of mobile phone technology can be attributed to the Nippon Telephone and Telegraph Company also termed NTT, in Japan around late 1970's. In addition, the Nordic Mobile Phone System

(NMTS), Advanced Mobile Phone System (AMPS), Total Access Communication System (TACS), and European Total Access Communication System (ETACS) also appeared as popular First Generation (1G) mobile communication systems in the 1980's [7]. The First Generation (1G) systems were analog in nature, they were based upon the concept of frequency modulation and frequency division multiple access (FDMA). These systems were designed to offer voice services only with speeds up to 2.4 *kbps*. Frequency of operation generally involved the 800 *MHz* and 900 *MHz* bands [7]. These First Generation (1G) systems owing to their analog nature were not secure and reliable, and offered limited coverage and capacity. Also, the concept of roaming was not supported and lack of standardization between different operating systems resulted in compatibility issues [8].

A major breakthrough in the history of mobile communication technology happened with introduction of Second Generation (2G) communication technology. Instead of analog signals, digital signals were used for the first time in order to provide secure and reliable communication services. Global System for Mobile Communication (GSM) offered the 2G services for the first time in Finland around 1991 and later on went to become a global standard for all future mobile communication system development [7]. The Second Generation (2G) communication systems adopted time division multiple access (TDMA) technology, provided security and better voice quality, supported the concept of roaming, and introduced exciting services like the short message service (SMS), multimedia message service (MMS), conference calls, call hold etc. The Second Generation (2G) GSM systems offered speeds of up to 64 *kbps* [9]. These systems were able to improve the compatibility, coverage and capacity issues faced by the First Generation (1G) systems. The frequency of operation primarily involved the 800 *MHz*, 900 *MHz*, 1800 *MHz*, and 1900 *MHz* bands [10]. Another system, based

upon the concept of code division multiple access (CDMA), was introduced by Qualcomm, around the mid 1990's, however GSM remained the most fundamental and famous Second Generation (2G) system. Efforts to improve the services and data rates offered by GSM led to development and deployment of two major and noteworthy systems the General Packet Radio Service (GPRS) and the Enhanced Data for GSM Evolution (EDGE) [8]. GPRS is famously referred to as the 2.5 G technology and provided data rates of up to 160 *kbps* whereas EDGE is popularly referred to as the 2.75 G technology and was successful in supporting data rates of up to 473 *kbps* [9].

The ever-increasing demand for high data rate applications led to the development of Third Generation (3G) communication technology systems. The Third Generation (3G) technology was primarily based upon Universal Mobile Telecommunications Systems (UMTS) and launched formally around 2000. These systems adopted the concept of packet switching and successfully provided appealing services like web surfing, map navigation, tracking, video conferencing, media streaming, social media, 3D gaming etc [7]. Data rates of up to 2 *Mbps* were offered by 3G systems. The major frequency bands utilized for providing 3G services ranged from 1.6 *GHz* to 2 *GHz* [10]. Devices known as smart phones were introduced to cater for the huge surge in applications supported by 3G systems. Further technological improvements led to the development of new systems known as High Speed Downlink Packet Access (HSDPA), High Speed Uplink Packet Access (HSUPA) and High Speed Packet Access Plus (HSPA+) [7]. All these systems aimed to enhance the data rate (up to 14 *Mbps*) and efficiency of the fundamental 3G communication network.

The Fourth Generation (4G) communication technology systems were developed to provide higher capacity and speed along with better quality. The Fourth Generation

(4G) technology is based upon Long Term Evolution (LTE) systems and was first put to commercial use around the year 2009 [7]. These systems allow the deployment of an Internet Protocol (IP) based network thereby providing sophisticated applications like cloud computing, high-definition Television, high-definition 3D gaming, mobile web access etc. The 4G systems are capable of offering data rates up to 1 *Gbps* [8]. Operational frequencies ranging from 2 *GHz* to 8 *GHz* are utilized for providing 4G services [10]. Advanced technologies such as Orthogonal Frequency Division Multiplexing (OFDM) and Multiple Input Multiple Output (MIMO) have been integrated into the Fourth Generation (4G) systems in order to deliver seamless and efficient services.

The massive growth of communication networks and modern applications called for further developments in communication system technology, giving rise to the current Fifth Generation (5G) communication technology. 5G aims at achieving much faster data rates with lower latency and also promises to provide a better connection density [7]. The systems being developed and deployed target a wireless system with an overall better coverage. Battery consumption issues of devices at the user end are also being dealt with. Initial 5G deployments will be based upon a non-standalone mode of configuration (along with 4G systems), but later on the proposed 5G technology systems will be gradually transferred into standalone configuration mode [8]. Advanced technologies such as Multiple Input Multiple Output (MIMO), Millimetre wave (mmWave) technology, cloud computing, New Radio (NR) and Internet of Things (IoT) have been integrated into modern 5G communication systems. These highly developed systems have been proposed to offer data rates up to 10 *Gbps* [11].

5G systems aim to completely transform human lifestyle. With the development and deployment of practical 5G systems, high end applications like self-driving cars, smart

cities, virtual and augmented reality, metaverse etc have become a possibility. The operating frequency range for 5G systems is quite diverse. Two frequency bands have been recommended in order to provide the 5G services, the sub 6 GHz band (frequencies lower the 6 GHz) and the mmWave band (24 GHz to 100 GHz) [12]. The sub 6 GHz band will primarily be used in the non-standalone mode whereas mmWave band will find applications in the future standalone mode of configuration for the 5G communication technology. The mmWave band, hence, may be termed as the sweet spot for 5G as its capabilities are widely unexplored.

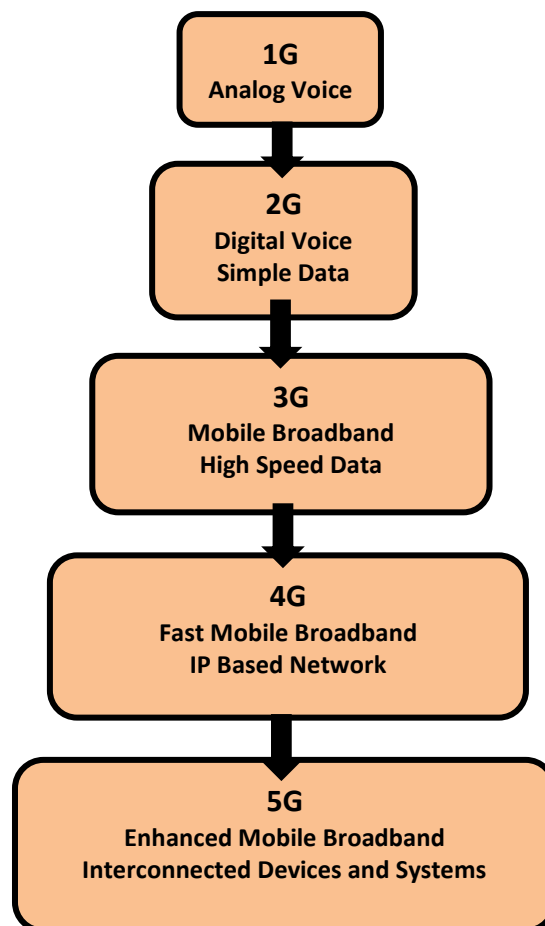


Figure 1.1 Evolution of Mobile Communication Generations – 1G to 5G

Figure 1.1 summarises the evolution of mobile communication generations by highlighting the significant achievement of every generation.

1.3 Significance of Antennas in Wireless Communication:

In order to establish a complete and comprehensive wireless communication system, many significant components are required like encoders, modulators, multiplexers etc. at the transmitter end and decoders, demodulators, demultiplexers etc. at the receiver end. However, the most important component that defines the very basic nature of a wireless communication system, that is, its 'wireless' nature, is the component known as an 'antenna'. Figure 1.2 represents the block diagram of a typical wireless communication system. An antenna is generally defined as "a means for radiating or receiving radio waves" [13]. It is one of the most crucial and vital component that is required by a wireless communication system to operate accurately. An efficiently designed antenna can therefore serve to enhance the overall performance of a wireless communication system. According to C. A. Balanis, antennas are the "Eyes" of a communication system [14].

The history of antenna originated when James Clark Maxwell published his famous Maxwell's Equations [15] and Rudolph Hertz established the first electromagnetic system [14]. Later on in 1901, Marconi performed his famous transatlantic transmission [14], thereby formally giving birth to the development of antenna technology. Initially, all antenna technology was based on the primitive wire antennas, but the World War II era led to the introduction and deployment of many other antenna types like horns and reflectors etc. [16]. 1950s saw massive developments in the field of antennas, with most popular being the induction of antennas used for Television reception [17]. About twenty years later, in 1970s a new radiating element was conceived, known as the microstrip patch antenna, this class of antennas continues to offer innovative and exciting applications [18]. The antenna technology development continues today, with latest and better performing antennas being developed for the existing as well as

upcoming wireless systems such as 4G and 5G communications including the mmWave applications.

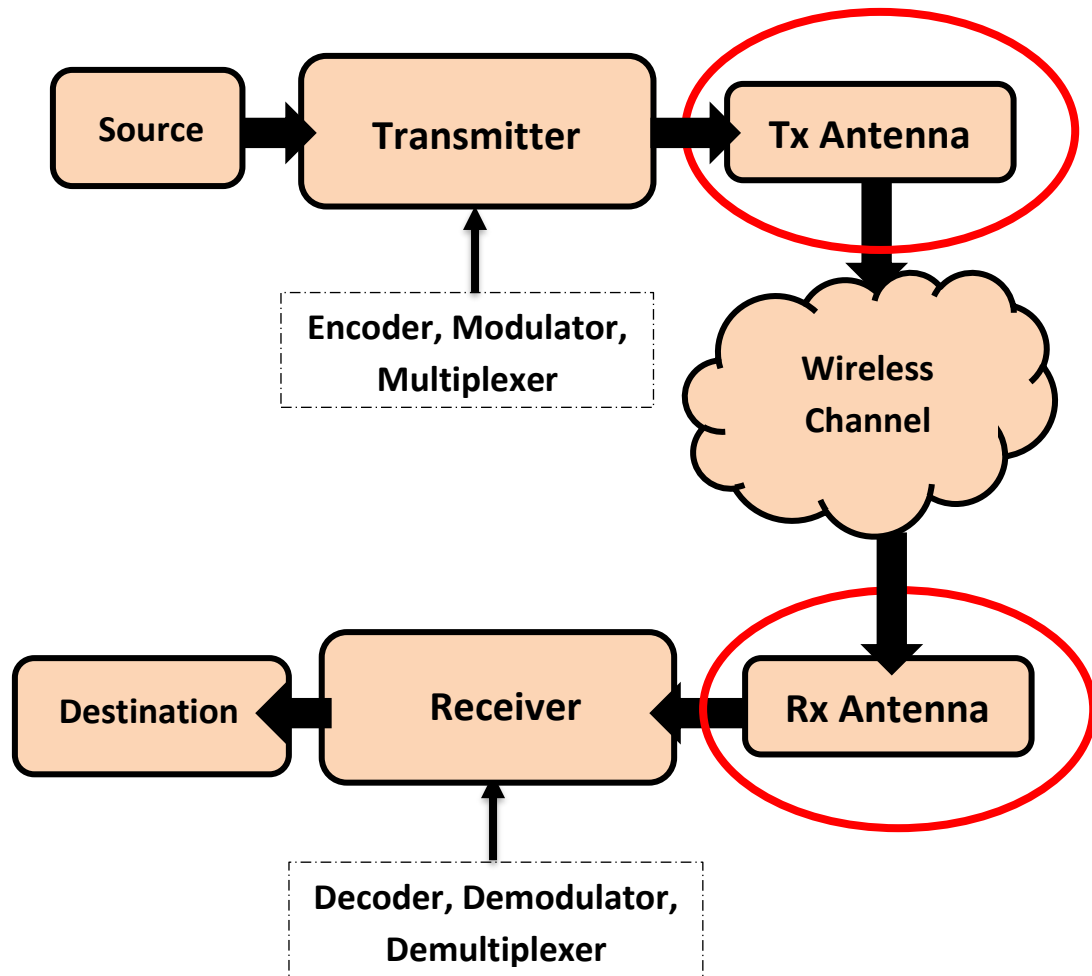


Figure 1.2 A Typical Wireless Communication System

1.4 Significance of Microstrip Patch Antennas in Wireless Communication:

Microstrip patch antennas have become more and more prevalent today due to their many advantages. The earliest concept of a microstrip patch antenna was given in a paper in 1953 [19], a patent on the same topic can also be tracked back to year 1955 [20]. The microstrip antennas are inherently simple, cost effective, easily realizable, have low profile, and are conformable. They can be readily manufactured using the widely available printed circuit board technology. The radiating element involved in

such antennas is termed 'patch'. Different performance characteristics of the antenna like operating frequency, radiation, polarization, and impedance characteristics can be determined by the shape and structure of the 'patch'. Due to their versatile nature, these antennas find applications today in a wide range of devices, especially devices used in modern communication systems, military, satellite, and space technology. These antennas generally consist of a metallic patch realized on a grounded substrate. The substrate usually is a dielectric sheet, made up of material having a dielectric constant anywhere between 2.2 and 12 [14]. The patch and feeding line are commonly printed using photoetching and laser printing on the substrate sheet.

Microstrip patch antennas due to their inherent advantages and adaptability are a popular choice for modern wireless communication systems today. These antennas find applications in mobile phones, laptops, wireless routers, base stations, and other wireless communication equipment. Microstrip antennas can be conveniently designed as per the device specifications and performance metrics and are also easily integrable. The desired frequency, bandwidth, polarization, and impedance characteristics can be easily achieved by the design diversity and versatility offered by microstrip patch antennas. Different design techniques are constantly being researched and developed, allowing this class of antennas to be used in a wide range of wireless communication equipment today.

1.5 Thesis Motivation:

Wireless communication technology has seen rapid advancements in recent times. With introduction of Fifth Generation (5G) technology, the world today is moving towards the concept of wireless systems and devices that are able to provide multiple services with high data rate and remain interconnected all the time. Such modern systems and

devices will find useful applications in many different areas of communication, government, and military facilities like Internet of Things (IoT), smart cities, modern mobile terminals, emergency health care etc. As a result, the already deployed Fourth Generation (4G) communication systems along with in-deployment Fifth Generation (5G) communication systems will experience an enormous growth and surge in terms of performance and capacity. Moreover, the Fifth Generation (5G) communication systems in their initial deployment phase will be deployed in non-standalone configuration and will coexist with the Fourth Generation (4G) communication systems, by utilizing the sub 6 GHz band. Later on, in advanced stages of deployment, the standalone Fifth Generation (5G) communication systems operating in the mmWave frequency range will also be deployed. Therefore, to cater the immense capacity growth and performance advancements of modern communication systems there is a huge demand for compact antenna designs that can operate on multiple bands for both non-standalone and standalone Fifth Generation (5G) communication systems. Since the non-standalone Fifth Generation (5G) communication systems will coexist with the Fourth Generation (4G) communication systems, using multiple antennas for these hybrid systems will contribute towards increasing the cost as well as complexity of wireless devices. Therefore, designing intelligent multiband antennas for different deployment configurations of Fifth Generation (5G) communication systems is a challenging task. Instead of using conventional antennas, there is a need to smartly design compact, efficient, and multiband antennas with low fabrication cost that are able to target the current and future operating frequency bands of the wireless communication system by performing effectively in the 4G/ 5G transitional (non-standalone 5G) deployment stage as well as in the advanced stages of 5G (standalone 5G) communication system deployment.

Existing literature regarding this research challenge concerning design of simple and compact multiband antennas for different deployment configurations of 5G communication systems is limited. Multiband antenna designs available in the literature mostly are dual or triple band designs primarily targeting the 3G/ 4G communication systems. Very limited research is available related to 5G multiband antenna designs that target operating frequencies from 3 GHz to 6 GHz (for the sub 6 GHz band of 5G communication systems). Interestingly 5G frequency bands above 3 GHz have been proposed for applications in a lot of world regions including China and Europe [21] as well as for many 5G New Radio (NR) services [22] and hence appear as potential bands of fascination for research related to 5G antenna development.

Also, many available antenna designs have complex multi-layered structures and are larger in size which limits their application in future wireless communication systems. Similarly, few efficient multiband antenna designs are available for the mmWave 5G band. The available mmWave multiband antenna designs are mostly either dual or triple band and are generally concentrated towards the 28 GHz band. The diversity and versatility of advanced 5G communication systems call for designing simple, low cost, compact, efficient, and multiband antennas targeting multiple proposed 5G frequency bands that are expected to be utilized in current as well as future wireless communication devices, for both non-standalone and standalone 5G deployment configurations. Microstrip patch antennas owing to their ease of fabrication, conformability, versatility, and adaptability can be smartly developed using modern and efficient design techniques for use in the transitional 4G/5G (non-standalone 5G) and advanced stages of 5G (standalone 5G) communication system deployment.

1.6 Thesis Contributions:

The thesis contributions include design, development, measurement, and analysis of three different compact, simple, smart, efficient, and low cost, multiband microstrip antennas for modern 5G communication systems. The research for this thesis was conducted between years 2019 and 2021. High Frequency Structure Simulator (HFSS) software has been used for simulation purposes. Two developed antenna designs have been published in reputed impact factor journals whereas the third developed antenna design has been presented and published in a reputable IEEE sponsored conference. Key characteristics and properties of each developed microstrip antenna design are briefly described below.

The first designed and developed smart microstrip patch antenna is based on a multi-reconfigurability approach. The antenna consists of a simple and compact circular loop type structure exhibiting frequency as well as bandwidth reconfigurability using PIN diodes. The antenna is able to target multiple frequency bands for 4G and 5G communication technology applications with high gain and radiation efficiency, and hence can be used in non-standalone deployment configuration of 5G communication systems. Frequency switching capability of antenna is demonstrated by operating the antenna in diodes 'ON' state in a tri band mode (at 2.21, 4.85, and 10.19 GHz) and then by operating the antenna in diodes 'OFF' state in dual band mode (at 3.42 and 8.02 GHz). On the other hand, bandwidth switching capability of antenna is demonstrated by operating the antenna in diodes 'ON' state in a wideband from 7.54 GHz to 12 GHz and then by operating the antenna in diodes 'OFF' state in a narrowband from 7.71 GHz to 8.48 GHz. The proposed antenna design offers a unique, smart, and intelligently futuristic approach of multi-reconfigurability that allows it to

be deployed in 4G devices, 5G devices, 4G/5G hybrid devices as well as devices utilizing both terrestrial and satellite communication services.

A multi-slotted, compact, quadband, two element Multiple Input Multiple Output (MIMO) microstrip patch antenna is designed and developed in the second phase of research for this thesis. The designed MIMO antenna is able to resonate at four different frequency bands (2.5, 3.7, 4.3, and 5.5 GHz) with reduced mutual coupling and compact size. A simple decoupler structure has been incorporated in the antenna design to improve the isolation performance without adding any design complexity. The antenna is able to resonate at all four frequency bands with a mutual coupling value of less than -20 dB. Radiation characteristics, efficiency and gain results of the proposed MIMO antenna authenticate the effective performance of proposed antenna design and render it appropriate for use in modern 4G and 5G communication applications. The proposed MIMO antenna due to its quadband nature, compact size and minimal structural loading is especially suitable for already present 4G applications and non-standalone 5G applications.

The third and final compact smart microstrip patch antenna developed for this research is based on a multiband mmWave array antenna design. Although the initial targeted area for 5G communication technology deployment is the sub 6 GHz band, primarily being used to offer 5G services in the non-standalone mode, the future scenario will however change and mmWave band will be needed to offer 5G services, due to its importance and need. The present mmWave antenna designs generally target the initial frequencies of the mmWave band. Also, many of the existing or proposed design structures operate in a single or dual band configuration. Hence a mmWave antenna array resonating at multiple frequency bands appears as a prospective candidate for future 5G communication applications. The proposed multi-slotted mmWave antenna

array structure is able to resonate at four different frequency bands (30.58 GHz, 34.5 GHz, 38.3 GHz, and 49.3 GHz) with high gain and radiation efficiency. The mmWave antenna array is designed using plain slot structures to avoid any additional complexities thereby keeping the proposed design very simple.

1.7 Thesis Organization:

The thesis is divided into six chapters.

Chapter 01 introduces the thesis topic by giving a background of wireless communication technology. The chapter also briefly narrates the evolution of wireless communication generations from 1G to 5G. Then the chapter discusses the basics of antennas. Importance of microstrip patch antennas along with thesis motivation is emphasized in context of their utility in modern communication systems. The chapter then briefly highlights the significant thesis contributions.

Chapter 02 describes the literature review carried out before proceeding with the three smart multiband microstrip patch antenna designs. Different research papers have been presented and discussed. The chapter highlights significant contributions of papers present in the previous literature. The chapter also attempts to emphasise the research gap and challenges that led to the development of microstrip patch antennas presented in this thesis. In the end a clear research approach, constituted in light of discussed research papers, has been elaborated.

Chapter 03 introduces and describes the design, development, and analysis of the first smart multiband microstrip patch antenna structure of this research. The antenna is based upon the concept of frequency as well as bandwidth reconfigurability using PIN diodes. The chapter introduces the concept of reconfiguration and discusses the relevant

available literature. The antenna design development is explored in detail. Later on, the simulated and measured results of different important antenna performance parameters have been presented, discussed, and analysed. The chapter also compares significant results of developed antenna with other relevant and recent antennas from literature in the form of a table.

Chapter 04 introduces and describes the design, development, and analysis of the second smart multiband microstrip patch antenna structure of this research. The antenna design is based upon the concept of Multiple Input Multiple Output (MIMO) technology. The chapter introduces the concept of MIMO antennas and discusses the relevant available literature. The design process of two element quadband multi-slotted MIMO antenna is explored in detail by this chapter. Then simulated and measured results of several significant individual as well as MIMO antenna performance metrics have been described and analysed in the chapter. Finally, before concluding, the chapter compares significant results of developed MIMO antenna with other relevant and recent MIMO antennas from literature in the form of a table.

Chapter 05 introduces and presents the design, development, and analysis of the third smart multiband microstrip patch antenna structure of this research. The antenna has been designed to operate in the mmWave range and utilizes the concept of an array structure. The chapter also discusses relevant available literature. The chapter explores design and development process of the antenna in detail. Several important simulated and measured results for different essential antenna parameters have been discussed and analysed in this chapter. In the end before concluding, the chapter compares important results of quadband microstrip patch antenna array with other relevant and recent antennas from literature in the form of a table.

Chapter 06 compares the three smart multiband microstrip patch antenna structures that have been designed and developed in this research. The chapter narrates significant features of all developed antennas and gives a comparative insight towards the unique performance capability offered by each design. The chapter ends by presenting the future work and conclusion.

Finally, at the end of the thesis, references used in writing this dissertation have been enlisted.

CHAPTER 02

LITERATURE REVIEW

A thorough literature survey was carried out before proceeding with the design of different smart multiband microstrip patch antennas. The literature survey comprised of studying, existing antenna structures for currently deployed communication systems, as well as techniques that allow an antenna to operate intelligently over multiple frequency bands. This chapter presents a generalized overview of certain significant papers that played a vital role in channelling the research of this thesis. First a comprehensive description of the recent trends in microstrip patch antenna design technology is presented followed by a review of frequency reconfigurable, MIMO and mmWave patch antenna designs.

2.1 Recent Trends in Microstrip Patch Antenna Design Technology:

Over the last decade microstrip patch antenna design technology has evolved substantially. Many new design techniques specially related to multiband patch antennas have been introduced in literature to meet the demand of modern communication, military, and satellite related equipment. A $60 \times 60 \times 1.56 \text{ mm}^3$ split ring resonator inspired triband patch antenna has been presented in [23]. Figure 2.1(a) represents layout of the antenna structure. The antenna top side consists of a square shaped slotted structure with four split ring resonators located at every corner of the square slot whereas a feedline is present on the bottom side of antenna. The complete structure is able to resonate at 2.7, 4.3, and 4.7 GHz. A dual band antenna utilizing the composite right- and left-hand transmission line zeroth order resonator (CRLHTR-ZOR) is presented in [24]. The CRLHTR-ZOR consists of a rectangular shaped

structure, a serpentine line, and a notch in the shape of trapezoid. In addition, a monopole and a triangle shaped radiator have also been included in antenna design. The complete antenna has a size of $105 \times 60 \times 0.8 \text{ mm}^3$ and is able to operate at two low frequency bands, $698 - 960 \text{ MHz}$ and $1710 - 2690 \text{ MHz}$ with a reflection coefficient value of less than -6 dB . However, when the reflection coefficient value of less than -10 dB is considered the antenna bandwidth becomes narrow for the first band (from $698 - 810 \text{ MHz}$) and second band vanishes completely. The antenna may find applications in 4G mobile devices.

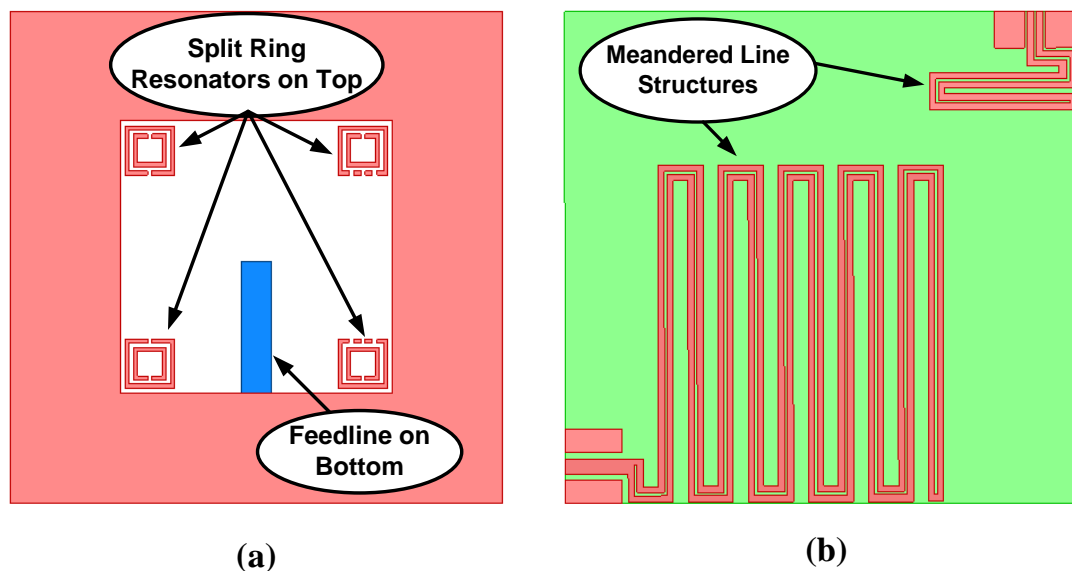


Figure 2.1 Antenna Geometry Presented in (a) [23] (b) [25]

A two-element triband antenna is proposed in [25]. The antenna design is based upon two different meandered line structures, which allow the antenna to resonate at $1.8, 2.4,$ and 2.6 GHz . The antenna however poses a large size of $85 \times 80 \text{ mm}^2$. Substrate used for antenna design is FR4 epoxy with a height of 0.035 mm . The two meandered line structures have been placed orthogonally to increase the isolation between two antenna elements to 15 dB . Figure 2.1 (b) represents the geometry of proposed antenna design. The antenna is suitable for LTE and WLAN applications; however, the antenna

prototype has not been fabricated and paper only contains simulated results. A transmission line metamaterial (TL-MTM) inspired antenna operating on dual frequency bands has been investigated in [26]. The TL-MTM is further based upon complementary split ring resonator structures and a mushroom type structure. F4B substrate of 3 mm thickness has been used to realize the antenna design. Four TL-MTM structures along with two ring shaped slots surrounding the antenna feed have been used in the design. Overall dimensions of the antenna including ground plane come out to be $30 \times 30 \text{ mm}^2$. The antenna is able to resonate at 2.4 GHz and 3.5 GHz but with a narrow bandwidth, particularly for the lower band. For 2.4 GHz band the measured bandwidth is 35 MHz whereas for 3.5 GHz band the measured bandwidth is 60 MHz. [27] presents another dual band antenna based upon a TL-MTM structure. The antenna consists of a single layered design containing four TL-MTM inspired structures along with two ring shaped slots on the top side. Overall dimensions of the antenna are $36 \times 36 \times 3 \text{ mm}^3$ and the design is able to resonate at 2.76 GHz and 5.23 GHz. The bandwidth for the first band is relatively narrow and ranges from 2.74 – 2.76 GHz whereas the bandwidth for second band ranges from 5.15 – 5.31 GHz.

A slotted multiband patch antenna is presented in [28]. The antenna utilizes multiple U-shaped slots on the top side along with two I shaped slots on the bottom side and ten metal vias in the structure to achieve multiband performance. Figure 2.2 represents the antenna geometry. The antenna is $40 \times 40 \times 1.964 \text{ mm}^3$ in size. The presented antenna, with three U-shaped slots on the top side, is able to resonate at 3.04, 3.83, 4.83, and 5.76 GHz, however the bandwidth achieved for all resonating bands is narrow. Operating bandwidth recorded at 3.04, 3.83, 4.83, and 5.76 GHz is 25, 25, 39, and 41 MHz respectively. For modern 5G communication devices at sub 6 GHz band a

bandwidth of 100 MHz is required between 2 to 6 GHz [29]. The efficiency of antenna falls between 42 % to 60 % for all resonating frequency bands.

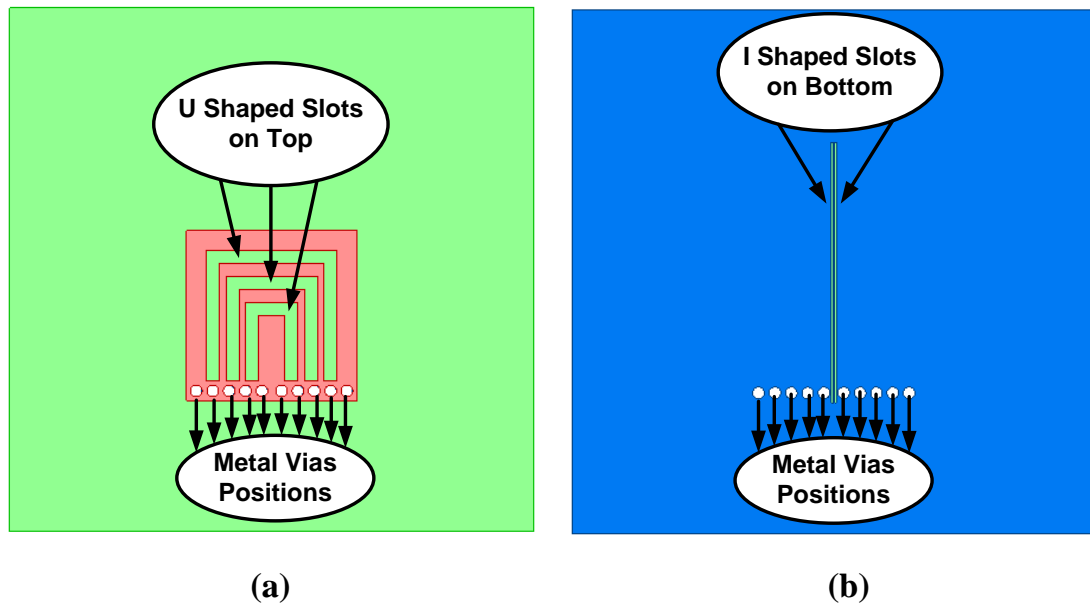


Figure 2.2 Antenna Geometry Presented in [28] (a) Top Side (b) Bottom Side

Another slotted patch antenna with a wideband has been presented in [30]. Conventional microstrip patch antennas generally suffer from the problem of narrow bandwidth. [30] investigates inclusion of a complementary structure in shape of a titled rectangular slot, in the ground plane of a patch antenna. The added structure is termed as a complementary rhombus resonator (CRR). Additional structures are usually added into a patch antenna for achieving desired performance results. The antenna design is represented in Figure 2.3 (a). CRR is placed just under the line feed to enhance the bandwidth, allowing the antenna to operate over a wideband from 5.5 to 6.7 GHz. The antenna structure has been created using FR4 epoxy substrate and has a size of $40 \times 49 \times 1 \text{ mm}^3$.

Design of a plain rectangular microstrip antenna with X shaped slots has been presented in [31]. Five X shaped slots have been inserted in the patch on the antenna top side

whereas a partial ground plane is present on the bottom side of the antenna structure. The complete layout of antenna is given in Figure 2.3 (b). The antenna is able to resonate at 9.9 GHz with a relatively wider bandwidth (from 8.49 – 11.3 GHz). Overall dimensions of the complete design are $20 \times 24 \times 0.01 \text{ mm}^3$, however only simulated results have been presented and no antenna prototype has been fabricated.

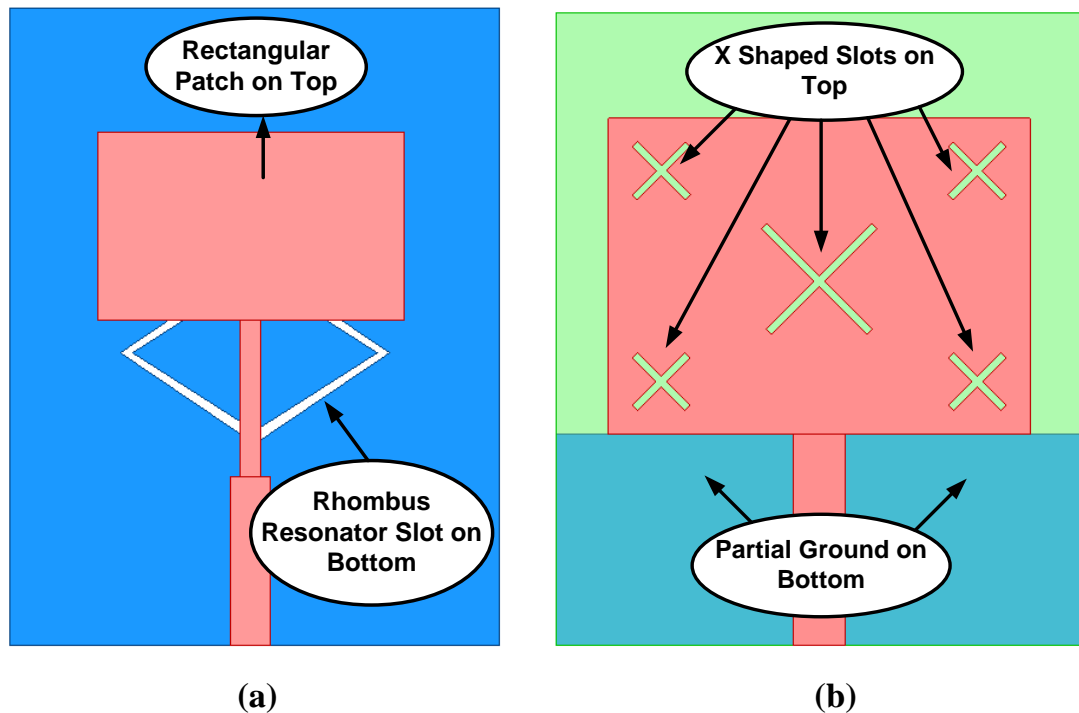


Figure 2.3 Antenna Geometry Presented in (a) [30] (b) [31]

A dual band square shaped single patch antenna for 3G/ 4G applications has been investigated in [32]. The antenna design structure is multi-layered and has been inspired from a rat race network arrangement with two feeding ports. The base of antenna structure is $160 \times 160 \text{ mm}^2$ in size. Two different substrates have been used; a polytetrafluoroethylene (PTFE) substrate is present at the bottom of antenna structure whereas FR4 epoxy substrate is present at the top of antenna structure. Both substrates have a separation of 16 mm among each other. Operating bands of antenna range from 1.59 to 2.34 GHz when port 1 is excited and from 1.88 to 2.76 GHz when port 2 is

excited. A wideband patch antenna for 3G/ 4G applications is presented in [33]. The antenna structure is non-planar and consists of two L shaped feeding probes placed between the ground layer and the patch layer. The Two L shaped feeding probes have been placed in an antisymmetric configuration to increase the operational bandwidth of the proposed antenna. The antenna is able to resonate from 1580 – 2750 MHz. A $200 \times 200 \text{ mm}^2$ ground plane is present at the base of antenna structure whereas a square shaped $50 \times 50 \text{ mm}^2$ patch is located at a height of 24 mm above the ground plane. Design of a stacked non-planar dual band antenna is given by [34]. The antenna structure is represented by Figure 2.4 (a). The antenna is multi-layered and uses four FR4 substrate sheets equipped with annular patches and ring-shaped slots. The antenna has an overall size of $60 \times 30 \times 21 \text{ mm}^3$ and is able to operate at 2.5 GHz and 3.5 GHz. The antenna may find suitable applications in WiMAX devices.

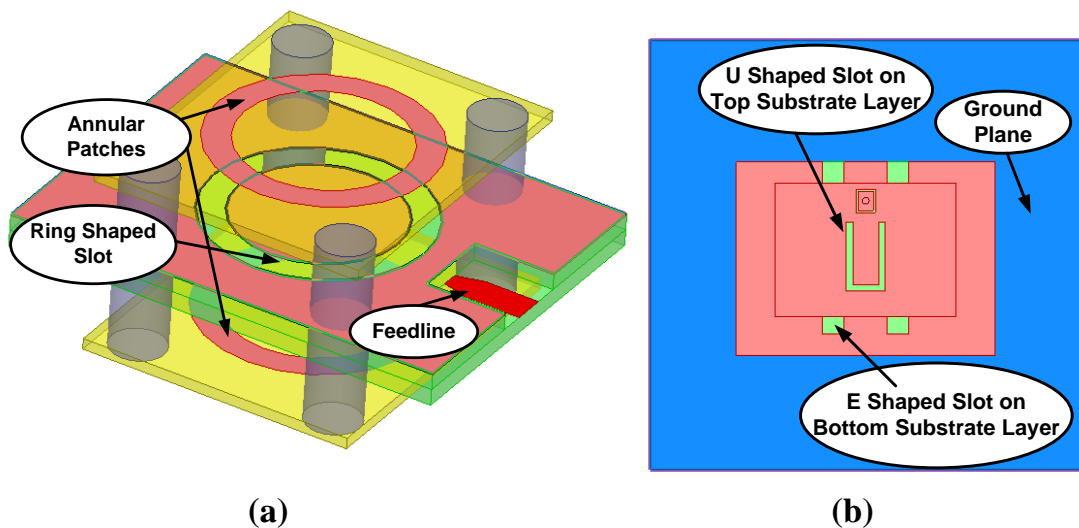


Figure 2.4 Antenna Geometry Presented in (a) [34] (b) [37]

A disc shaped multi-layered dual band patch antenna is proposed in [35]. Two-disc shaped substrate layers (each with a radius of 30.8 mm) of Rogers RO4003C have been incorporated in the antenna structure. The upper substrate layer consists of two

radiators, a square shaped radiator on the top side and a circular radiator on the bottom side. The top circular radiator further consists of four slots placed symmetrically with respect to each other whereas the bottom square shaped radiator contains a U-shaped slot. Ground is present on bottom side of the lower substrate. Two substrate discs are connected with the help of four metallic posts. The complete antenna structure targets resonant frequencies of 2.45 and 5.8 GHz. Another multi-layered multiband antenna structure is proposed by [36]. Five different substrate layers have been used to realize the antenna design with improved efficiency. Four substrate layers are composed of FR4 epoxy material whereas one substrate layer is composed of Rogers RT/Duroid 5880 material. Each substrate layer used has similar area of $74 \times 70 \text{ mm}^2$, however the thickness of each substrate layer is different. Moreover, each substrate layer contains patches of different shapes and dimensions. Antenna is able to operate in dual band configuration from 2.25 – 2.9 GHz and from 4.95 – 5.94 GHz thereby targeting the WLAN frequency bands. A multiband E shaped antenna with two layers is proposed in [37]. Figure 2.4 (b) highlights the antenna structure. The antenna has two substrate layers, the top substrate layer contains a patch with U-shaped slot whereas the bottom substrate layer contains a patch with an E-shaped slot. On the base of the antenna a $100 \times 100 \text{ mm}^2$ ground plate has been provided. Height of the complete structure is 12 mm. Antenna design operates from 2.4 – 2.48 GHz and 3.4 – 3.61 GHz and is suitable for use in WLAN and WiMAX application devices.

A rectangular patch antenna design with a parasitic element for 4G/ LTE applications is researched in [38]. The antenna design is given in Figure 2.5 (a). Parasitic element has been inserted to enhance the operating bandwidth of the design. The antenna is able to operate in the frequency range from 800 – 2400 MHz. Antenna has been realized using FR4 epoxy substrate of 1.6 mm thickness. The presented antenna has an overall

large size of $140 \times 120 \text{ mm}^2$. Also, no measured results have been discussed by the paper. Another multiband patch antenna utilizing the defected ground approach has been presented in [39]. Figure 2.5 (b) highlights the antenna design. The antenna has been created using Rogers RO4350 substrate with a thickness of 0.76 mm . The overall antenna size is $18.8 \times 20 \text{ mm}^2$. The design targets the WLAN frequency bands. Considering the -6 dB bandwidth the antenna is able to operate at 2.43 GHz (with 40 MHz bandwidth) and at 5.2 GHz (with 1.2 GHz bandwidth). However, when -10 dB bandwidth criterion is considered, the first operating frequency band almost vanishes whereas the second frequency band then ranges from and the second band ranges from 4.8 to 5.6 GHz . Also, the antenna has a gain of -1.7 dB at 2.43 GHz and a gain of 2.4 dB at 5.2 GHz .

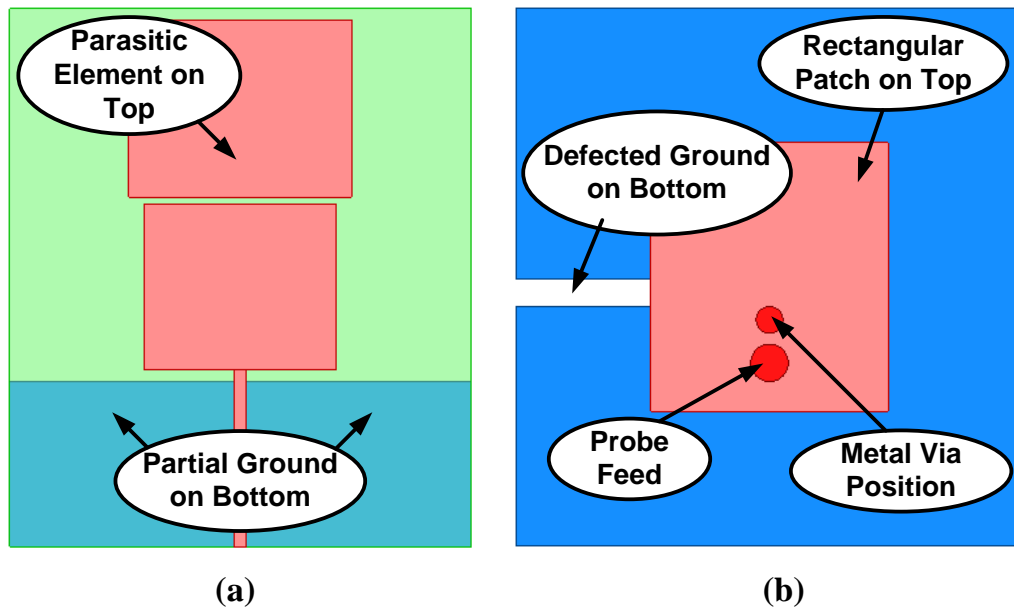


Figure 2.5 Antenna Geometry Presented in (a) [38] (b) [39]

It can be assessed from the presented literature that many different techniques can be used to design microstrip patch antennas like split ring resonator structures, transmission line based structures, meandered line inspired structures, slotted structures, or structures involving parasitic elements or defected ground. However,

most of the developed antennas are either dual band or triple band in nature and generally cater for the operating frequencies around or below 2 GHz . Also, many designs have relatively large size and are complex involving multi-layered nonplanar structures.

2.2 Review of Frequency Reconfigurable Microstrip Patch Antenna Design Technology:

Need for smaller electronic equipment with multiband performance has led to research in achieving antenna compactness. Many ideas have been presented to reduce the size of antenna; one such idea is that of a frequency reconfigurable antenna. These antennas are able to change their operating frequency in real time.

The printed antenna in [40] proposes a reconfigurable antenna using two lumped components (a chip inductor and a PIN diode) placed in a C shaped monopole inspired patch structure. The inductor is inserted in the middle rectangle of C shaped monopole structure whereas PIN diode is inserted in the top rectangle of C shaped monopole structure. Arlon CuClad 217 with a height of 0.787 mm has been used as the antenna substrate. The total size of the antenna is $20 \times 28.5\text{ mm}^2$. It is observed that in the 'ON' state the antenna resonates at 2.2 GHz whereas in the 'OFF' state the resonance band shifts to 2.4 GHz . The antenna has a relatively low gain, 0.05 dB at 2.2 GHz and 0.65 dB at 2.4 GHz . The presented antenna may find applications in devices utilized for providing UMTS and WLAN communication services. An aperture coupled frequency reconfigurable antenna with two substrates has been proposed in [41]. The antenna design is represented in Figure 2.6 (a). The antenna utilizes the concept of defected ground structure (DGS). The upper substrate contains a rectangular patch on the top side whereas the bottom substrate contains the DGS with two dumbbell shaped

geometries on top side and aperture coupled feedline on the bottom side. A switch has been placed in the feedline to realize the frequency reconfigurability operation. When the switch is in ‘ON’ state the antenna resonates at 8.85 GHz while the antenna resonates at 7.5 GHz when the switch is in ‘OFF’ state.

Another dual band frequency reconfigurable antenna is given by [42]. Two similar metasurfaces inspired from meandered line structures have been placed on top of the main slotted radiating element. Mechanically controlling the arrangement and positioning of two metasurfaces executes the frequency reconfigurability operation. The dimensions of radiating element and metasurfaces are $65 \times 65\text{ mm}^2$, whereas the two metasurfaces have been placed at a distance of 2 mm from each other. Overall height of the complete structure is 6 mm . Antenna is able to resonate in three different states; in state 1 the antenna operates from 3.1 to 3.3 GHz and from 4.4 to 4.7 GHz , in state 2 the antenna operates from 3.3 to 3.5 GHz and from 4.65 to 4.8 GHz , and finally in state 3 the antenna operates from 3.53 to 3.69 GHz and from 4.83 to 5.07 GHz .

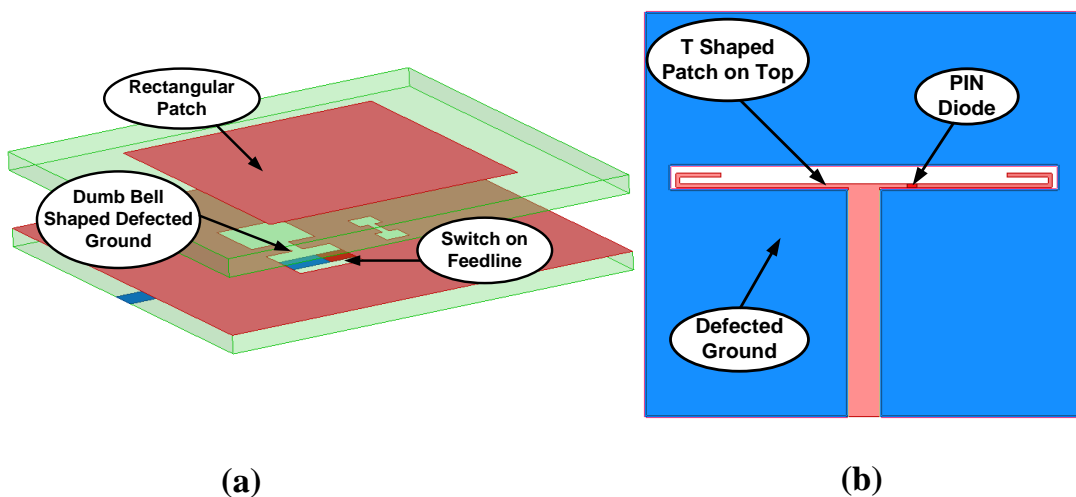


Figure 2.6 Antenna Geometry Presented in (a) [41] (b) [43]

A dual band coplanar waveguide-based frequency reconfigurable antenna is presented in [43]. Figure 2.6 (b) highlights the antenna design. The patch consists of a T shaped

radiator with a PIN diode. When the switch is operating in the ‘ON’ state the antenna operates at 1.59 GHz whereas when the switch is turned ‘OFF’ the antenna starts to operate in dual band configuration at 1.55 GHz and 3.65 GHz. The proposed antenna has a size of $82 \times 80 \text{ mm}^2$. A rectangular microstrip antenna with full ground a slotted feed line capable of offering frequency reconfigurability has been proposed by [44]. A T-shaped slotted feedline equipped with three PIN diodes is responsible for implementing the reconfiguration operation. The antenna has an overall size of $120 \times 120 \text{ mm}^2$. Based upon different configuration states of PIN diodes the antenna can resonate at either 1.8, 2.3, or 2.4 GHz. However, only simulated results have been presented and no prototype has been fabricated. A frequency reconfigurable antenna for LTE and WLAN application devices is proposed in [45]. The antenna design is represented in Figure 2.7 (a). The antenna structure consists of four similar rectangular dielectric resonators separated by feed line containing PIN diodes. Four different narrow operating bands at 1.89, 2.14, 2.53, and 2.77 GHz can be achieved by operating the three PIN diodes in different configurations. The biasing circuit placed besides the antenna structure consists of many components, and contains two dc bias lines, two inductors and a resistor for every PIN diode and four capacitors in total.

Another frequency reconfigurable microstrip patch antenna based on a conventional dipole structure is given by [46]. The dipole arms have been equipped with split ring resonator structures. Four PIN diodes have been placed in gaps of each split ring resonator structure. Antenna has a size of $40 \times 70 \text{ mm}^2$ and is capable of switching from a single resonant band at 2.5 GHz to dual resonant bands at 1.55 GHz and 2.6 GHz. A frequency reconfigurable antenna based upon a very basic square shaped radiating patch is presented in [47]. Figure 2.7 (b) illustrates the antenna structure.

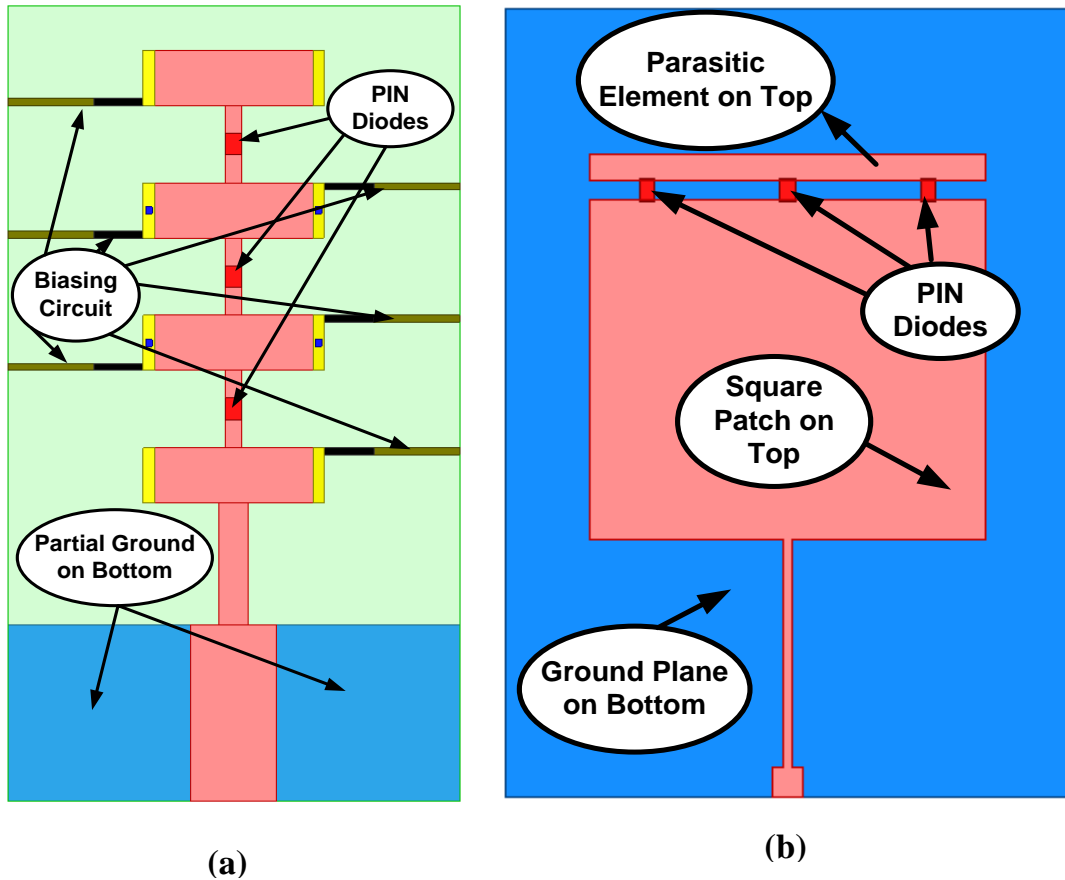


Figure 2.7 Antenna Geometry Presented in (a) [45] (b) [47]

The antenna also contains a parasitic rectangular radiating element which is connected with the square shaped patch using three PIN diodes. When all diodes are turned ‘OFF’ the antenna operates at 2.45 GHz but when all diodes are turned ‘ON’ the antenna starts to operate at 2.2 GHz . Proposed antenna design has a size of $80 \times 56\text{ mm}^2$. Another frequency reconfigurable antenna designed for LTE and GPS mobile handset applications is proposed by [48]. The design consists of an L shaped feeding strip and two grounded strips (one short and one long). The long-grounded strip is made to connect with four inductors using an RF switch. These connections between the inductors and the RF switch are used to exhibit the frequency reconfiguration operation. Overall dimension of the antenna is $140 \times 70\text{ mm}^2$. Considering the -6 dB

bandwidth, proposed antenna structure can offer operating frequencies from 683 – 960 MHz and 1460 – 2820 MHz based upon the RF switch configuration. From the presented literature it can be observed that the concept of frequency reconfigurability can be used to effectively design microstrip patch antennas, with reduced antenna size, that can intelligently operate on different frequency bands, thereby enhancing the efficiency of the antenna structure.

2.3 Review of Multiple Input Multiple Output (MIMO) Microstrip Patch Antenna

Design Technology:

Another smart and intelligent antenna design approach for modern communication devices is offered by Multiple Input Multiple Output (MIMO) antenna design technology. Different microstrip patch antennas have been designed using this approach. Few investigated MIMO antenna designs have been presented in this section.

A small size multiple input multiple output (MIMO) antenna for UMTS and LTE applications, operating in two frequency bands is proposed in [49]. L shaped radiating elements have been utilized to design the antenna structure. Coplanar waveguide (CPW) feeding technique with a slotted circular shaped ground has been adopted. Parasitic strips along with slits have also been incorporated to improve the isolation performance. Figure 2.8 (a) shows the complete antenna structure. Antenna has a total size of $120 \times 120 \times 0.8 \text{ mm}^3$. The final antenna design exhibits a dual band resonance with centre frequencies of 0.7 GHz and 1.8 GHz. The antenna, however, has low gain value of -6.5 dB for the lower resonant band. The isolation is more than 13 dB for both resonant bands. A multiband MIMO antenna with high isolation is proposed in [50]. The antenna utilizes radiating elements in the shape of trapezoids. Moreover, defected ground structure (DGS) and meander line structures have been included in the

design to reduce mutual coupling and improve the overall antenna performance. The size of proposed two element MIMO antenna is $17 \times 42 \times 1.6 \text{ mm}^3$. The MIMO antenna is able to operate in two frequency bands centred around 7.2 GHz and 8.6 GHz . The antenna has an isolation greater than 17 dB for both operating frequency bands due to the insertion of a defected ground structure.

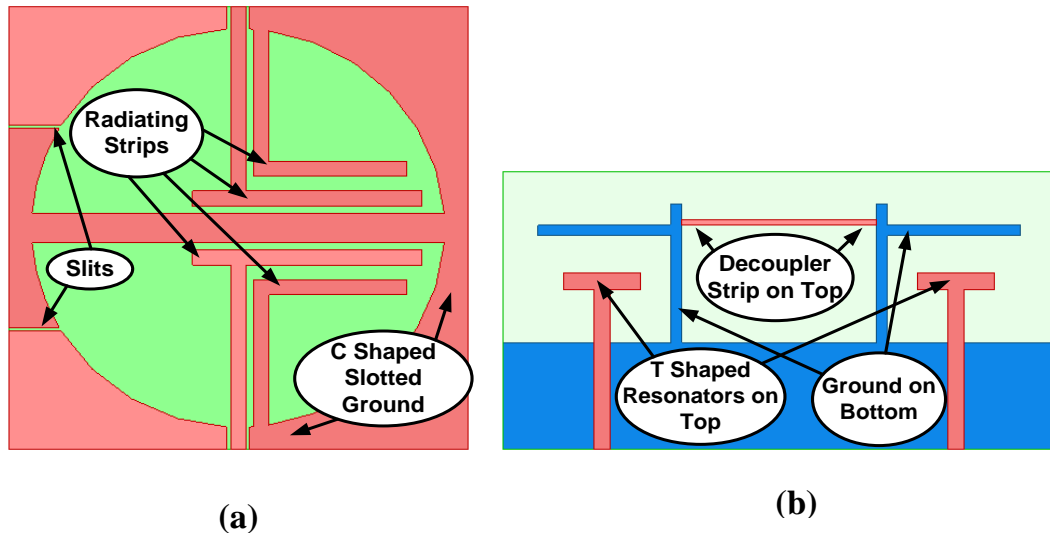


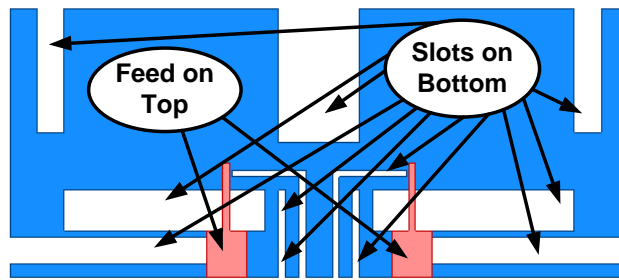
Figure 2.8 Antenna Geometry Presented in (a) [49] (b) [51]

Another MIMO antenna design for WLAN applications with reduced mutual coupling is presented in [51]. The fundamental antenna element has been created using T shaped resonators. A simple metal strip is used to decrease the mutual coupling between the two antenna elements. The design is able to resonate in two different frequency bands. Complete antenna geometry is given in Figure 2.8 (b). Total size of the MIMO antenna comes out to be $26 \times 50 \times 0.8 \text{ mm}^3$. The reduced mutual coupling two element MIMO antenna is able to operate in two frequency bands centred around 2.5 and 5.5 GHz . Moreover, the isolation between antenna elements is more than 20 dB . A dual band MIMO antenna for WLAN devices inspired from inverted F shaped antenna design has been reported by [52]. The antenna structure also utilizes a T shaped slot on the ground

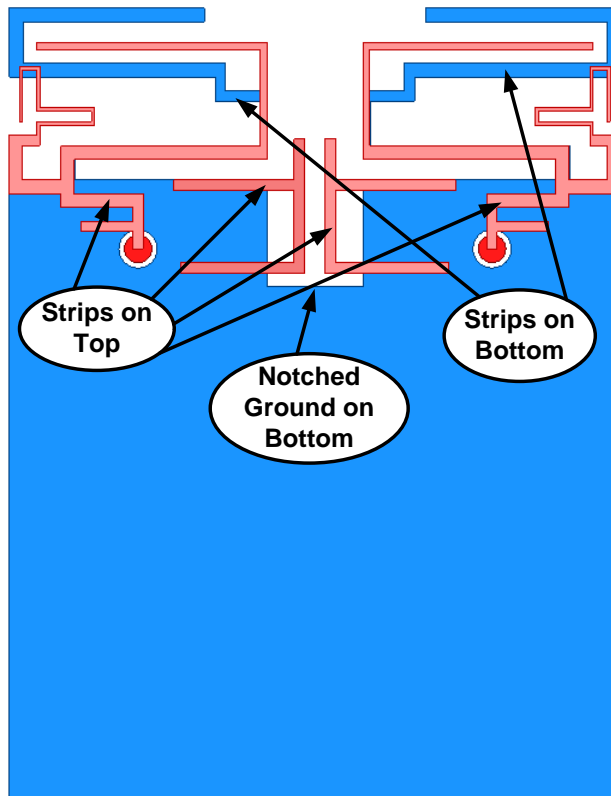
along with a meandered line to improve the isolation performance. Two U-shaped slits have also been incorporated in the design to enhance the return loss performance. The antenna has a size of $52 \times 77.5 \times 1.6 \text{ mm}^3$ and is able to operate from 2.4 to 2.8 GHz and from 5.15 to 5.825 GHz with an isolation of 15 dB for both resonant frequency bands.

An interesting multiport MIMO antenna design for WLAN devices resonating in dual band configuration is presented in [53]. The antenna design is represented in Figure 2.9 (a). The antenna utilizes multiple rectangular slots along with a T-shaped slot to achieve the desired performance. Overall structure is a combination of a two-port antenna resonating from 2.4 to 2.5 GHz with a four-port antenna resonating from 4.9 to 5.725 GHz. The antenna has a total dimension of $46 \times 20 \times 1.6 \text{ mm}^3$ but possesses relatively lower isolation of 12 dB between antenna ports. A multi-layered MIMO antenna operating at two different frequency bands is presented in [54]. The antenna operates at 3.7 GHz and 4.1 GHz. The main radiator consists of a simple rectangular patch for both MIMO antenna elements. An H shaped decoupler has also been inserted along with the two rectangular patches in the antenna design. Moreover, a layer of modified decoupling surface, comprising of rectangular slots and plus shaped structures, has also been added to enhance the isolation between two MIMO antenna elements to 30 dB. The antenna has an overall large dimension of $48.5 \times 60.6 \times 20 \text{ mm}^3$.

Another planar MIMO antenna design is given by [55]. Figure 2.9 (b) illustrates the structure of proposed antenna. The antenna design consists of two similar elements utilizing simple and meandered striplines on the top side and plain striplines with a notched ground plane on the bottom side.



(a)



(b)

Figure 2.9 Antenna Geometry Presented in (a) [53] (b) [55]

Overall size of the antenna is $89 \times 115 \times 0.3 \text{ mm}^3$ and the design is able to resonate from 890 to 960 MHz as well as from 1.88 to 2.69 GHz. A parasitic element has been utilized to improve the MIMO antenna isolation performance. The isolation between two antenna elements comes out to be 10 dB. It can be seen from the survey conducted on MIMO antennas, that efficiency and performance of a microstrip patch antenna can

be increased by utilizing this technology, however, special attention needs to be paid towards the isolation between antenna elements. Generally, reduction of isolation between MIMO antenna elements may result in an increased antenna size if an efficient decoupler structure is not used.

2.4 Review of mmWave Microstrip Patch Antenna Design Technology:

As discussed in chapter 1, mmWave frequencies have been proposed for the 5G technology. Antenna designing for mmWave is a popular research topic today. Few of the explored papers have been described in this section.

A mmWave dual band printed antenna array is given by [56]. The single element antenna consists of a T shaped radiator placed on antenna top side whereas a triangle shaped radiating structure with a triangle shaped slot is present on antenna bottom side. Six elements have been combined to form an array with an overall dimension of $35 \times 25 \times 1.575 \text{ mm}^3$. The antenna array is able to resonate at 28 GHz and 38 GHz . However no fabricated prototype has been demonstrated and only simulated results have been depicted. [57] reports a single band single element mmWave antenna for applications targeting the concept of Internet of Things (IoT). The antenna structure is highlighted by Figure 2.10 (a). The antenna resonates at a frequency of 60 GHz . Geometry of proposed antenna consists of a rectangular loop type structure containing two U-shaped parasitic patches on the top side and a full ground on the bottom side. The overall dimensions of mmWave antenna are $14 \times 10.5 \times 1.15 \text{ mm}^3$.

A proximity feeding based stacked mmWave microstrip antenna using three substrate layers is proposed by [58]. The first substrate layer contains two feedlines on the top side and a full ground plane on the bottom side, whereas on the top side of second

substrate a square shaped patch and two strip lines are present. The third substrate layer contains a square slotted radiating element. The dimensions of antenna come out to be $10 \times 10 \times 0.387 \text{ mm}^3$. The final antenna design is able to resonate at 28 GHz and 39 GHz . A slotted H shaped microstrip patch antenna structure is presented in [59]. Figure 2.10 (b) highlights the antenna design. The antenna operates in a dual band configuration at 37 GHz and 54 GHz . Size of complete structure is $7.2 \times 5 \times 0.787 \text{ mm}^3$. The realized gain at 37 GHz is 5 dBi whereas the realized gain at 54 GHz is 6 dBi . Moreover, no antenna prototype has been fabricated and only simulated results have been presented.

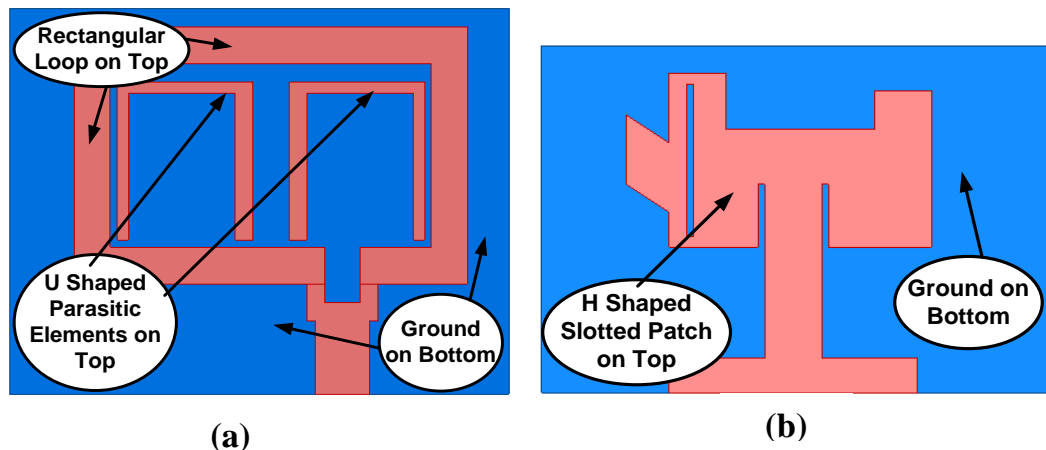


Figure 2.10 Antenna Geometry Presented in (a) [57] (b) [59]

A multi-layered double cavity backed microstrip antenna array is investigated by [60]. The single element is composed of a double cavity slotted antenna with 8 stacked layers. Four single elements have been combined to form a mmWave antenna array that is able to resonate at 28 GHz and 38 GHz . However, the achieved bandwidth for both resonant bands is relatively narrow. The designed antenna array has an overall size of $20.04 \times 3.065 \times 0.905 \text{ mm}^3$. A triple band mmWave patch antenna is reported in [61]. The antenna structure has been represented in Figure 2.11 (a). The antenna design utilizes a fractal structure with partial ground plane approach. Moreover, an

electromagnetic band gap structure has also been incorporated in the basic antenna design to enhance the gain. The complete antenna structure is able to resonate at 29.05 GHz, 35.75 GHz, and 41 GHz. The realized antenna has a size of $20 \times 20 \times 0.762 \text{ mm}^3$.

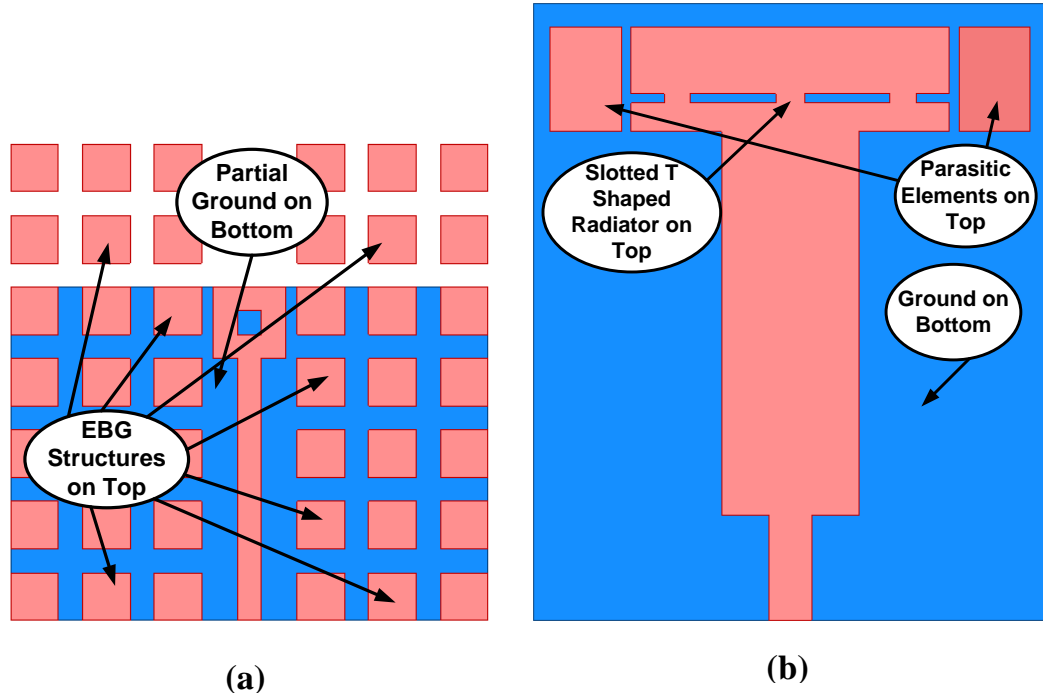


Figure 2.11 Antenna Geometry Presented in (a) [61] (b) [63]

A multi-layered wideband stacked four element mmWave antenna array design is presented in [62]. Detailed single element antenna design consists of two Rogers 4350 substrate layers and four metallic layers. The sandwiched metallic layers contain coupling slots whereas the top metallic layer contains a multi-slotted structure of 16 slots and the bottom metallic layer four radiating structures and antenna feed line. The size of antenna structure comes out to be $12 \times 12 \times 0.762 \text{ mm}^3$. Operating frequency of antenna ranges from 71 GHz to 86 GHz. Design of another dual band mmWave antenna is investigated in [63]. Figure 2.11 (b) shows the layout of the proposed antenna structure. Antenna design consists of a T-shaped radiating structure containing four different slots for performance enhancement. The complete antenna structure has a size

of $12.5 \times 10.1 \times 0.87 \text{ mm}^3$ and it resonates at 27.5 GHz and 35.7 GHz . However, no antenna prototype has been manufactured and only simulated results have been presented. In [64] 2×2 microstrip patch antenna arrays with different substrates have been realized and investigated. The basic antenna design consists of four rectangular patches excited using inset feeds. The designed arrays are made to operate in a single band configuration at 28 GHz . The best and efficient antenna design has been realized using Astra M77 substrate and has a size of $14.5 \times 14.5 \times 0.35 \text{ mm}^3$. It can be observed from the reviewed literature on mmWave antenna designs that most designs are dual band or triple band designs and target operating frequencies around 28 GHz . Also, mechanisms and techniques need to be investigated and adopted in order to improve the gain and radiation efficiency of this class of antennas. Moreover, mmWave antennas will find potential applications in future standalone 5G communication devices.

2.5 Summary:

The conducted comprehensive literature review greatly helped in channelling the direction of this research. It can be asserted that microstrip patch antennas are an effective and in-demand antenna type for future wireless communication devices. The basic design of microstrip patch antennas need to be intelligently and smartly modified in order to adapt these antennas to be used in future communication applications and devices. Microstrip patch antennas with efficient and effective multiband operation need to be designed for current 4G, and upcoming 5G non-standalone and standalone devices. Reconfigurable antennas offering frequency switching capability may present an interesting antenna solution to modern wireless communication applications. Moreover, MIMO antennas resonating on multiple frequency bands of 4G and 5G

technology can also offer a smart and crafty design solution for future communication devices. Also, mmWave technology-based antennas can be designed smartly for future stand-alone 5G communication devices.

Three different smart, compact, efficient, multiband microstrip antenna structures were developed and analysed in the next phase of this research. The upcoming chapters describe the design and results of the three developed antennas in detail along with a more specific literature review focused on the techniques utilised for antenna structure development and evolution to meet the desired performance specifications.

CHAPTER 03

ANTENNA DESIGN 1: A MULTI-RECONFIGURABLE ANTENNA BASED ON CIRCULAR LOOP DESIGN

3.1 Introduction:

Advances in modern wireless communications has resulted in congestion of the available electromagnetic spectrum. Frequency reconfigurable microstrip patch antennas have been proposed as one effective solution to overcome this congestion issue. These antennas have been successfully able to gain a lot of attention during the past few years. In addition, frequency reconfigurable antennas offering switching between different frequency bands lessen the complexity of involved hardware because they offer several functions in a single design. The frequency reconfigurable antennas can decrease the cost, complexity, and overall size of an antenna structure, thereby improving the efficiency and performance of a wireless system. These antennas therefore can be a very promising choice for modern 4G and 5G wireless communication system devices.

As discussed in chapter 2, many techniques have been explored in literature to attain frequency reconfigurability. A lot of these techniques are based on changing the flow of current in an antenna structure. Different current paths are developed with the help of strips, stacking structures and addition of elongated arms in the shape of an antenna. But many such adopted techniques rely on the involvement of a larger ground plane and can increase structural complexity of the antenna design [65]. LC (inductor-capacitor) resonator loading is one other technique that has been adopted to induce the reconfigurability operation. The method relies on embedding different LC components

into the patch antenna structure, these components then allow the antenna to operate at different frequency bands [66]. Techniques exploiting defected ground structures for frequency reconfigurability are also present in literature [67]. Moreover, frequency reconfigurability operation using ring shaped structures has also been explored [68].

The reconfigurability operation offered by microstrip patch antennas is not limited to the operating frequency only. Antenna performance parameters such as radiation pattern, bandwidth, and polarization can also be targeted using the reconfigurability approach. Usually, the number of active components involved in antenna design structure determine the number of executed reconfigurability operations [14] [69]. In order to allow the microstrip patch antenna structure to attain the reconfigurability function, generally mechanical switches or electronic switches are utilized. Common examples of mechanical switches include use of reed switches for achieving reconfigurability, whereas PIN diodes are a typical example of electronic switches used for achieving reconfigurability in an antenna design. Varactor diodes and radio frequency (RF) microelectromechanical systems (MEMS) switches are also employed in design of reconfigurable patch antennas [70] [71]. Low switching speeds of around 1 to 200 μs are generally provided by RF MEMS switches for most applications [70], whereas PIN diodes provide relatively faster switching speeds of around 1 to 100 ns [72]. Integration of mechanical switches on patch antennas creates heavy and complex structures while on the other hand, PIN diodes are easily integrated on patch antenna substrates making them a comfortable and potentially appropriate choice for reconfigurable antenna designs. PIN diodes have been used to achieve reconfigurability operations targeting frequency, polarization, and radiation pattern [73] – [75]. Moreover, idea of bandwidth reconfigurability for 4G applications has also been explored [76]. Ideas of incorporating slits, slotted structures, modified ground planes

and parasitic patches along with PIN diodes have been exploited in literature to attain reconfigurability targeting different antenna parameters [77] [78].

In this chapter the first antenna design for this research is presented. The antenna is based on a circular loop structure exhibiting frequency as well as bandwidth reconfigurability using PIN diodes. The antenna is able to target multiple frequency bands for 4G and 5G communication technology applications. The detailed design, development, results, and analysis of the proposed antenna structure are explored in subsequent sections of the chapter.

3.2 Design of Proposed Multi-Reconfigurable Antenna:

The design of proposed multi-reconfigurable antenna is based primarily on a circular loop shaped structure. The loop has been evolved to fit in two PIN diodes. The antenna design is represented in Figure 3.1. The two PIN diodes have been smartly placed in such a way that both these diodes can be simultaneously turned ON and OFF. The antenna is able to resonate at three different frequency bands, 2.21, 4.85, and 10.19 GHz when both diodes are in ON state. While a dual band operation at 3.54 and 8.02 GHz is observed when both diodes are in OFF state. Moreover, bandwidth reconfigurability is also noticed, from narrowband to wideband, when both diodes are turned ON. Hence the proposed multi-reconfigurable antenna is able to offer both frequency and bandwidth reconfigurability approaches.

The proposed multi-reconfigurable antenna design is based on a circular loop design [79]. A modified ground plane approach has been used in design. High Frequency Structure Simulator (HFSS), which is a full wave 3D electromagnetic software has been used for antenna design and analysis. A multiband microstrip antenna can be designed using rings or circular loops [80]. At the beginning a typical circular loop antenna was

designed. The radius of the loop r was taken as 10 mm . The strip width d was taken as 1.5 mm .

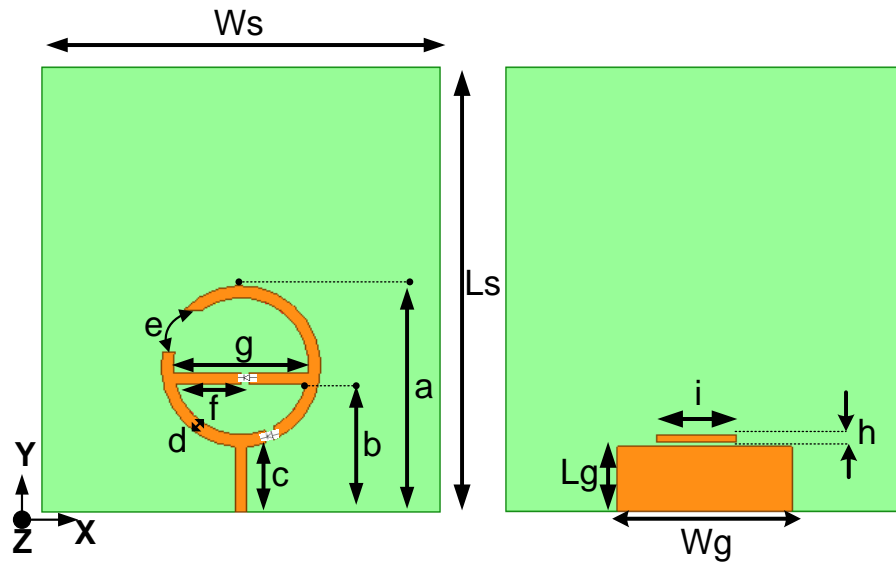


Figure 3.1 Final Design of Proposed Multi-Reconfigurable Antenna, Patch Structure (Left) and Modified Ground Structure (Right)

Wire radius can be obtained from given strip width using the following equation [81]:

$$\text{Wire Radius } (wr) = \frac{\text{Strip Width } (d)}{4}$$

The wire radius in this case can be computed by inserting the value of strip width d as 1.5 mm .

$$\text{Wire Radius } (wr) = \frac{1.5\text{ mm}}{4}$$

$$\text{Wire Radius } (wr) = 0.375\text{ mm}$$

For loop antennas an interesting parameter termed the thickness factor can be determined from the values of loop and wire radius. Any loop antenna can be categorized as a thick or thin antenna based upon the value of thickness factor. Thin

antennas are efficiently able to operate at multiple frequencies [81]. Thickness factor can be determined using the following equation [82]:

$$TF = 2 \ln \left(\frac{2\pi r}{wr} \right)$$

The thickness factor can hence be calculated by inserting the values of loop and wire radius as 10 mm and 0.375 mm respectively.

$$TF = 2 \ln \left(\frac{2\pi 10}{0.375} \right)$$

$$TF = 10.24$$

Thus, the initially designed loop antenna has a thickness factor value of 10.24. Loop antennas having thickness factor values of greater than 9 are characterized as thin antennas [82]. Therefore, the initially designed loop antenna structure can be categorized as a thin antenna, capable of exhibiting multiband operation.

The antenna is designed using commonly available FR4 epoxy substrate with a thickness of 1.6 mm. The complete layout of antenna design is given in Figure 3.1. The dimensions highlighted in Figure 3.1 are detailed in Table 3.1.

Table 3.1 Detailed Dimensions of Multi-Reconfigurable Antenna

Dimension	Value (mm)	Dimension	Value (mm)
<i>L_s</i>	55	<i>f</i>	8.19
<i>W_s</i>	50	<i>g</i>	17
<i>a</i>	28	<i>h</i>	1
<i>b</i>	15.75	<i>i</i>	10
<i>c</i>	8.02	<i>L_g</i>	8
<i>d</i>	1.5	<i>W_g</i>	22
<i>e</i>	5.25		

As represented in Figure 3.1 the final patch design is based on a fundamental circular loop structure. A horizontal strip of length g and width d has been inserted in middle of the loop and an arc of length e has been taken out from the loop to obtain the final design of proposed antenna. The antenna is excited using a 50Ω microstrip line feed. The addition of horizontal strip in middle of circular loop [83], removal of arc from the circular loop [79], and insertion of a partial ground plane [84] into the antenna structure allow the proposed antenna to achieve multiband resonance as well as increased bandwidth. Finally, a small strip of 1 mm width and 10 mm length, in the shape of a rectangle is placed 0.5 mm above the partial ground plane to further enhance the bandwidth and efficiency of proposed antenna structure.

3.2.1 Antenna Design Evolution:

Figure 3.2 represents important evolution steps involved in the antenna design. In order to observe the impedance matching performance, Figure 3.3 represents the corresponding reflection coefficient plots for every design in Figure 3.2.

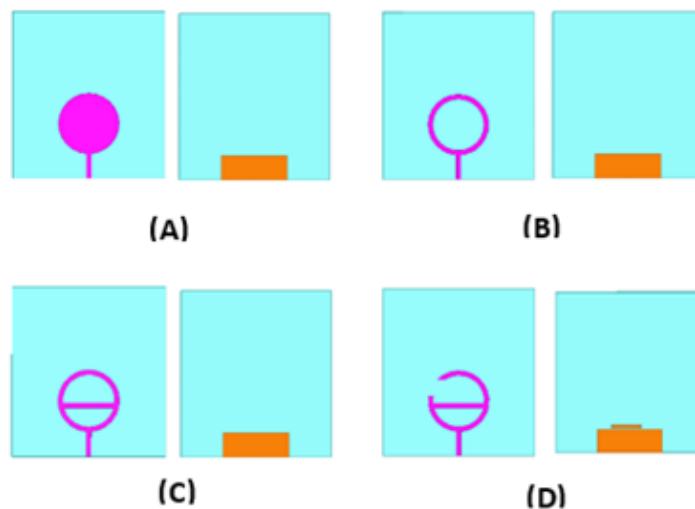


Figure 3.2 Evolution Steps for Antenna Design (top and bottom): (A) Design A (B) Design B (C) Design C (D) Design D

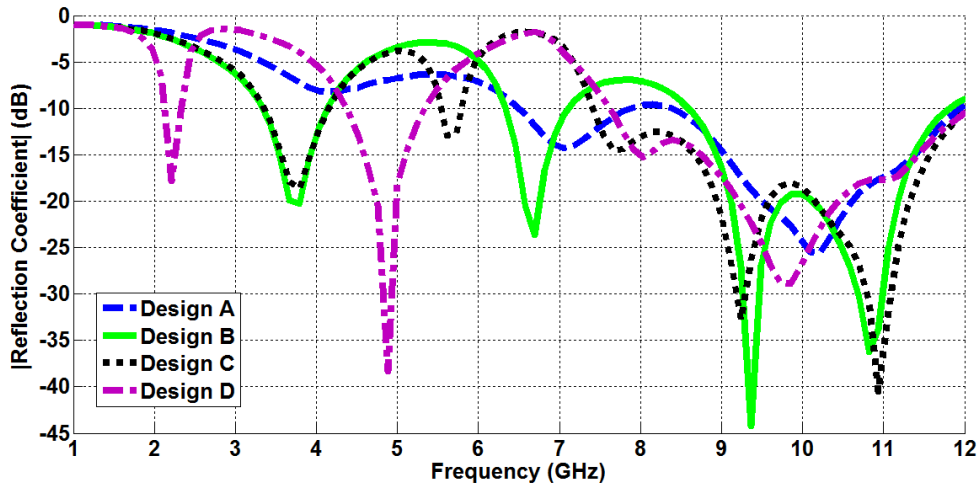


Figure 3.3 Reflection Coefficient Results for Antenna Evolution Steps

Design A highlights the first step in the antenna design evolution process. As it can be seen Design A consisted of a plain circular patch and a rectangular partial ground plane. The corresponding reflection coefficient plot for Design A in Figure 3.3 shows the antenna resonating around X band (8.4 to 12 GHz), as well as from 6.5 to 8 GHz. Design A was then evolved into Design B by converting plain circular patch into a circular loop structure in order to allow the antenna to resonate at multiple frequencies. Reflection coefficient results of Design B in Figure 3.3 highlight a multiband operation. More precisely Design B is able to resonate at three different frequency bands from 3.1 to 4.1 GHz, 6.4 to 7.1 GHz, and 8.6 to 11.7 GHz. Next step in the design evolution process involved further adjustment of resonant frequencies and bandwidth of the X band. In Design C a horizontal strip of length 17 mm and width 1.5 mm is added in the middle of circular loop structure [83]. The corresponding reflection coefficient results for Design C in Figure 3.3 represent a triband operation. Design C was able to resonate from 3.1 to 4.1 GHz, 5.6 to 5.8 GHz, and 7.4 to 12 GHz. Hence Design C is able to operate in the entire X band. Lastly Design D was developed by taking out an arc of

length 5.25 mm from the circular loop structure on the top side of antenna design [79], and by placing a small strip above the partial ground on the bottom side of antenna design [84]. Design D, as it can be seen in Figure 3.3, was able to operate from 2.16 to 2.27 GHz, 4.3 to 5.3 GHz, and 7.54 to 12 GHz.

3.2.2 Parametric Analysis:

In order to clearly understand the impact of various radiating elements present in the final antenna design a detailed parametric study was carried out targeting certain geometric parameters. In the beginning the arc length e taken out from circular loop structure was changed from 1.25 mm to 7.75 mm . Figure 3.4 represents the corresponding reflection coefficient results for different arc length values. It can be assessed from the reflection coefficient plots that change in removed arc length affects the operating frequency of the first band. Increasing the value of removed arc length gradually increases the centre frequency of the first resonant band. For the final design value of removed arc length has been chosen as 5.25 mm in order to attain the desired operating frequency of 2.21 GHz.

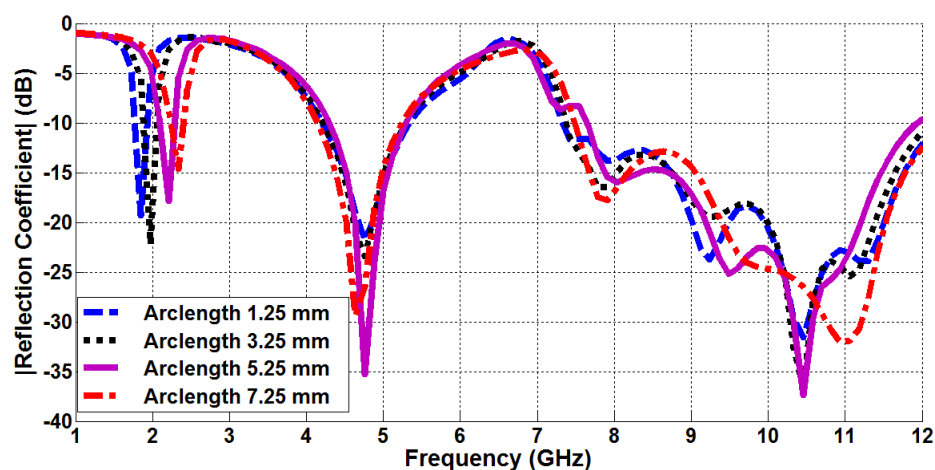


Figure 3.4 Reflection Coefficient Results for Removed Arc Length Variation

Next parametric study was carried out on length of horizontal strip present in centre of the circular loop structure. Length of the horizontal strip has been represented as g . Length of horizontal strip was changed from 5 mm to 17 mm by keeping it intact with the right side of circular loop structure. Corresponding reflection coefficient results have been plotted in Figure 3.5. The results clearly indicate that length of horizontal strip controls the second resonant band. Also increase in bandwidth of X band, the third resonant band, depends on length of horizontal strip. The position for first PIN diode was mainly selected based on this specific parametric analysis. It can be observed that best results are achieved when length of horizontal strip is taken as 17 mm and it is connected to the circular loop structure from both ends.

Another parametric study was performed based upon variation of the strip length d . As discussed previously strip length d plays an important role in determining the thickness factor of the loop antenna design.

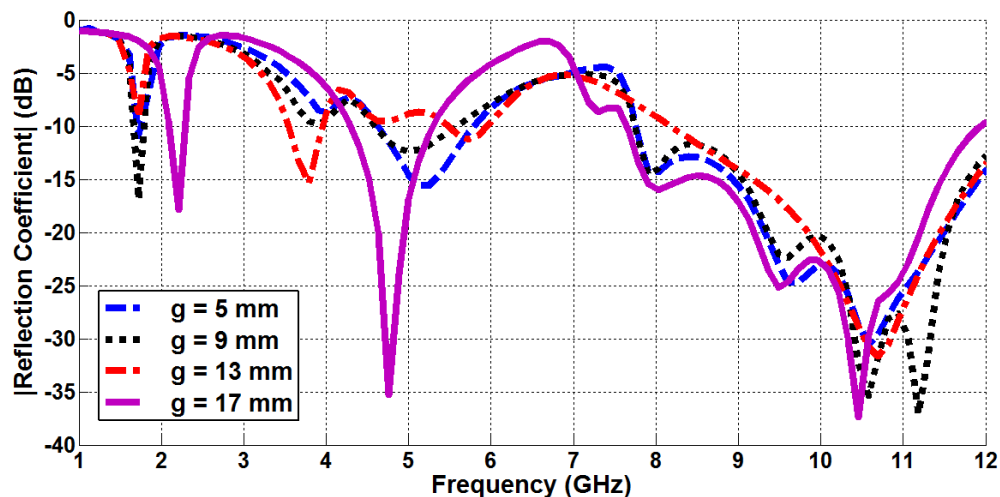


Figure 3.5 Reflection Coefficient Results for Horizontal Strip Length Variation

This significance of strip length is also evident through the executed parametric study. The strip length d was altered from 1.5 mm to 4.5 mm. The corresponding reflection

coefficient results have been presented in Figure 3.6. It can be seen that a thin antenna, as defined previously can operate at different frequency bands. The strip width of 1.5 mm has been selected for the final antenna design. Increase in value of strip width strongly affects the second resonant band and it starts to disappear.

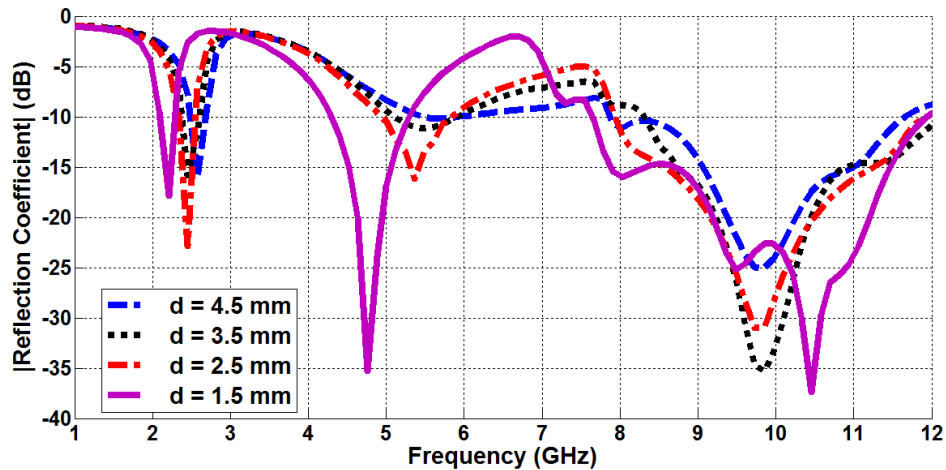


Figure 3.6 Reflection Coefficient Results for Strip Width Variation

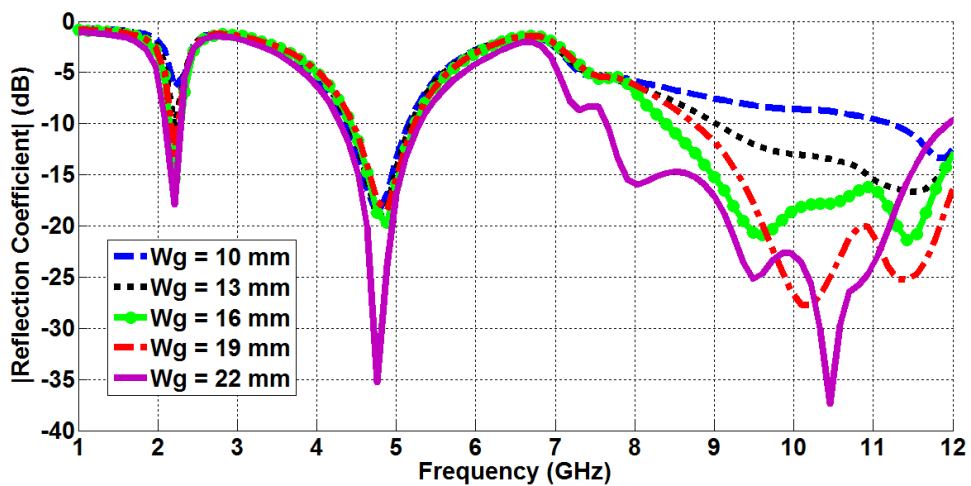


Figure 3.7 Reflection Coefficient Results for Partial Ground Length Variation

In order to observe the effects of partial ground on antenna performance another parametric study was carried out. This particular study targeted the length of rectangular partial ground, referred to as Wg . The length of partial ground was altered from 10 mm to 22 mm . Reflection coefficient results for partial ground length alterations are shown

in Figure 3.7. It can be seen that change in length of partial ground affects reflection coefficient values of all three resonant bands. Moreover, bandwidth of the third resonant band (X band) also changes with partial ground length variation. Optimum results are attained when length of partial ground is taken as 22 mm.

The final antenna design with selected optimum dimensions as represented in Figure 3.1, is able to successfully exhibit a triband operation from 2.16 to 2.27 GHz, 4.3 to 5.3 GHz, and 7.54 to 12 GHz. The final antenna design can be realized using a $22 \times 30 \text{ mm}^2$ substrate, but the substrate dimensions were later increased to comfortably adjust the PIN diodes and their DC biasing circuit.

3.2.3 Integration of PIN Diodes in Final Antenna Design:

In order to introduce the reconfigurability approach, PIN diodes positions were identified after the triband antenna has been designed and optimized. Identification of PIN diodes positions involved understanding and analysis of triband antenna design, close examination of implemented parametric studies and assessment of the surface current on designed antenna structure. Identified PIN diode positions are highlighted in Figure 3.8, which depicts the patch of antenna under consideration. The dimension '*j*' in Figure 3.8 has a value of 1 mm. PIN diode positions were selected in such a way that multiple paths could be provided to RF current from feed to patch, thereby altering the electrical length of antenna structure. After position identification PIN diodes were integrated into the antenna structure. From Figure 3.8 it can clearly be assessed that two PIN diodes have been placed in the antenna design. The diode at position 1 is responsible for controlling the 2.21 GHz frequency band. On the other hand, bandwidth of the X band is controlled by diode at position 2. Moreover, simultaneous operation of both PIN diodes results in switching between the 3.42 GHz and 4.85 GHz frequency

bands. It is pertinent to mention that both PIN diodes have been placed in the antenna structure in such a way that they can be operated simultaneously, that is both PIN diodes can be turned into ‘OFF’ and ‘ON’ states simultaneously.

RLC boundary conditions were exploited to include PIN diode structures in HFSS simulation. The effects of PIN diodes on impedance matching and radiation characteristics of the designed antenna were carefully optimized after inclusion of PIN diodes in the simulation model. In order to realize PIN diodes in HFSS simulation a small rectangle shaped strip was assigned the RLC boundary. In particular for realizing the ‘OFF’ diode state, a $1\text{ k}\Omega$ resistor was placed in parallel with a 0.1 pF capacitor, this component arrangement was then placed in series with a 0.5 nH inductor. On the other hand, to realize the ‘ON’ diode state a 0.5 nH inductor was put in series with a $0.8\ \Omega$ resistor [85]. When the PIN diodes are turned ‘OFF’, the antenna operates in dual band configuration and the frequency band from 2.16 GHz to 2.27 GHz gets suppressed. While the antenna is able to operate in tri band configuration when the PIN diodes are turned ‘ON’, this happens due to provision of constant current path to the antenna patch.

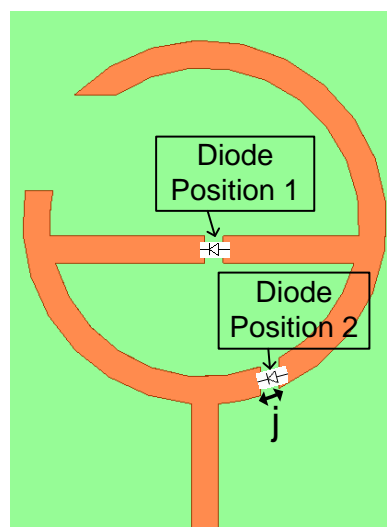


Figure 3.8 Marked Diode Positions on Antenna Radiating Patch

3.2.4 Investigation of Surface Current Distribution for Designed Antenna:

To better understand resonance behaviour of the designed antenna, surface current distribution for different resonant frequencies has been plotted in Figures 3.9 and 3.10. Contribution of different antenna sections in generation of respective frequencies can be clearly assessed from these figures. Figure 3.9 represents the surface current distribution plot of designed antenna in PIN diodes 'OFF' state, for both radiating patch and ground structure at frequencies of 3.42 GHz and 8.02 GHz. The figure has two sub parts, Figure 3.9 (A) represents the surface current distribution at 3.42 GHz. It can be seen that horizontal rectangle shaped strip placed in centre of circular loop along with lower half of circular loop supports generation of 3.42 GHz resonant frequency. Figure 3.9 (B) on the other hand, highlights the antenna sections responsible for generation of 8.02 GHz operating frequency. Lower and upper both halves of circular loop play important part in realization of 8.02 GHz frequency. It can also be evidently seen in Figure 3.9 that the small horizontal rectangle shaped strip on antenna bottom side has also a significant role in generation of the 8.02 GHz operating frequency.

Figure 3.10 highlights the surface current distribution plots of designed antenna in PIN diodes 'ON' state, for both radiating patch and ground structures at frequencies of 2.21, 4.85, 8.02 and 10.19 GHz. Surface current distribution at 2.21 GHz has been plotted in Figure 3.10 (A), it can be seen that both PIN diodes contribute towards generation of 2.21 GHz operating frequency. Moreover, the rectangle shaped horizontal strip placed in centre of circular loop along with upper and lower sections of the circular loop also contribute towards attainment of 2.21 GHz operating frequency.

Observing Figure 3.10 (B) reveals that PIN diode at position 2 plays significant role in realization of 4.85 GHz operating frequency along with lower section of the circular

loop structure of radiating patch. Surface current distributions corresponding to 8.02 GHz and 10.19 GHz, for PIN diodes ‘ON’ state, have been plotted in Figure 3.10 (C) and Figure 3.10 (D) respectively.

It can be assessed that wideband from 7.54 GHz to 12 GHz is achieved when both PIN diodes are turned ‘ON’, as whole antenna structure is responsible for generation of 10.19 GHz operating frequency, which can also be noticed in Figure 3.10 (D). Moreover, contribution of partial ground structure in generation of all three operating frequency bands can also be evidently appreciated from Figure 3.10.

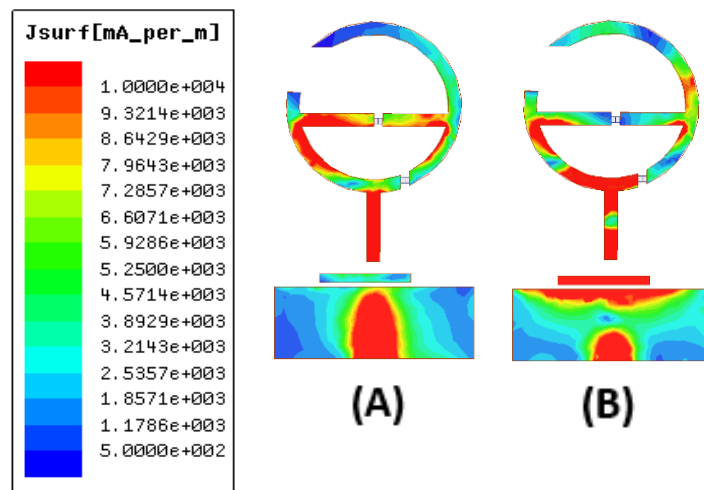


Figure 3.9 Surface Current Distribution (for patch and ground) in PIN diodes ‘OFF’ state at: (A) 3.42 GHz and (B) 8.02 GHz

3.3 Significant Antenna Results and Analysis:

In order to validate and estimate the effectiveness of final antenna design, a prototype of the proposed antenna structure was fabricated using FR4 epoxy substrate with a loss tangent value of 0.02, relative permittivity of 4.4 and a height of 1.6 mm. PIN diodes manufactured by Skyworks having part number SMP 1322 were incorporated in the fabricated prototype [85].

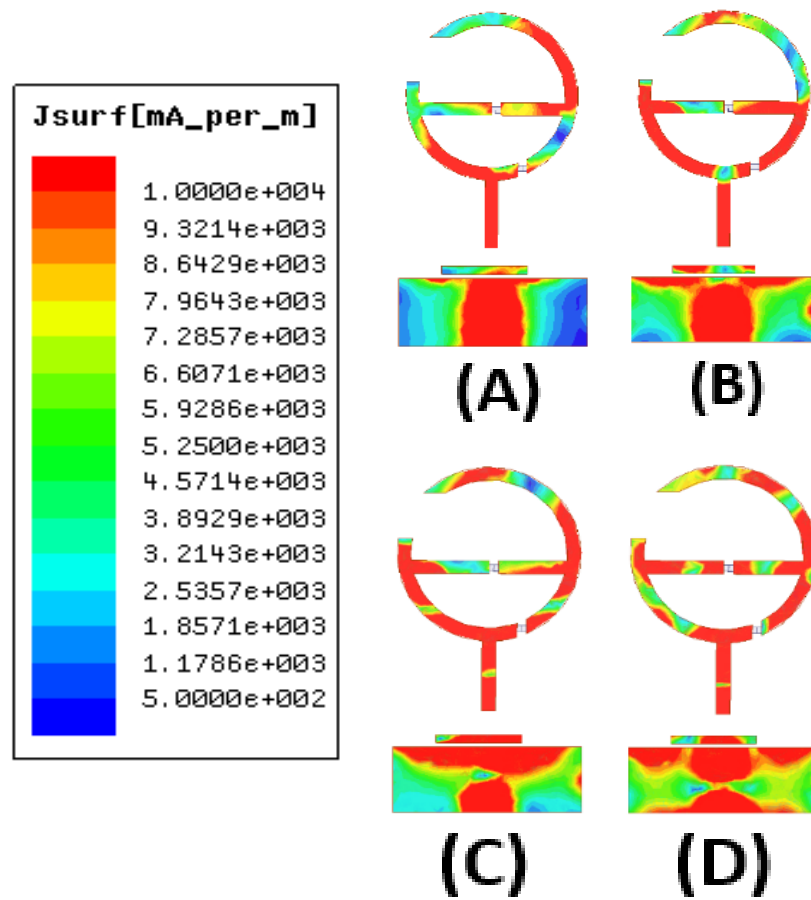


Figure 3.10 Surface Current Distribution (for patch and ground) in PIN diodes ‘ON’ state at: (A) 2.21 GHz (B) 4.85 GHz (C) 8.02 GHz and (D) 10.19 GHz

RF chokes produced by Minicircuit having part number ADCH-80A were also integrated in the developed prototype in order to separate DC currents from RF currents. ADCH-80 A chokes were chosen as they offer decreased parasitic capacitance, decreased DC resistance and high impedance for the selected frequency range [86]. The fabricated antenna prototype is illustrated in Figure 3.11.

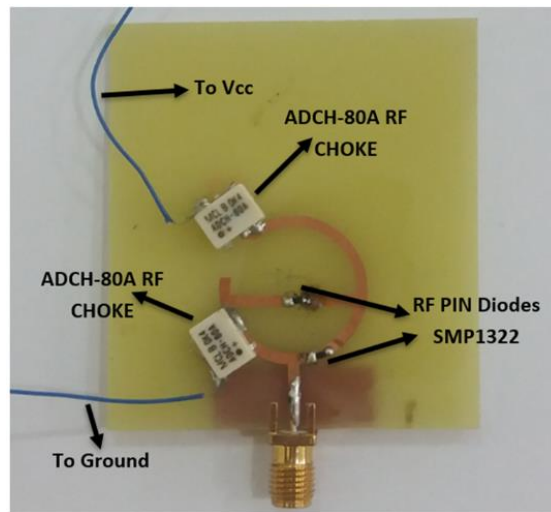


Figure 3.11 Fabricated Antenna Prototype

3.3.1 Reflection Coefficient Results:

To assess impedance matching of the proposed design, magnitude reflection coefficient results of the fabricated prototype were measured using a well calibrated Network Analyzer (Agilent N5245B PNA-X). Measured results presented a good agreement with the simulated results. However, nonideal PIN diode behaviour and fabrication imperfections can be held responsible for small differences between the measured and simulated results. Despite small differences the simulated and measured magnitude reflection coefficient values remain below -10 dB for all operating frequency bands in both diodes ‘OFF’ and ‘ON’ states. Simulated magnitude reflection coefficient results for all four possible configurations related to the two PIN diodes are represented by Figure 3.12. Role of PIN diode 2 in generation of 4.85 GHz resonant band can be evidently observed from Figure 3.12. Moreover, significant contribution of PIN diode 2 in controlling the bandwidth of X band can also be comprehended from Figure 3.12.

It can also be seen that both PIN diodes 1 and 2 are responsible for generation of 2.21 GHz and 3.42 GHz resonant bands.

Figure 3.13 illustrates the simulated and measured magnitude reflection coefficient results for PIN diodes 'OFF' and 'ON' states. As stressed previously the placement positions of both PIN diodes allow them to be turned 'ON' and 'OFF' simultaneously. It can be seen that antenna resonates at 3.42 GHz and 8.02 GHz when both diodes are turned 'OFF' while the antenna resonates at 2.21, 4.85 and 10.19 GHz when both diodes are turned 'ON'. From Figure 3.13 it can be noticed that the resonant frequency band at 3.42 GHz present in the PIN diodes 'OFF' state shifts to 4.85 GHz when both PIN diodes are turned 'ON'. Increase in bandwidth of third resonant band (X band) can also be observed evidently when PIN diodes switch from 'OFF' state to 'ON' state.

Table 3.2 records the detailed magnitude reflection coefficient and bandwidth results for PIN diodes 'OFF' and 'ON' states. From Table 3.2 and Figure 3.13 it can be observed that the proposed antenna design offers both frequency as well as bandwidth switching capability. Therefore, the proposed antenna design can be attributed as a multi-reconfigurable antenna design.

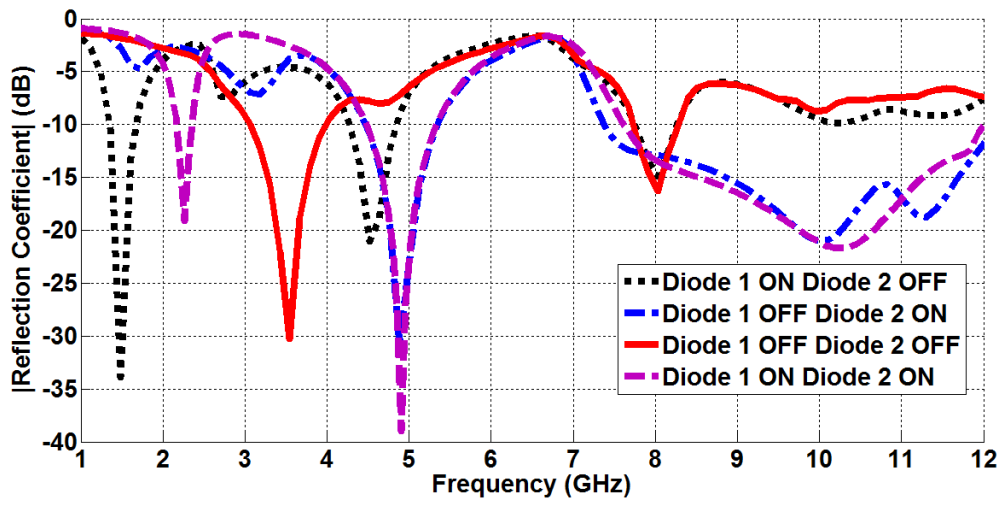


Figure 3.12 Simulated Reflection Coefficient Results for Four Possible Configurations of PIN Diodes

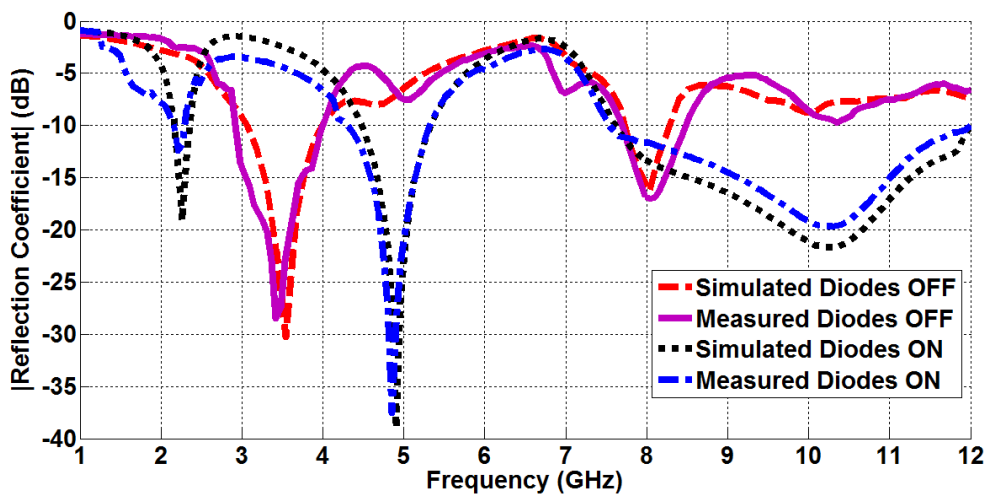


Figure 3.13 Simulated and Measured Reflection Coefficient Results for PIN Diodes 'OFF' and 'ON' States

Table 3.2 Detailed Magnitude Reflection Coefficient Results

	Diodes State ON	Diodes State OFF
Simulated Results	<p>Band 1: 2.155 GHz to 2.34 GHz (Bandwidth = 0.185 GHz) Centre Frequency = 2.265 GHz ($s_{11} = -19.12 \text{ dB}$)</p> <p>Band 2: 4.52 GHz to 5.29 GHz (Bandwidth = 0.77 GHz) Centre Frequency = 4.905 GHz ($s_{11} = -38.99 \text{ dB}$)</p> <p>Band 3: 7.625 GHz to 12 GHz (Bandwidth = 4.375 GHz) Centre Frequency = 10.35 GHz ($s_{11} = -21.63 \text{ dB}$)</p>	<p>Band 1: 3.061 GHz to 4.025 GHz (Bandwidth = 0.964 GHz) Centre Frequency = 3.54 GHz ($s_{11} = -30.23 \text{ dB}$)</p> <p>Band 2: 7.73 GHz to 8.36 GHz (Bandwidth = 0.63 GHz) Centre Frequency = 8.03 GHz ($s_{11} = -16.31 \text{ dB}$)</p>
Measured Results	<p>Band 1: 2.16 GHz to 2.27 GHz (Bandwidth = 0.11 GHz) Centre Frequency = 2.21 GHz ($s_{11} = -12.4 \text{ dB}$)</p> <p>Band 2: 4.3 GHz to 5.3 GHz (Bandwidth = 1 GHz) Centre Frequency = 4.85 GHz ($s_{11} = -37.5 \text{ dB}$)</p> <p>Band 3: 7.54 GHz to 12 GHz (Bandwidth = 4.46 GHz) Centre Frequency = 10.19 GHz ($s_{11} = -19.7 \text{ dB}$)</p>	<p>Band 1: 2.92 GHz to 3.97 GHz (Bandwidth = 1.05 GHz) Centre Frequency = 3.42 GHz ($s_{11} = -28.48 \text{ dB}$)</p> <p>Band 2: 7.71 GHz to 8.48 GHz (Bandwidth = 0.77 GHz) Centre Frequency = 8.02 GHz ($s_{11} = -17.03 \text{ dB}$)</p>

3.3.2 Far Field Results:

In order to understand the far field properties of proposed antenna, radiation pattern results were plotted in PIN diodes ‘OFF’ and ‘ON’ states. Figure 3.14 illustrates the simulated and measured radiation pattern plots in PIN diodes ‘OFF’ state whereas

Figure 3.15 illustrates the simulated and measured radiation pattern plots in PIN diodes ‘ON’ state. The radiation patterns were measured using an anechoic chamber facility.

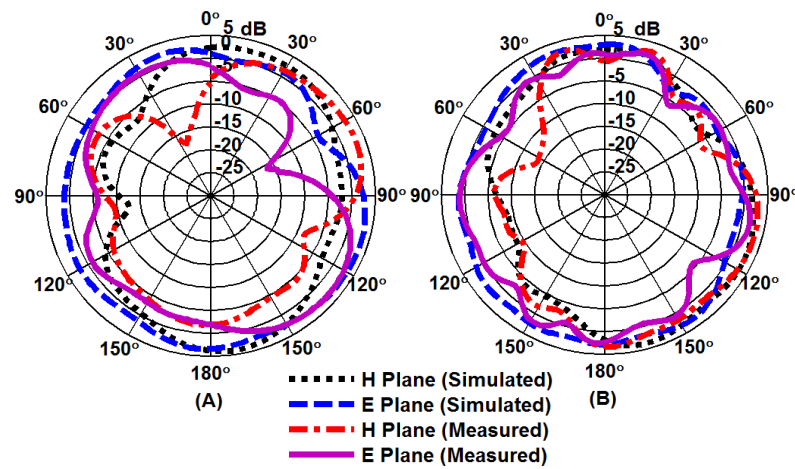


Figure 3.14 Simulated and Measured Radiation Patterns for PIN Diodes ‘OFF’ State at (A) 3.42 GHz and (B) 8.02 GHz

E plane (yz plane) and H plane (xz plane) radiation patterns have been plotted in Figure 3.14 at 3.42 GHz and 8.02 GHz. Whereas E plane (yz plane) and H plane (xz plane) radiation patterns have been plotted in Figure 3.15 at 2.21, 4.85, 8.02 and 10.19 GHz. It can be inferred from comparison that simulated and measured results agree with one another. Nonideal PIN diode behaviour, fabrication and testing equipment imperfections can be deemed responsible for slight disagreements between simulated and measured results. Simulated and measured radiation efficiency and peak gain values for diodes ‘OFF’ and ‘ON’ states at different resonant frequencies are given in Table 3.3. Peak gains have been evaluated in the E plane. It can be noticed that although the radiation pattern at 8.02 GHz attains the same plot in diodes ‘OFF’ and ‘ON’ states however the value of peak gain in ‘OFF’ state is higher than the value of peak gain at 8.02 GHz in the ‘ON’ state. This decrease in the peak gain value at 8.02 GHz can be attributed to integration of active devices (PIN diodes) in the antenna structure.

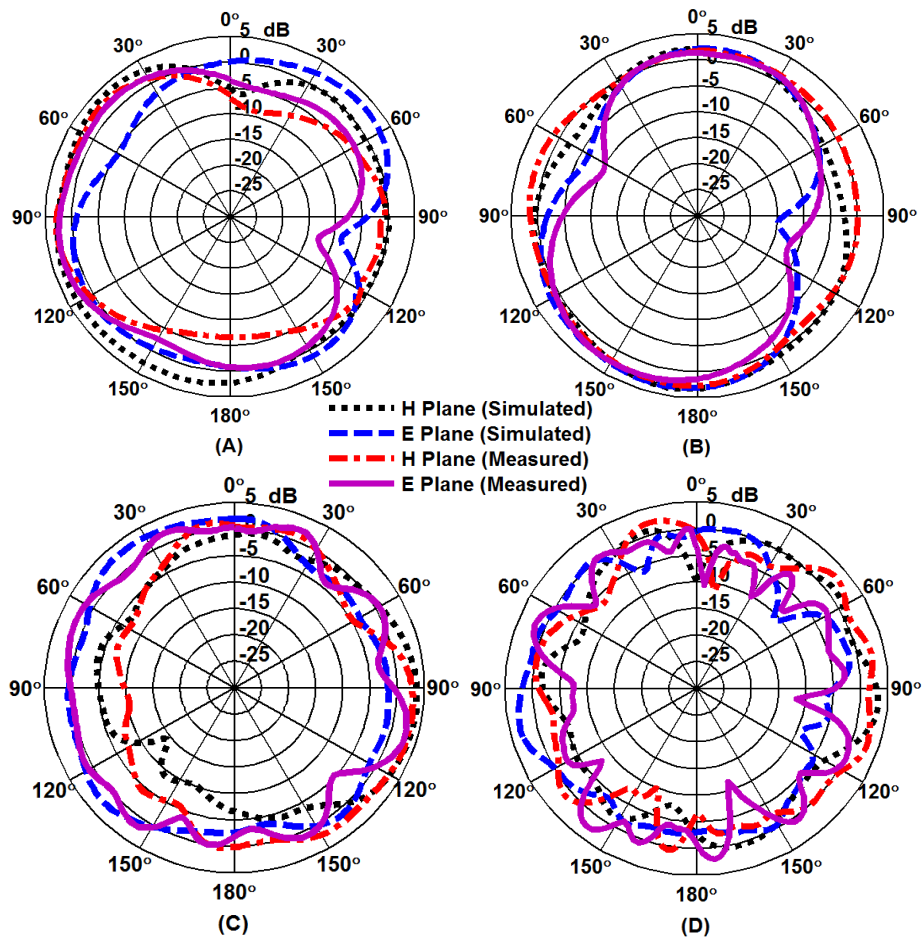


Figure 3.15 Simulated and Measured Radiation Patterns for PIN Diodes ‘ON’ State at

(A) 2.21 GHz (B) 4.85 GHz (C) 8.02 GHz and (D) 10.19 GHz

Table 3.3 Peak Gain (dBi) and Radiation Efficiency (%) Results

Diodes State	Freq (GHz)	Simulated Results		Measured Results	
		Peak Gain (dBi)	Radiation Efficiency (%)	Peak Gain (dBi)	Radiation Efficiency (%)
OFF	3.42	4.09	88.03	3.03	82.48
OFF	8.02	3.82	86.67	3.37	81.31
ON	2.21	3.53	89.42	3.06	83.27
ON	4.85	3.49	85.56	2.81	78.64
ON	8.02	3.78	85.14	3.26	77.39
ON	10.19	3.32	84.26	2.92	78.48

The highest measured radiation efficiency of 82.48 % is recorded at 3.42 GHz in PIN diodes ‘OFF’ state whereas highest measured radiation efficiency of 83.27 % is recorded at 2.21 GHz in PIN diodes ‘ON’ state.

3.3.3 Comparison with Related Literature:

A comparison of proposed multi-reconfigurable antenna design with related literature is presented in Table 3.4. The advantages of proposed antenna design can be assessed from this comparison. It can be noticed from literature comparison that the proposed design is unique in offering frequency and bandwidth switching capability not only concerning the 4G and 5G communication frequencies but also the X band frequency.

Table 3.4 Related Literature Comparison

Ref	Antenna Shape/ Targeted Parameter	Antenna Size (mm ²)/ Switching Elements	Operating Frequency Bands	Biasing Network	Peak Gain
[70]	Octagon/ Polarization	50.8×50.8/ 4 MEMS Switches	3.8 GHz	Microstrip lines and radial stubs	4.9 dBi
[71]	Dual Side Vivaldi/ Frequency	30×30/ Varactor Diode	6.16 – 6.6 GHz	External Biasing Tee	6.77 dBi
[72]	Annular Slot/ Frequency, Radiation Pattern	50×50/ 4 PIN Diodes	5.2, 5.8 & 6.4 GHz	Microstrip radial stubs	-
[73]	Square Ring/ Frequency, Polarization	60×65/ 2 PIN Diodes	2.4, 3.4 & 4.18 GHz	RF Chokes	4.01, 3.65 & 3.07 dBi
[74]	Planar Inverted F/ Frequency	42.5×80/ 3 PIN Diodes	1.8, 2.1, 2.4, 3.5, 3.7 & 5.8 GHz	RLC Circuit	3.34, 2.8, 5.16, 3.95, 5.05 & 6.98 dBi

[76]	Slotted Rectangle/ Bandwidth	25×50/ 2 PIN Diodes	2.4 – 5.5 GHz	RLC Circuit	-
[78]	Ring Slot Inspired/ Frequency, Bandwidth	60×80/ 2 PIN Diodes & 2 Varactor Diodes	1.35 – 6.2 GHz, 2.55 – 3.2 GHz	RF Chokes	5.12 dBi
This Work	Circular Loop Inspired/ Frequency, Bandwidth	50×55/ 2 PIN Diodes	2.21, 3.42, 4.85, 8.02, 10.19 GHz	RF Chokes	3.53, 4.09, 3.49, 3.82 & 3.32 dBi

3.4 Summary:

A smart and intelligent multi-reconfigurable antenna design is proposed in this chapter. The antenna is capable of offering not only frequency switching but also offers bandwidth switching capability. PIN diodes have been incorporated in the antenna design to execute the switching operation. The antenna results indicate that PIN diodes can efficiently control the operating frequency and bandwidth of a microstrip patch antenna. Switching operation can be implemented to selected desired operational bands as and when required. Frequency switching capability of antenna is demonstrated by operating the antenna in diodes ‘ON’ state in a tri band mode (at 2.21, 4.85 and 10.19 GHz) and then by operating the antenna in diodes ‘OFF’ state in dual band mode (at 3.42 and 8.02 GHz). The 2.21 GHz band present in diodes ‘ON’ state gets suppressed in the diodes ‘OFF’ state whereas the 4.85 GHz band present in diodes ‘ON’ state shifts to 3.42 GHz in the diodes ‘OFF’ state. Bandwidth switching capability of antenna is demonstrated by operating the antenna in diodes ‘ON’ state in a wideband from 7.54 GHz to 12 GHz and then by operating the antenna in diodes ‘OFF’ state in a narrowband from 7.71 GHz to 8.48 GHz. The proposed antenna design was fabricated and tested. Measured results validate the antenna design.

The proposed antenna design can be used in 4G and 5G communication devices such as devices used in 4G Advanced Wireless Services (AWS from 2180 to 2200 MHz [87]), WiMAX applications (3400 to 3600 MHz [88]), 5G New Radio service bands like n48 (3550 to 3700 MHz [22]) and n78 (3300 to 3800 MHz [22]), licensed 5G bands in China (3300 to 3600 MHz, 4800 to 5000 MHz [21]), licensed 5G bands in Europe (3400 to 3800 MHz [21]) and X band (8 to 12 GHz [89]) satellite services (fixed and mobile). The antenna design offers a unique, smart, and intelligently futuristic approach of multi-reconfigurability that allows it to be deployed in 4G devices, 5G devices, 4G/5G devices as well as devices utilizing both terrestrial and satellite communication services.

CHAPTER 04

ANTENNA DESIGN 2: A QUADBAND MIMO ANTENNA BASED ON A MULTI SLOTTED STRUCTURE

4.1 Introduction:

5G services in their initial deployment phase will be provided in a non-standalone configuration and will share operating bands with the already deployed 4G networks [90]. Deployment of Multiple Input Multiple Output (MIMO) antenna technology for providing 4G and 5G services can result in significant improvement of channel capacity as well as spectrum utilization without any increase in the transmission bandwidth and power. Many antenna designs exploiting the MIMO technology have been proposed in literature [91 – 98]. These proposed antenna designs target a variety of operating frequency bands. A MIMO antenna resonating at 0.75 GHz and 1.9 GHz has been presented in [91]. A MIMO antenna with a relatively larger size of $33.5 \times 22 \times 5.4 \text{ mm}^3$, based on an inverted F shape design structure is presented in [92]. A MIMO antenna consisting of four elements and operating at 2.4 GHz and 5.5 GHz is reported in [94]. [95] proposes another MIMO antenna structure consisting of two elements and resonating at 7.2 GHz and 8.6 GHz, the proposed structure however suffers from low isolation.

A key challenge in designing MIMO antenna structures is to mitigate the mutual coupling, a parameter which signifies the extent of electromagnetic contact between multiple antenna elements [99]. Generally, if distance between multiple antenna elements is small then the electric field radiated out of one antenna element can alter the current distribution of other antenna elements [100]. Many different solutions have

been reported in literature for reduction of mutual coupling between different elements of a MIMO antenna. Some notable solutions include use of electromagnetic band gap (EBG) structures [101] [102], artificial metamaterials [103], parasitic branching [104] and neutralization lines [105] [106]. Literature also reports structures termed as ‘decouplers’, with various different shapes, slits, and slots, which have been incorporated in MIMO antenna designs to reduce mutual coupling [107] [108]. MIMO antenna design for the sub 6 GHz 5G band is an interesting research phenomenon today as this band offers huge integration capability with the already existing 4G communication technology systems. At the same time design of MIMO antennas with compact structures and low mutual coupling is a daunting endeavour. MIMO antennas with increased isolation and low mutual coupling, operating on multiple frequency bands are in great demand nowadays.

In this chapter a smart two element MIMO antenna based on a multi slotted structure is proposed. The designed antenna is able to resonate at four different frequency bands with reduced mutual coupling and compact size. A simple decoupler structure has been incorporated in the antenna design to improve the isolation performance. Subsequent sections of the chapter highlight detailed development of antenna design, results and analysis of significant parameters including MIMO antenna performance parameters.

4.2 Detailed Design Development of Proposed Antenna Structure:

Development of proposed antenna structure began with design of a single element antenna. Once successfully realized, the single element antenna was then transformed into proposed two element MIMO antenna design. A simple decoupler structure has also been incorporated in final two element MIMO antenna design to enhance the isolation performance.

4.2.1 Development of Single Element Antenna:

Figure 4.1 represents complete layout of the developed single element antenna structure. Total size of the antenna is $18.5 \times 28 \text{ mm}^2$, which corresponding to the lowest operating frequency of 2.5 GHz comes out to be $0.154 \lambda_o \times 0.233 \lambda_o$. The single element antenna structure is conceived using FR4 epoxy substrate having a relative permittivity value of 4.4 and height of 1.6 mm. The formulation of single element antenna began with a simple rectangular patch without any slots. Antenna design evolution led to incorporation of a multi-slotted patch structure on the antenna top side along with introduction of a partial ground structure on the antenna bottom side.

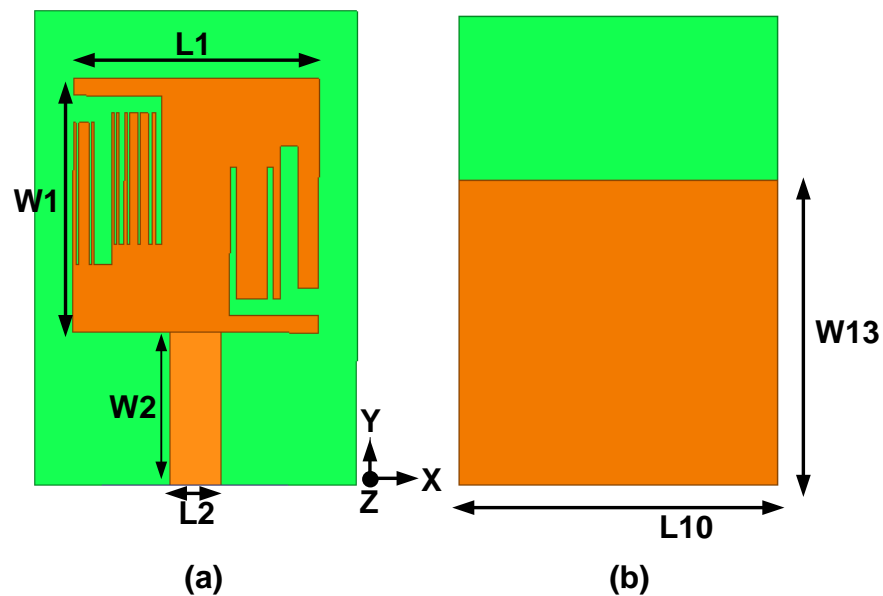


Figure 4.1 Complete Layout of Single Element Antenna (a) Top (b) Bottom

The incorporated multi-slotted structure enables the single element antenna to resonate at multiple frequencies targeting the 4G and 5G communication technologies. The multi-slotted structure consists of L shaped and I shaped slots. The slots are smartly placed on opposite edges of the initial rectangular patch structure. The introduced slots allow the antenna to not only resonate at multiple frequencies but also enable the

antenna structure to achieve compactness [109 – 111]. Further optimization and tuning of slot dimensions led to gain and bandwidth improvement along with miniaturization and multiband resonance [112]. The complete multi-slotted patch structure in detail is represented by Figure 4.2. Dimensions involved in Figures 4.1 and 4.2 are given by Table 4.1.

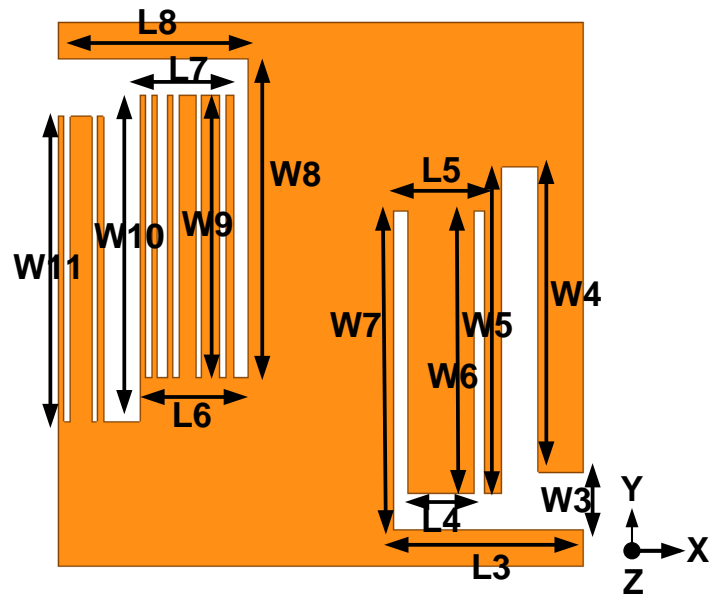


Figure 4.2 Detailed View of Multi-Slotted Rectangular Patch Loaded with L and I Shaped Slots

Table 4.1 Dimensions Involved in Figures 4.1 and 4.2

Dimension	Value (mm)	Dimension	Value (mm)
Figure 4.1			
<i>L1</i>	14.5	<i>W1</i>	15
<i>L2</i>	3	<i>W2</i>	9
<i>L10</i>	18.5	<i>W13</i>	18.25
Figure 4.1			
<i>L3</i>	5.25	<i>W5</i>	9
<i>L4</i>	1.8375	<i>W6</i>	7.8
<i>L5</i>	2.5375	<i>W7</i>	8.8
<i>L6</i>	2.8375	<i>W8</i>	8.8
<i>L7</i>	2.6	<i>W9</i>	7.8
<i>L8</i>	5.25	<i>W10</i>	9
<i>W3</i>	1.6	<i>W11</i>	8.4
<i>W4</i>	8.4		

Analysis of Figure 4.2 reveals that a total of eight I-shaped slots together with a single L-shaped slot exist on the dense slot side (the left side) of rectangular patch structure. The eight I-shaped slots on the dense slot side have different dimensions. While on the sparse slot side (the right side) a total of two I-shaped slots together with a single L-shaped slot are present. The two I-shaped slots on the sparse slot side possess different dimensions.

Considering Figure 4.2, five different width measurements (towards the x-axis) for L-shaped and I-shaped slots can be noticed. The values for these width measurements have been taken as 0.1625, 0.2, 0.3, 0.4, and 1 mm. Also, the dense and sparse slot sides have been placed in an upside-down position with respect to each other, on the opposite sides of the initial rectangular patch structure, in order to achieve compactness in antenna size [113]. A comprehensive design evolution process, based upon the targeted performance parameters and consisting of many iterations, helped in selection of the number, size and respective locations of L- and I-shaped slots present in the final single element antenna structure. Figure 4.3 highlights the significant design evolution steps. The corresponding reflection coefficient results of different design evolution steps are represented in Figure 4.4. The design evolution process started with development of a simple rectangular based patch antenna resonating at 4.3 GHz, with the help of already founded empirical formulas [14]. Two L-shaped slots were then incorporated in the rectangular patch, in an upside-down position and on opposite edges (Design A in Figure 4.3), in order to achieve multiband operation with compact size [113]. As it can be seen in Figure 4.4 that Design A was able to operate at 3.4 GHz and 4.3 GHz. To introduce further multiband operation, an I-shaped slot was inserted individually with both L-shaped slots (Design B in Figure 4.3). After incorporation of I-shaped slots, Design B was able to operate at 2.7, 4.1, and 4.6 GHz as indicated by

Figure 4.4. The simple rectangular patch structure produced a single operating frequency, the other two resonant frequencies for Design B can be attributed to the L- and I-shaped slot incorporation.

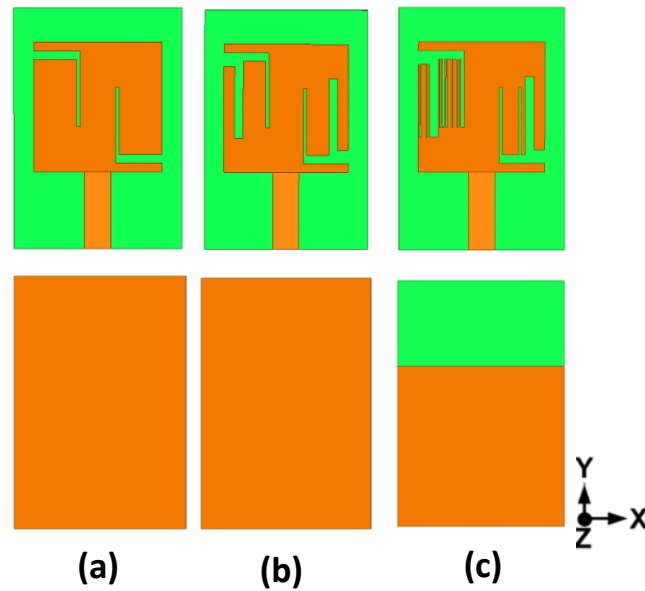


Figure 4.3 Design Evolution Steps

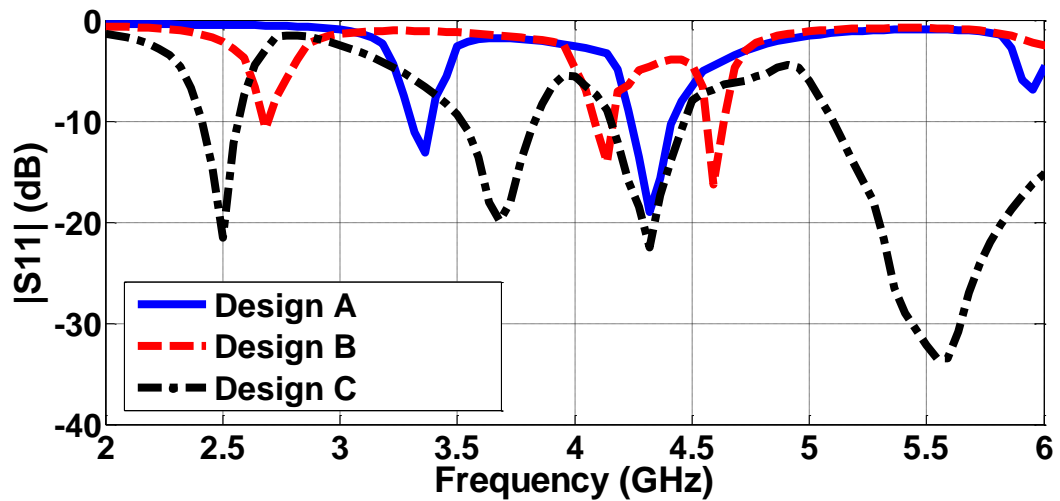


Figure 4.4 Magnitude Reflection Coefficient Results for Figure 4.3

Next stage in the evolution process was to tune the resonant frequencies to desired levels as well as introduce another resonance at 5.5 GHz. To achieve this objective,

multiple L- and I-shaped slots with different number, size and placement positions were merged and evaluated. A partial rectangular shaped ground was also introduced on the antenna bottom side to improve the operating bandwidth [114]. In order to properly tune the antenna to desired resonant frequencies the number, size and respective locations of the involved slots were continuously altered in an iterative process. Finally, after many iterations Design C as highlighted in Figure 4.3 was achieved. Design C as represented in Figure 4.4 was able to successfully operate at 2.5, 3.7, 4.3, and 5.5 GHz.

4.2.2 Development of Two Element MIMO Antenna:

The single element antenna design was finalized with attainment of quadband frequency operation. The developed single element antenna design was then converted into a two element MIMO antenna. The two antenna elements involved in creating the MIMO antenna design were put in an upside-down position with respect to each other in order to improve the isolation performance [115]. The two element MIMO antenna design is depicted in Figure 4.5. The dimensions involved in Figure 4.5 are given by Table 4.2.

On the top side, two antenna elements are separated by a distance of 8 mm. 50 Ω microstrip line feed structure is used to feed the MIMO antenna. The two element MIMO antenna design was conceived using FR4 substrate with a height of 1.6 mm. A simple decoupler, comprising of three rectangle shaped strips having a width of 1 mm each, has been introduced on the bottom side of MIMO antenna design. The simple decoupler structure serves to enhance the isolation performance of MIMO antenna by reducing mutual coupling between the two antenna elements. A strong decoupling method is offered by the three rectangular strips as they are able to provide dummy load and reactive loading to the MIMO antenna design.

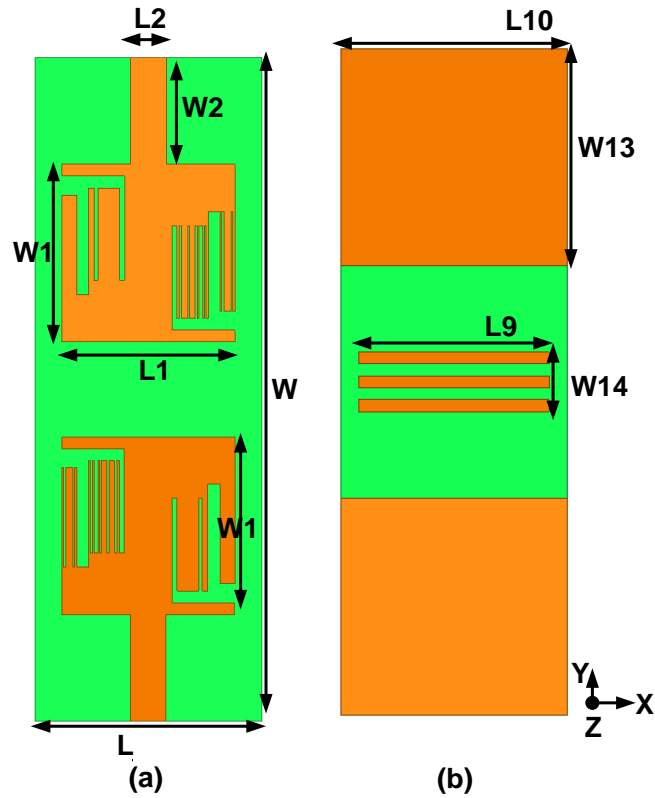


Figure 4.5 Two Element MIMO Antenna Design (a) Top (b) Bottom

Table 4.2 Dimensions Involved in Figure 4.5

Dimension	Value (<i>mm</i>)
L	18.5
W	56
$L9$	16
$W14$	5

4.2.3 Investigation of Surface Current Distribution for Two Element MIMO

Antenna:

In order to understand and interpret the radiation as well as decoupling mechanism of the proposed two element MIMO antenna, surface current distribution has been plotted in Figure 4.6. Figure 4.6 has been divided into four sub-parts, where each sub-part

represents the surface current distribution plot corresponding to a specific operating frequency. The contribution of decoupler structure in reduction of mutual coupling between two antenna elements is clearly highlighted by the current distribution plots. For all operating frequency bands, a mutual coupling value of less than -20 dB has been attained due to reactive loading. Hence it can be asserted that dummy loads serve as band stop filters. From Figure 4.6 it can be seen that current is concentrated towards the righthand side port (excited port) of MIMO antenna. The three strips of decoupler structure enhance the isolation performance of MIMO antenna by reducing coupling current of nonexcited antenna element thereby limiting current propagation and decreasing the mutual coupling.

Contribution of multi-slotted structure on antenna top side along with partial ground plane on antenna bottom side in generation of all four operating frequencies can be witnessed effectively in Figure 4.6. Thus Figure 4.6 can be used to conveniently interpret the radiation mechanism of proposed two element MIMO antenna design. As represented in Figure 4.6 (a) the 2.5 GHz operating frequency is generated primarily by the central area of rectangular patch together with a major section of the sparse slot side. Meanwhile the 3.7 GHz operating frequency is generated majorly by the dense slot side of the rectangular patch along with some contribution by outer edges of the sparse slot side as indicated by Figure 4.6 (b). Resonant frequency of 4.3 GHz is generated due to contribution from both sparse and dense slot sides as highlighted by Figure 4.6 (c). Lastly the operating frequency of 5.5 GHz is generated by significant portion of two L shaped slots present in the rectangular patch structure as seen in Figure 4.6 (d). Contribution of partial ground structure, on the MIMO antenna bottom side, in bandwidth improvement and impedance matching at all operating frequencies can also be assessed from Figure 4.6.

4.3 Important Antenna Results and Analysis:

The proposed two element MIMO antenna design was manufactured and tested for several antenna performance parameters. The simulated and measured antenna results along with their analysis are presented in the subsequent sub-sections.

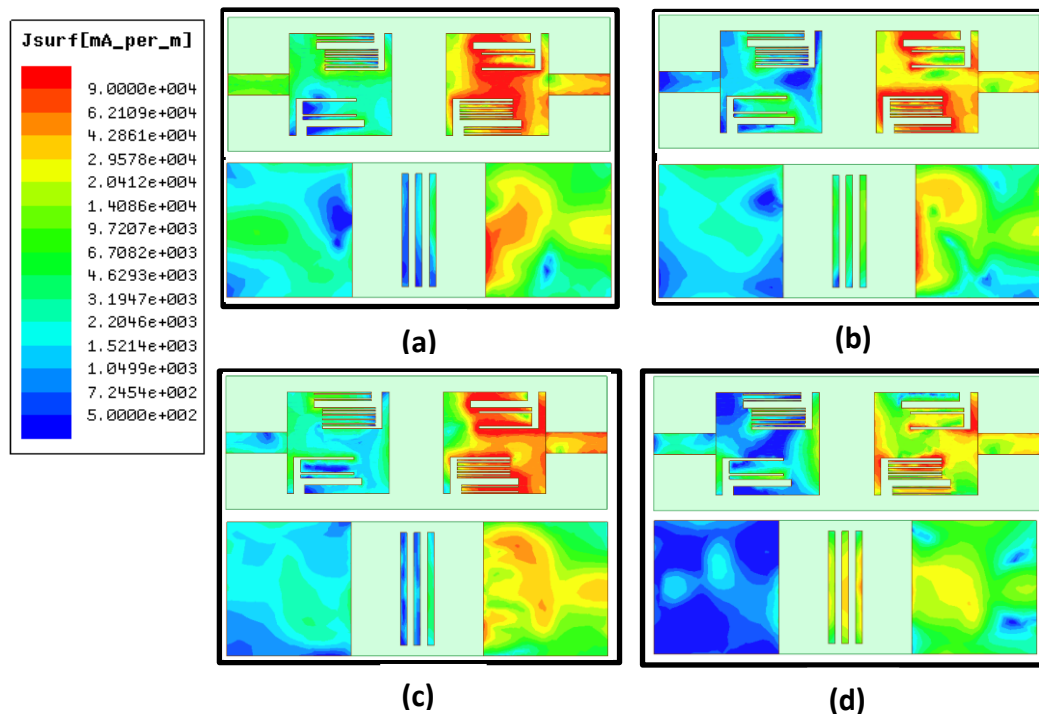


Figure 4.6 Surface Current Distribution for MIMO Antenna (Top and Bottom) (a) 2.5 GHz (b) 3.7 GHz (c) 4.3 GHz (d) 5.5 GHz

4.3.1 Reflection Coefficient Results:

Figure 4.7 illustrates the simulated and measured magnitude reflection coefficient ($|S_{11}|$) results for the proposed two element MIMO antenna design. The simulated results shown in Figure 4.7 include results with as well as without the decoupler structure. Agilent N5245B PNA-X vector network analyzer was used to measure the magnitude reflection coefficient ($|S_{11}|$) results.

Due to symmetry of antenna elements, results were measured at port 1 of MIMO antenna while port 2 was terminated with a $50\ \Omega$ load. The simulated and measured results agree well with each other. Slight disagreements between the simulated and measured results can be associated with fabrication imperfections. From Figure 4.7, it is evident the proposed MIMO antenna is able to resonate at four frequency bands. From the measured results the four operating frequency bands, where magnitude reflection coefficient ($|S_{11}|$) has a value of less than $-10\ \text{dB}$, come out to be 2.43 to 2.57 GHz, 3.37 to 3.8 GHz, 4.25 to 4.5 GHz, and 5.09 to 6.25 GHz. Also, from Figure 4.7 the measured magnitude reflection coefficient values corresponding to centre frequency of each resonating band can be recorded as $-13.64\ \text{dB}$ at 2.5 GHz, $-15.24\ \text{dB}$ at 3.7 GHz, $-16.35\ \text{dB}$ at 4.3 GHz, and $-25.43\ \text{dB}$ at 5.5 GHz.

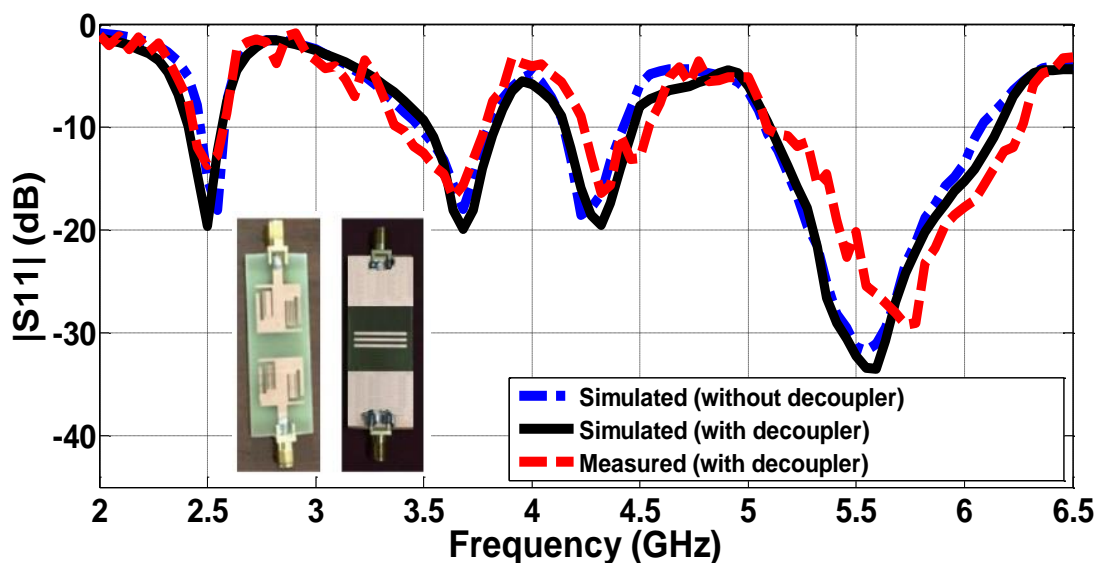


Figure 4.7 Magnitude Reflection Coefficient ($|S_{11}|$ (dB)) Results of Proposed MIMO Antenna

4.3.2 Mutual Coupling Results:

Figure 4.8 highlights the simulated and measured results for mutual coupling between the MIMO antenna elements. The simulated results in Figure 4.8 have been plotted with as well as without the decoupler structure. The role of decoupler structure in suppressing mutual coupling and improving the isolation performance of proposed MIMO antenna is evidently depicted by Figure 4.8. With the incorporation of decoupler structure in MIMO antenna design, $|S_{21}|$ remains below -20 dB for all operating frequency bands. The measured $|S_{21}|$ values at central operating frequencies of all four resonant bands come out to be -28.98 dB at 2.5 GHz, -26.33 dB at 3.7 GHz, -22.44 dB at 4.3 GHz, and -27.82 dB at 5.5 GHz. A good concurrence between simulated and measured results validates the role of reactive loading on MIMO antenna bottom side to improve the overall isolation performance. It can also be inferred from Figure 4.8 that positioning of single antenna elements with respect to each other together with the decoupler structure allow the proposed MIMO antenna to resonate with reduced mutual coupling.

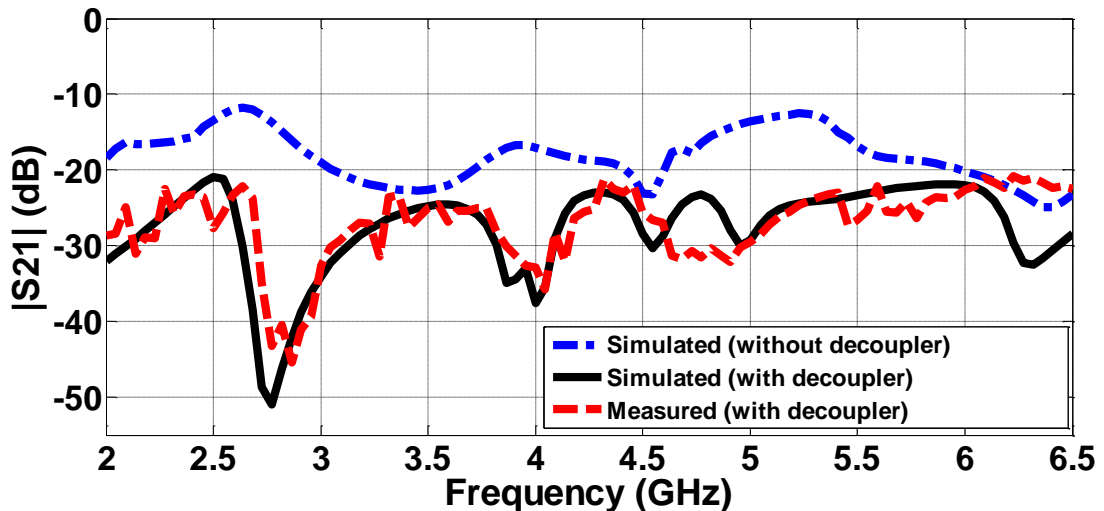


Figure 4.8 Mutual Coupling ($|S_{21}|$ (dB)) Results of Proposed MIMO Antenna

4.3.3 Radiation Characteristics:

Simulated radiation patterns of proposed MIMO antenna design are represented by Figure 4.9 whereas the measured radiation patterns of proposed MIMO antenna design are given by Figure 4.10. Both Figures 4.9 and 4.10 have been divided into four subparts where each subpart corresponds to a particular operating frequency. An in-depth inspection of the radiation pattern plots reveals that the H plane pattern at all four resonant frequencies (2.5, 3.7, 4.3, and 5.5 GHz) is omnidirectional in nature, the E plane pattern on the other hand, has a shape resembling that of a dipole pattern without any nulls. The nature and shape of radiation patterns render the proposed MIMO antenna suitable for use in modern and future practical communication applications. An overall agreement between the simulated and measured radiation patterns can also be ascertained from Figures 4.9 and 4.10. Nonetheless few differences between the results can be attributed to measurement apparatus limitations and fabrication defects.

4.3.4 Peak Gain and Radiation Efficiency Results:

The simulated and measured peak gain values for proposed MIMO antenna are illustrated by Figure 4.11. The simulated values have been plotted for two cases, without the decoupler structure and with the decoupler structure. It can be observed from the figure that peak gain values with decoupler structure are greater than the peak gain values without the decoupler structure. The simulated peak gain values (with the decoupler structure present) at the operating frequencies of 2.5, 3.7, 4.3, and 5.5 GHz come out to be 4.13, 3.38, 3.34, and 2.85 *dBi* respectively. It can also be assessed by observing Figure 4.11 that the measured peak gain for all operating frequencies remains greater than 2.5 *dBi*. The measured peak gain at the operating frequencies of 2.5, 3.7, 4.3, and 5.5 GHz comes out to be 3.49, 2.97, 2.93, and 2.54 *dBi* respectively.

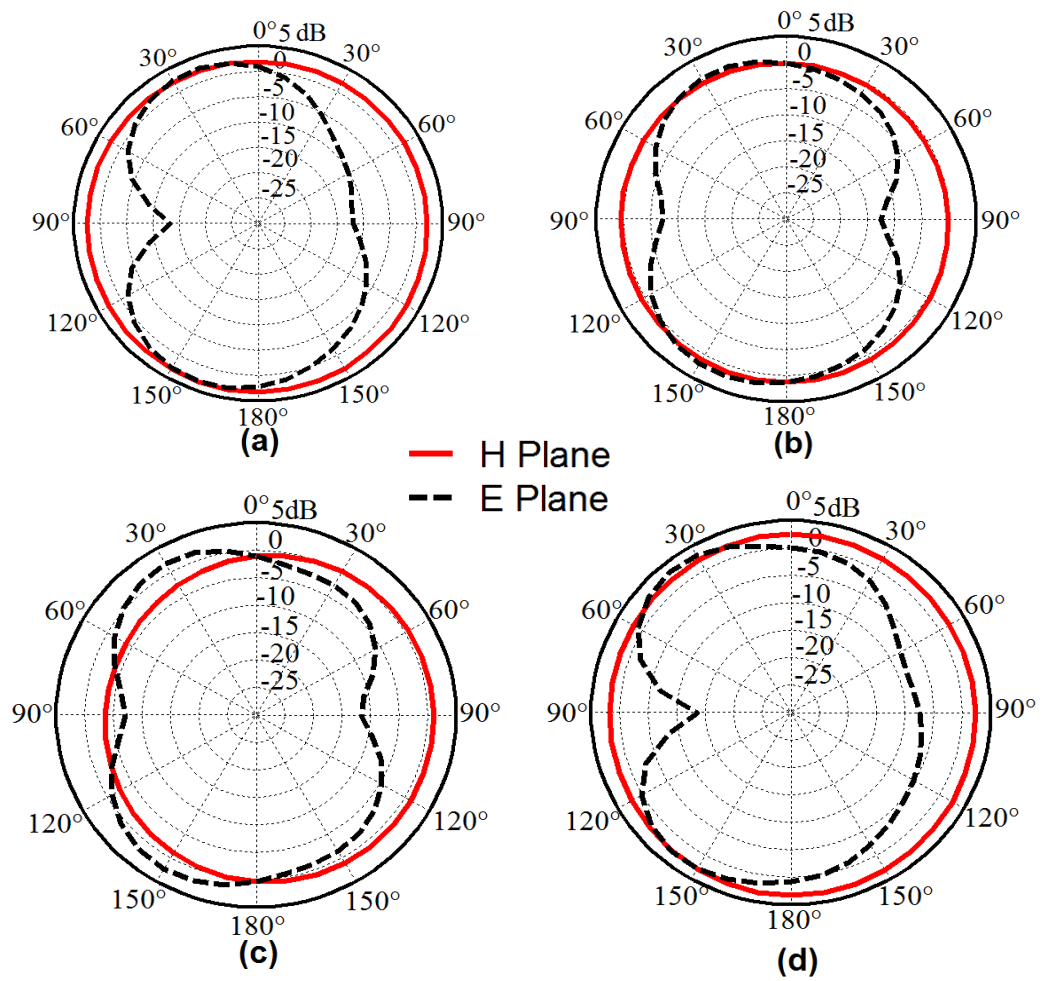


Figure 4.9 Radiation Pattern Plots (Simulated) of Proposed MIMO Antenna at (a) 2.5 GHz (b) 3.7 GHz (c) 4.3 GHz (d) 5.5 GHz

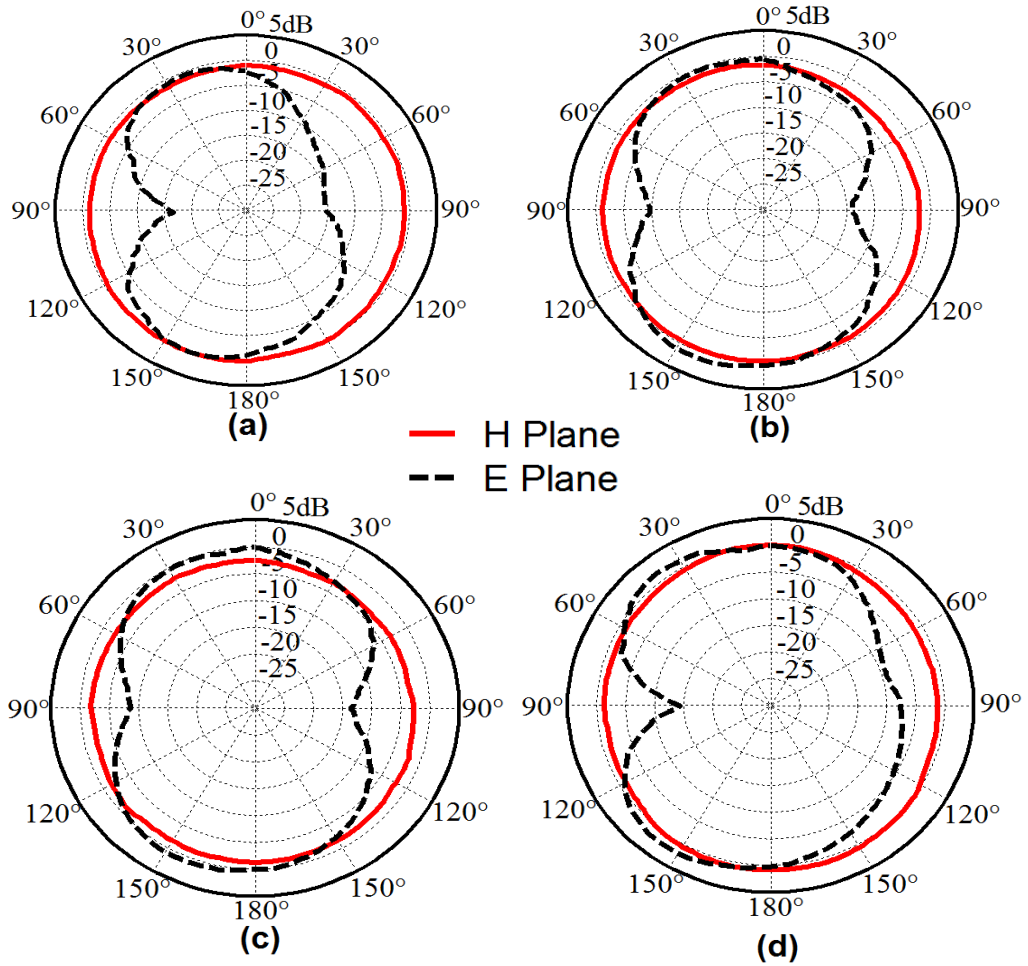


Figure 4.10 Radiation Pattern Plots (Measured) of Proposed MIMO Antenna at (a)

2.5 GHz (b) 3.7 GHz (c) 4.3 GHz (d) 5.5 GHz

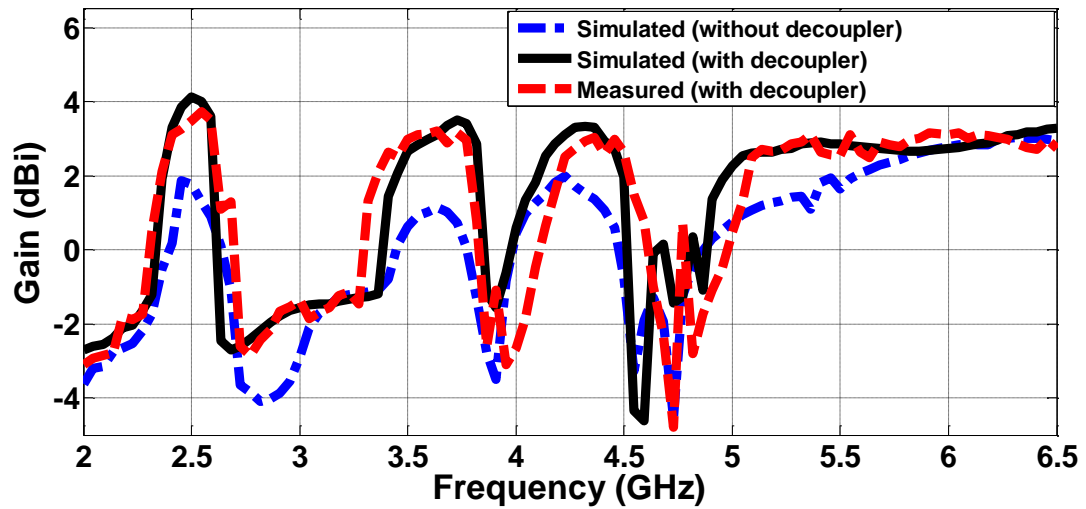


Figure 4.11 Simulated (with and without decoupler) and Measured Peak Gain Results

Figure 4.12 illustrates the simulated and measured radiation efficiency results for the proposed MIMO antenna design. The simulated results have been plotted for two cases, with the decoupler structure and without the decoupler structure. Again, it can be evidently observed from Figure 4.12 that the radiation efficiency values with the decoupler structure present are higher than the radiation efficiency values without the decoupler structure. Simulated (with the decoupler structure present) radiation efficiency values at the operating frequencies of 2.5, 3.7, 4.3, and 5.5 GHz come out to be 90.8%, 87.5%, 86.8%, and 85.4% respectively. It can also be ascertained from inspecting Figure 4.12 that the measured radiation efficiency remains above 79.5% for all operating frequencies. Slight differences between the measured and simulated radiation efficiency results can be effectively ascribed to SMA connector soldering and fabrication tolerances. The measured radiation efficiency values at operating

frequencies of 2.5, 3.7, 4.3, and 5.5 GHz come out to be 87.3%, 82.5%, 81.4%, and 79.7% respectively.

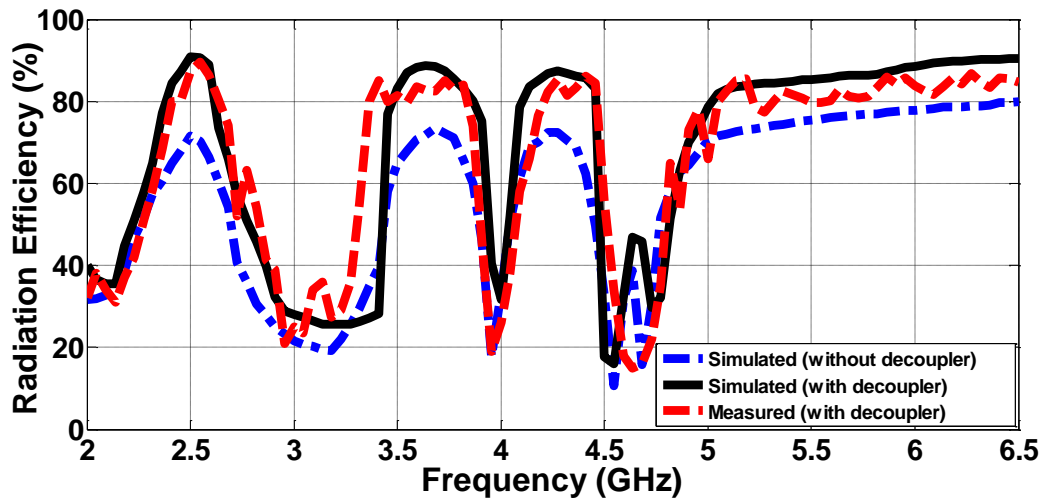


Figure 4.12 Simulated (with and without decoupler) and Measured Radiation Efficiency Results

4.4 MIMO Antenna Performance Results:

Certain parameters like the envelope correlation coefficient (ECC), channel capacity loss (CCL), total active reflection coefficient (TARC) and diversity gain (DG) are used to describe and assess the performance and behaviour of a MIMO antenna. These parameters have been evaluated for the proposed two element MIMO antenna design and are presented in the subsequent sections.

4.4.1 Envelope Correlation Coefficient:

Envelope correlation coefficient (ECC) is a significant parameter that is used to assess the cross-correlation performance and channel capacity of a MIMO system. Ideally the value of ECC must be zero. Nevertheless, for practical MIMO systems a value of ECC less than 0.5 is considered acceptable as an optimum performance measure [116]. ECC for the proposed MIMO antenna design can be calculated using far field radiation results through the following equation [117]:

$$ECC = \frac{|\iint E_{\theta i} \cdot E_{\theta j}^* + E_{\phi i} \cdot E_{\phi j}^* d\Omega|^2}{(\iint E_{\theta i} \cdot E_{\theta i}^* + E_{\phi i} \cdot E_{\phi i}^* d\Omega)(\iint E_{\theta j} \cdot E_{\theta j}^* + E_{\phi j} \cdot E_{\phi j}^* d\Omega)}$$

where ‘*i*’ and ‘*j*’ represent port numbers and *E* represents the electric field vector.

Simulated and measured ECC results are represented by Figure 4.13. The simulated results have been plotted for both cases, without the decoupler structure and with the decoupler structure. It can be conveniently observed from Figure 4.13 that ECC remains below 0.05 for all resonant bands, thereby authenticating optimum MIMO antenna performance with respect to the correlation coefficients.

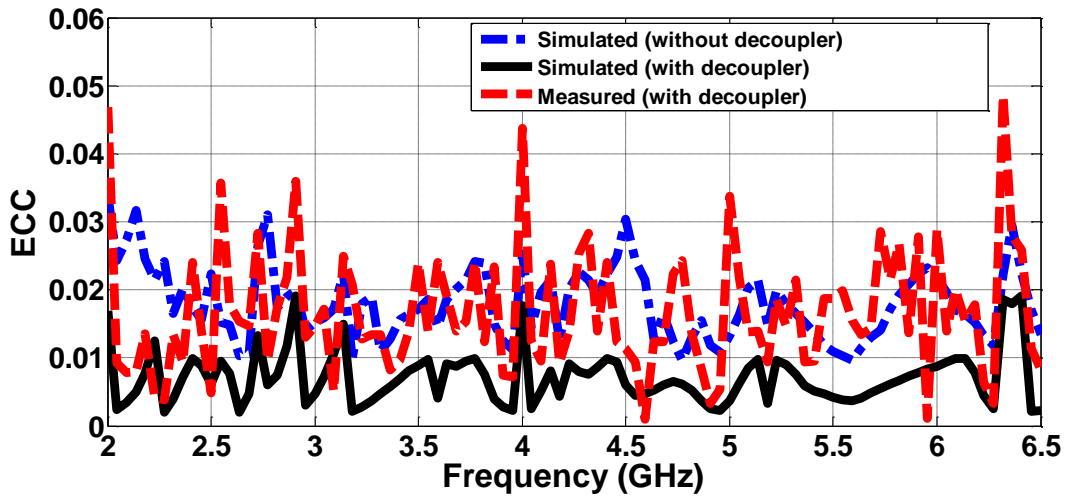


Figure 4.13 Simulated (with and without decoupler) and Measured ECC Results

4.4.2 Channel Capacity Loss:

Channel capacity loss (CCL) is another significant parameter that is used to depict the performance of a MIMO antenna. CCL allows the expression of lost transmission bits for high data rate transmission scenarios. For the proposed two element MIMO antenna design, CCL has been computed numerically using equations given in [118]. The simulated and measured CCL results are represented in Figure 4.14. The simulated results have been plotted for both cases, without the decoupler structure and with the decoupler structure. Inspection of Figure 4.14 highlights the fact that measured CCL

values remain below 0.4 bits/s/Hz for all resonant frequency bands, thereby validating an efficient MIMO antenna performance along with high throughput [118].

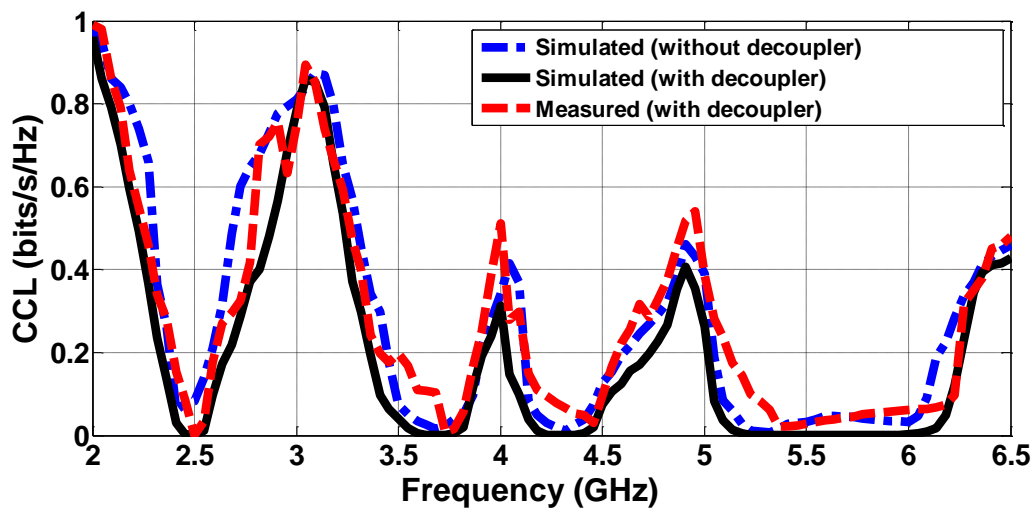


Figure 4.14 Simulated (with and without decoupler) and Measured CCL Results

4.4.3 Total Active Reflection Coefficient:

Total active reflection coefficient (TARC) represents the complete return loss of a MIMO antenna system. TARC is a notable parameter that is used to analyse the diversity performance of a MIMO antenna. TARC for the proposed two element MIMO antenna is determined using the computation mechanism given in [119]. The computation mechanism involves calculating square root of total reflected power to the total incident power. For an effective MIMO system, the value of TARC should be below 0 dB [119]. The simulated (with and without decoupler structure) and measured TARC results for the proposed two element MIMO antenna are represented in Figure 4.15. As indicated by Figure 4.15, the values of TARC remain less than -10 dB at all resonant frequency bands, hence validating an effective performance of the proposed MIMO antenna.

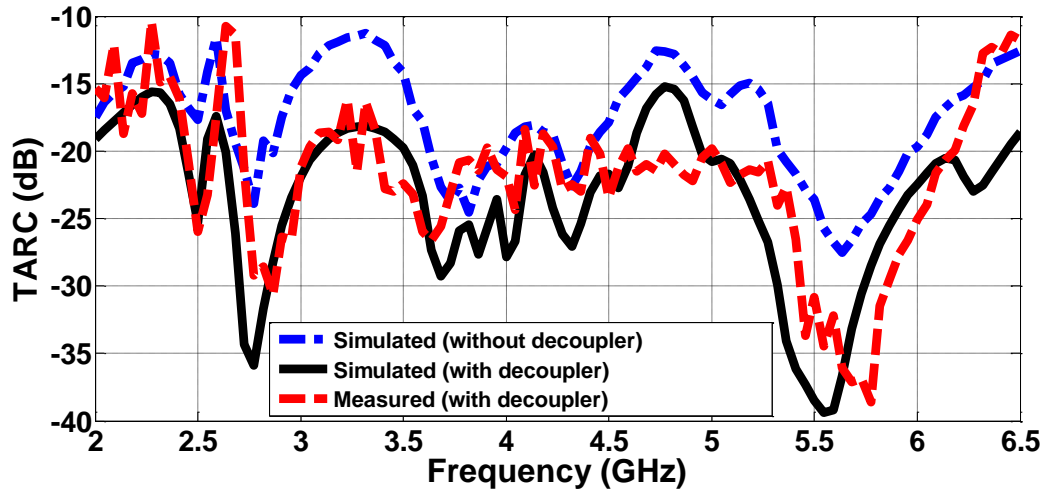


Figure 4.15 Simulated (with and without decoupler) and Measured TARC Results

4.4.4 Diversity Gain:

Diversity gain (DG) is another important parameter that is used to ascertain the diversity performance of a MIMO antenna. DG can be computed from the previously determined ECC values using the following equation [120]:

$$DG = 10 \times \sqrt{1 - |ECC|^2}$$

The simulated (with and without decoupler structure) and measured DG values have been plotted in Figure 4.16. It can be assessed that the DG values remain above 9.98 dB at all operating frequency bands representing an effective antenna performance.

From Figures 4.13 to 4.16 the significant role of decoupler structure in improving MIMO antenna performance can be evidently witnessed. Improved performance in ECC, CCL, TARC and DG plots for simulated results with decoupler structure is clearly indicated as compared to the simulated results without the decoupler structure.

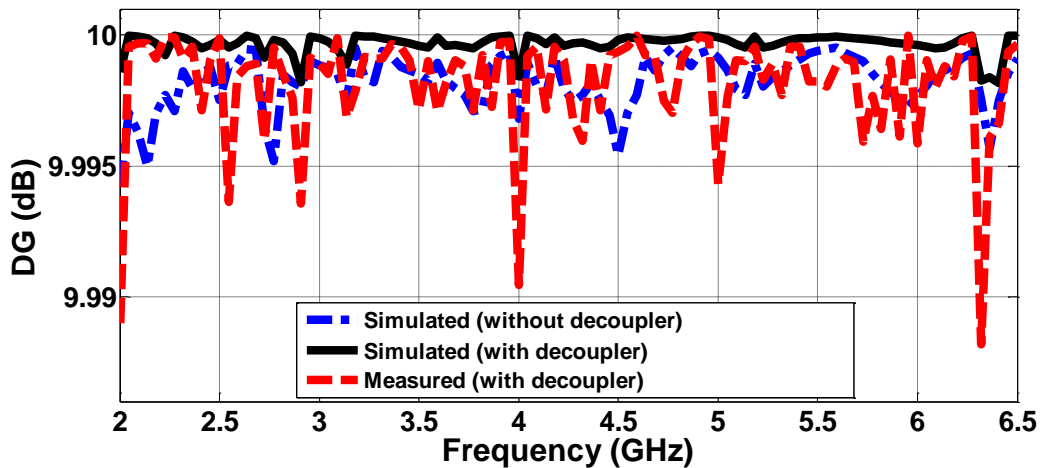


Figure 4.16 Simulated (with and without decoupler) and Measured DG Results

4.5 Comparison with Related Literature:

Comparison of the proposed two element MIMO antenna design with recent work presented in the literature is given in Table 4.3. The list of papers quoted in the table is not all inclusive but still provides a decent comparison. Number of MIMO antenna elements, resonant frequencies, size, isolation and far field ECC values have been recorded in the comparison table. It can be observed from the comparison presented in the table that many antennas are not compact in size and fail to resonate at the frequency bands targeted by the proposed two element MIMO antenna. On the other hand, antennas which are compact in size involve complex design structures and resonate at higher frequency bands. Some recent published work does not include ECC values computer using the far field parameters. It can, hence, be ascertained that the proposed MIMO antenna design is compact, effective, and has the capability to resonate at four different operating frequency bands, with a mutual coupling value of less than -20 dB and ECC value of less than 0.05 at all resonant frequencies.

Table 4.3 Comparison of Proposed MIMO Antenna with Related Literature

Ref	Number of Elements	Central Frequency of Operating Bands (GHz)	Antenna Size (mm ²)	Mutual Coupling (dB)	ECC (using far field parameters)
[91]	2	0.75 / 1.9	120 x 120	< -13	< 0.13
[92]	2	1.8/2.4/5.2	44 x 70	< -20	Not Given
[93]	2	2.4 / 5.2 / 5.8	50 x 26	< -20	Not Given
[94]	4	2.4 / 5.5	50 x 50	< -17.5	< 0.0576
[95]	2	7.2 / 8.6	17 x 42	< -13	Not Given
[96]	4	3.5	150 x 75	< -17	< 0.1
[97]	4	4.1 / 5.3	52 x 53	< -23	Not Given
[98]	4	3.4 /4.7 /5.4	150 x 75	< -17	< 0.1
This Work	2	2.5 / 3.7 / 4.3 / 5.5	18.5 x 56	< -20	< 0.05

4.6 Summary:

The design and analysis of a quadband two element MIMO antenna based on a multi-slotted structure has been presented in this chapter. The proposed MIMO antenna is able to operate at 2.5, 3.7, 4.3, and 5.5 GHz with a magnitude reflection coefficient ($|S_{11}|$) of less than -10 dB. The multi-slotted structure present at the antenna top side comprises of L and I shaped slots. In order to improve the MIMO antenna isolation performance a simple decoupler structure consisting of three rectangular strips has been incorporated on the antenna bottom side. The antenna is able to resonate at all four frequency bands with a mutual coupling ($|S_{21}|$) value of less than -20 dB. The simulated and measured results are in good concurrence with each other. Apart from conventional antenna performance parameters, certain other parameters were also

evaluated to ascertain the MIMO performance of proposed antenna design. It was noticed that ECC remains below 0.05 and TARC value remains lower than -10 dB at all resonant frequencies. The novelty of the proposed two element MIMO antenna is suggested by (i) incorporation of multi-slotted structure (consisting of L- and I-shaped slots) for attaining compact antenna size, multiband resonance, gain improvement and bandwidth enhancement, (ii) reduction of mutual coupling between antenna elements by introducing reactive loading on the antenna bottom side instead of using EBGs or metamaterial which would have resulted in additional structural loading and design complexities, (iii) MIMO antenna performance evaluation through parameters like ECC, CCL, TARC and DG, and (iv) comparison of proposed MIMO antenna design with recent literature to emphasise compact size, effective isolation and ECC results.

Radiation characteristics, efficiency and gain results of the proposed MIMO antenna authenticate the effective performance of proposed antenna design and render it appropriate for use in modern 4G and 5G communication applications. The proposed MIMO antenna due to its quadband nature, compact size and minimal structural loading is especially suitable for already present 4G applications and non-standalone 5G applications. The proposed two element MIMO antenna can find applications in current LTE networks operating at 2.5, 3.5, and 5.2 GHz [121]. The proposed MIMO antenna can also be deployed in WiMAX networks operating at 2.5, 3.5, and 5.8 GHz [122] as well as WLAN networks operating at 2.4, 3.6, 4.3, and 5.9 GHz [123, 124]. Moreover, the proposed MIMO antenna is an effective candidate for 5G New Radio n7 band operating from 2.5 to 2.57 GHz as well as the 5G New Radio n48 band operating from 3.55 to 3.7 GHz [121].

CHAPTER 05

ANTENNA DESIGN 3: COMPACT MMWAVE MULTIBAND

ANTENNA ARRAY

5.1 Introduction:

As discussed in chapter 1, the suggested frequency bands for 5G communication technology can be divided into two main categories, the sub 6 GHz band (focusing on frequencies below 6 GHz) and the mmWave band (from 24 GHz to 100 GHz) [21]. Although the initial targeted area for 5G communication technology deployment is the sub 6 GHz band, primarily being used to offer 5G services in the non-standalone mode, the future scenario will however change and mmWave band will be needed to offer 5G services, due to its importance and need. mmWave band can be referred to as the sweet spot for 5G communication services as a lot of capabilities and properties of this band are still widely unexplored. mmWave band has the capacity to provide higher data rates and throughput with relatively much smaller antenna sizes. As higher frequencies are dealt with by the mmWave band a key drawback can be the higher propagation loss [125]. Hence device components including antennas having higher efficiency and gains need to be designed for this particular band.

Microstrip patch antennas have been a popular choice for current and proposed communication system devices. These antennas with evolved architecture and design can also be employed for the proposed mmWave band based 5G communication applications. [126] suggests a mmWave antenna resonating at 28 GHz but the proposed design is relatively complex in nature. Another antenna operating at 37 GHz and 54 GHz has been proposed in [127]. A complex mmWave antenna array with a triple

layered design has been presented in [128]. The presented antenna is able to resonate at 45,67, and 76 GHz. [129] suggests a microstrip antenna with defected ground structure resonating at 28 GHz and 38 GHz.

Another array structure taking advantage of the proximity coupling feeding method and resonating at 28 GHz is presented in [130]. Whereas an array consisting of sixteen elements operating from 27.5 to 28.35 GHz is proposed in [131]. [132] proposes a wideband complex antenna array structure operating from 24.35 GHz to 31.13 GHz. A wideband antenna array resonating from 50 GHz to 67.8 GHz is also suggested by [133]. An antenna array design derived from a clover like structure and operating from 24 GHz to 28 GHz is proposed by [134]. Another array design resonating from 23 GHz to 29 GHz is suggested by [135] but again the design is structurally complex. [136] highlights the design of an array operating at 28 GHz and inspired by a shell shape design.

The present mmWave antenna designs generally target the initial frequencies of the mmWave band. Also, many of the existing or proposed design structures operate in a single or dual band configuration. Hence a mmWave antenna array resonating at multiple frequency bands appears as a prospective candidate for future 5G communication applications.

This chapter presents the design, results, and analysis of a simple mmWave antenna array structure that is able to resonate at four different frequency bands. The antenna array design is based on a multi-slotted structure. The proposed mmWave antenna array provides high gain values at all four operating frequencies. The mmWave antenna array is designed using plain slot structures to avoid any additional design complexities thereby keeping the proposed design very simple. The detailed antenna design, results

and analysis of the proposed antenna array are presented in the subsequent sections of this chapter.

5.2 Detailed Design of the Proposed Antenna Array:

The detailed design of the proposed antenna array is represented in Figure 5.1. As it can be observed from Figure 5.1 that the top side of proposed antenna array structure consists of eight multi-slotted rectangular elements, whereas on the bottom side a complete ground structure is present. The dimensions highlighted in Figure 5.1 have been provided in Table 5.1. Moreover, the feedline involved in proposed antenna array structure has a width of 0.5 mm . The multi-slotted single element rectangle shaped structure on the top consists of six similar sized rectangular slots. A single slot involved in the multi-slotted structure has a size of 0.5 mm (along the y-axis) and 0.7 mm (along the x-axis).

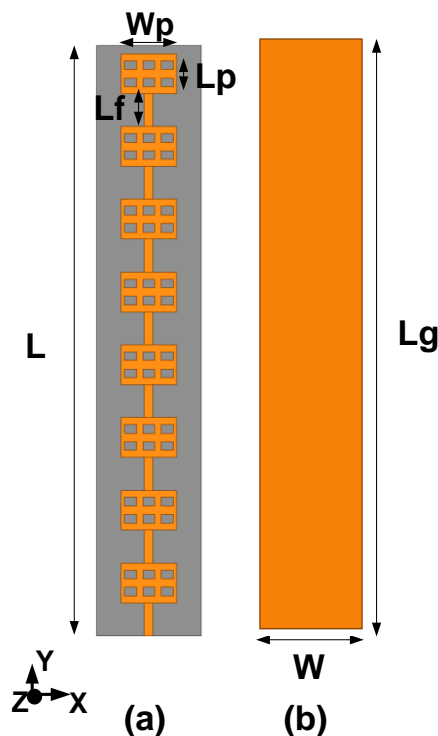


Figure 5.1 Detailed Antenna Array Design (a) Top (b) Bottom

Table 5.1 Dimensions Involved in Figure 5.1

Dimension	Value (<i>mm</i>)
<i>L</i>	34
<i>W</i>	6
<i>L_p</i>	2.29
<i>W_p</i>	3.2
<i>L_f</i>	1.9
<i>L_g</i>	34

5.2.1 Antenna Design Evolution:

At the beginning a plain rectangular patch antenna resonating at 34.5 GHz was realized with the help of empirical formulae provided in [14]. Multiple rectangle shaped slots were then incorporated into the design, in order to make it resonate at different frequency bands [109]. The single element antenna structure was then transformed into an array structure consisting of eight similar elements. The number, location, and size of rectangle shaped slots on antenna array top side were selected carefully to allow the antenna array to resonate at targeted frequency bands. Rogers RT Duroid 5880 (relative permittivity 2.2 and loss tangent 0.0009) has been used as the substrate to realize the proposed antenna array structure. Figure 5.2 highlights the significant steps involved in antenna design evolution. It can be seen that only top side of antenna structure is altered in the design evolution process. On the bottom side of all antennas shown in Figure 5.2 a complete ground structure is present. The corresponding reflection coefficient ($|S_{11}|$ dB) results for each step involved in the antenna design evolution have been plotted in Figure 5.3. It can be observed clearly from Figure 5.3 that the proposed mmWave antenna array structure, referred to as Design D, is able to resonate at four distinct frequency bands and is hence quadband in nature.

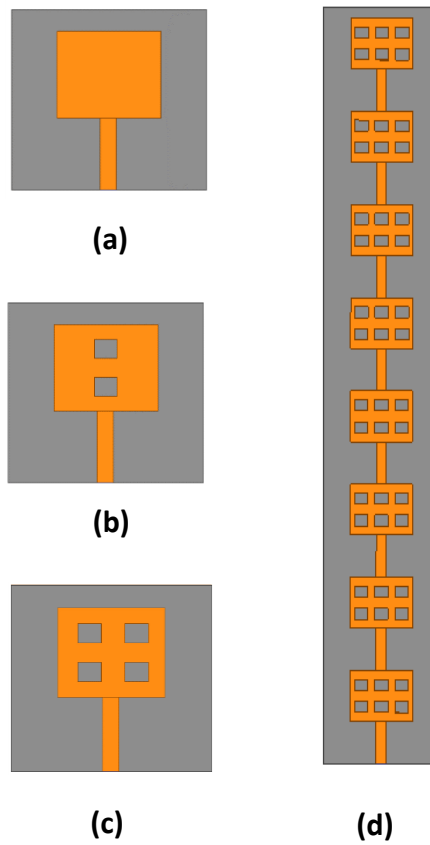


Figure 5.2 Antenna Design Evolution Steps (a) Design A (b) Design B (c) Design C
(d) Design D

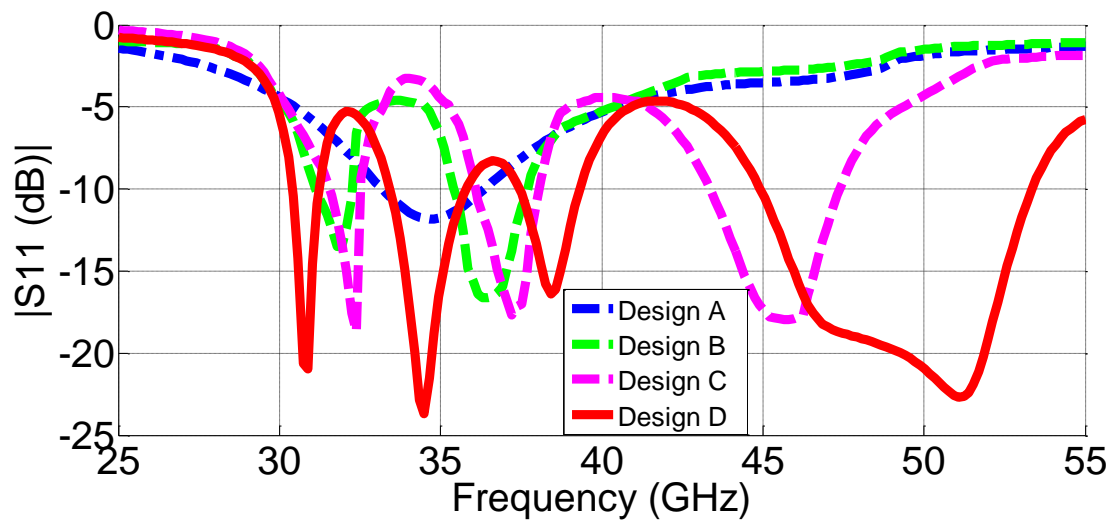


Figure 5.3 Reflection Coefficient Results ($|S_{11}|$ dB) for Design Evolution Steps

Shown in Figure 5.2

5.2.2 Analysis of Current Distribution Plots:

The surface current distribution for the single element involved in the proposed array structure has been plotted at all four resonant frequencies. Through the surface distribution results, the single element antenna regions responsible for generation of respective resonant frequencies can be identified and their contribution can be assessed. The surface current distribution results are shown in Figure 5.4. The figure has four subparts, where each subpart corresponds to a particular resonant frequency. It can be observed from Figure 5.4 (a) that the vertical walls (along the y-axis) of all six rectangular slots, specially the upper three rectangular slots have a significant contribution in generation of first operating frequency band centred at 30.58 GHz. From Figure 5.4 (b) it can be assessed that all six rectangular slots are involved in generation of second operating frequency band centred around 34.5 GHz. However, again the vertical walls (along the y-axis) of all six rectangular slots and the bottom three slots have a relatively stronger contribution in generation of the second operating frequency band centred around 34.5 GHz. The third operating frequency band with centre frequency of 38.3 GHz is being generated due to contribution from all rectangular slots specially the outermost vertical walls (along the y-axis) lying around the boundary of the single element top side, as can be evidently witnessed from Figure 5.4 (c). Lastly the contribution of rectangular slots in production of fourth operating frequency band centred around 49.3 GHz can be observed from Figure 5.4 (d). It can be seen that the uppermost and lowermost horizontal walls (along the x-axis) lying around the boundary of the single element top side have a more significant contribution towards generation of this particular resonant frequency band.

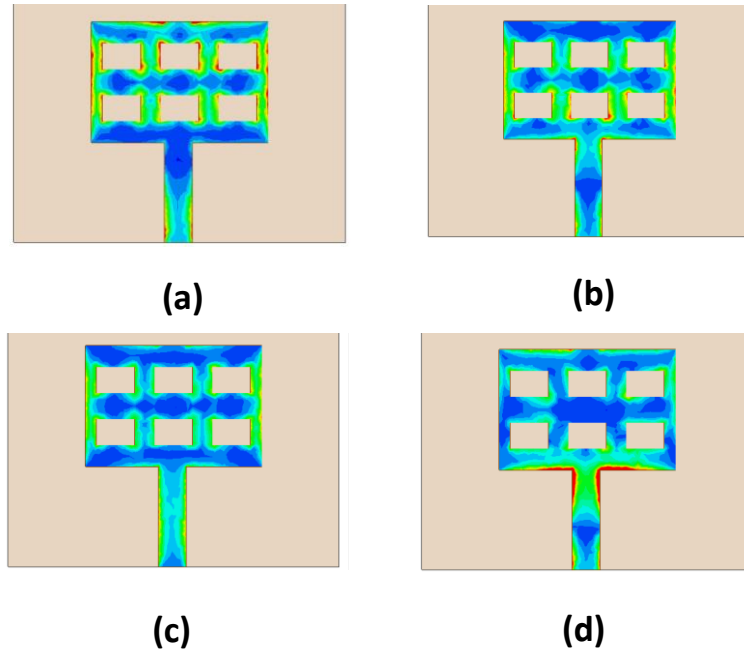


Figure 5.4 Single Element Surface Current Distribution at (a) 30.58 GHz (b) 34.5 GHz (c) 38.3 GHz (d) 49.3 GHz

5.3 Significant Results and Analysis of the Proposed mmWave Antenna Array:

Proposed antenna array structure has also been manufactured and tested using Rogers RT Duroid 5880 of 0.5 mm height as substrate. Different important performance parameters were tested, measured, and analysed for the proposed antenna array design. Manufactured prototype of the proposed array design is shown in Figure 5.5.

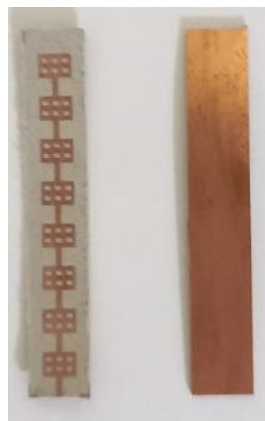


Figure 5.5 Manufactured Antenna Array Top and Bottom View

The presented antenna array structure is capable of resonating at four frequency bands in the mmWave region thereby rendering it a quadband array design. The proposed mmWave antenna array was tested for different significant parameters and the obtained results were analysed. The obtained results and their analysis are presented in the subsequent subsections under this heading.

5.3.1 Reflection Coefficient Results:

The proposed antenna array structure has the ability to operate at four mmWave frequency bands. The simulated and measured reflection coefficient ($|S_{11}|$ dB) results have been plotted in Figure 5.6. From the measured results the operating frequency bands can be identified as 30.27 to 30.88 GHz, 33.3 to 35.6 GHz, 37.3 to 38.9 GHz, and 45.1 to 53.5 GHz.

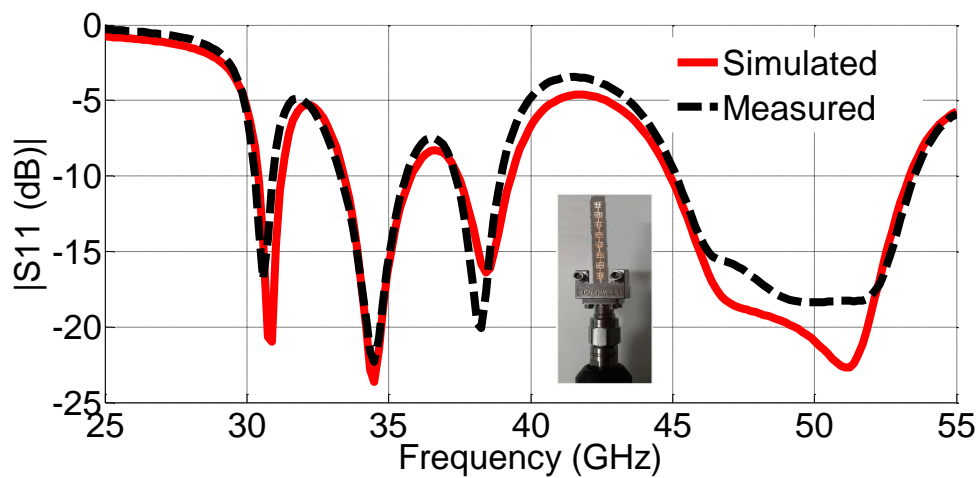


Figure 5.6 Reflection Coefficient Results ($|S_{11}|$ dB) Simulated and Measured

Table 5.2 represents in-depth simulated and measured results concerning the reflection coefficient in terms of bandwidth and centre frequency. The four operating frequency band possess a simulated bandwidth of 0.78, 2.21, 1.68, and 8.2 GHz respectively. The corresponding measured bandwidths for the four resonating bands, on the other hand,

come out to be 0.61, 2.3, 1.6, and 8.4 GHz respectively. Slight variations between the simulated and measured results can be ascribed to the manufacturing process and connector losses.

Table 5.2 In-depth Simulated and Measured Reflection Coefficient ($|S_{11}|$ dB)

Results

Results	Parameters	1 st Band	2 nd Band	3 rd Band	4 th Band
Simulated Results	Operating Frequency Range	30.42 to 31.2 GHz	33.5 to 35.71 GHz	37.52 to 39.2 GHz	45 to 53.2 GHz
	Bandwidth	0.78 GHz	2.21 GHz	1.68 GHz	8.2 GHz
	Centre Frequency	30.85 GHz	34.5 GHz	38.42 GHz	49.1 GHz
	$ S_{11} $ dB at Centre Frequency	-20.51 dB	-23.22 dB	-16 dB	-19.4 dB
Measured Results	Operating Frequency Range	30.27 to 30.88 GHz	33.3 to 35.6 GHz	37.3 to 38.9 GHz	45.1 to 53.5 GHz
	Bandwidth	0.61 GHz	2.3 GHz	1.6 GHz	8.4 GHz
	Centre Frequency	30.58 GHz	34.5 GHz	38.3 GHz	49.3 GHz
	$ S_{11} $ dB at Centre Frequency	-16.34 dB	-22.14 dB	-20.06 dB	-17.75 dB

5.3.2 Radiation Characteristics of the Proposed mmWave Antenna Array:

Figure 5.7 illustrates the simulated and measured radiation pattern plots for the proposed mmWave antenna array structure. The figure has been divided into four subparts, where each subpart represents the radiation pattern plot of a particular resonant frequency at 30.58, 34.5, 38.3, and 49.3 GHz. Both E plane and H plane radiation patterns have been plotted in Figure 5.7. The radiation patterns were measured in an anechoic chamber facility. By observation of the radiation pattern plots it can be seen that the H plane radiation pattern plots are almost omnidirectional in nature. The

E plane radiation pattern plots, on the other hand, appear to be more directional in nature.

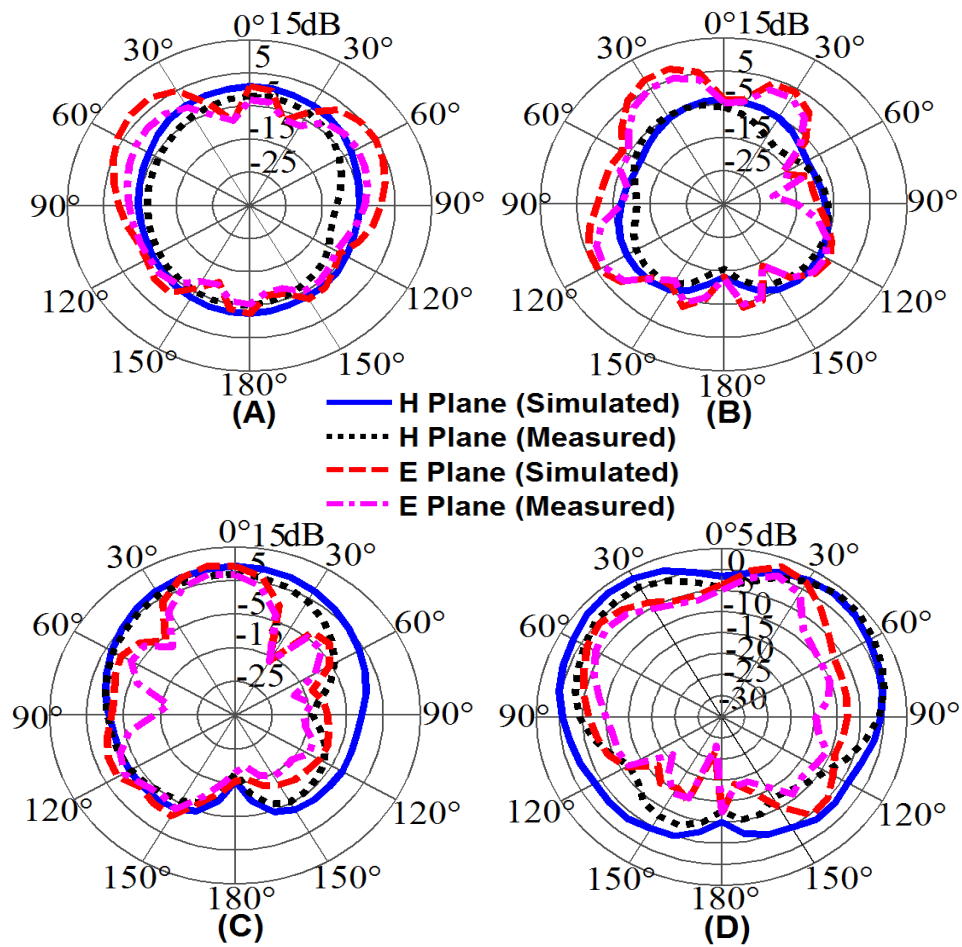


Figure 5.7 Simulated and Measured Radiation Pattern Plots at (a) 30.58 GHz, (b) 34.5 GHz, (c) 38.3 GHz, and (d) 49.3 GHz

5.3.3 mmWave Antenna Array Peak Gain Results:

The simulated and measured peak gain results, at all four operating frequencies, for the proposed mmWave antenna array structure are provided in Table 5.3. It can be evidently observed from the table that for all operating frequencies simulated peak gain values are greater than 8.53 dBi whereas for all operating frequencies measured peak gain values are greater than 7.98 dBi. Maximum simulated peak gain of 10.62 dBi is

observed at 38.3 GHz, whereas the maximum measured peak gain of 9.93 dBi is also observed at the same operating frequency of 38.3 GHz.

Table 5.3 Simulated and Measured Peak Gain Results for Proposed mmWave

Antenna Array

Frequency (GHz)	Simulated Peak Gain (dBi)	Measured Peak Gain (dBi)
30.58	8.53	7.98
34.5	9.24	8.43
38.3	10.62	9.93
49.3	10.45	9.87

5.3.4 mmWave Antenna Array Radiation Efficiency Results:

The simulated and measured radiation efficiency results, at all four operating frequencies, for the proposed mmWave antenna array structure are provided in Table 5.4. It can be evidently observed from the table that for all operating frequencies simulated radiation efficiency values are greater than 85.22% whereas for all operating frequencies measured radiation efficiency values are greater than 78.45%. Maximum simulated radiation efficiency is recorded as 88.04% at 30.58 GHz, meanwhile maximum measured simulated radiation efficiency is recorded as 84.71% also at 30.58 GHz.

Table 5.4 Simulated and Measured Peak Gain Results for Proposed mmWave

Antenna Array

Frequency (GHz)	Simulated Radiation Efficiency (%)	Measured Radiation Efficiency (%)
30.58	88.04	84.71
34.5	86.16	82.03
38.3	85.22	78.45
49.3	85.86	79.68

Tables 5.3 and 5.4 present an insight into the high gain and radiation efficiency performance of the proposed mmWave antenna array structure thereby validating the proposed array to be used effectively in future mmWave 5G applications.

5.4 Comparison with Related Literature:

Table 5.5 highlights a comparison of the proposed mmWave antenna array with related work in the literature. It can be evidently observed the proposed antenna array is compact in size, offers quadband resonance ability and is very simple in design. Many of the array design structures in Table 5.5 include a complex design approach, whereas the proposed design is quite simple and can be fabricated and deployed without any additional design complexity.

Table 5.5 Comparison of Proposed mmWave Antenna Array with Recent Literature

Ref	Center Operating Frequency (GHz)	Antenna Size (mm ²)	Simulated Peak Gain (dBi)	Design Complexity / Array
[126]	28	15 × 9	8.5	High/ No
[127]	37.2, 54.5	7.2 × 5	5, 6	Low/ No
[128]	45.2, 67.3, 76	10 × 8.9	8.65	High/ Yes
[130]	28	102 × 96.5	21	High/ Yes
[132]	28.3	99.2 × 17.5	19.88	High/ Yes
[134]	25.7	41.5 × 4	9	Medium/ Yes
[137]	28.65	30 × 15	6.49	Medium/ No
This Work	30.58, 34.5, 38.3, 49.3	34 × 6	8.53, 9.24, 10.62, 10.45	Low/Yes

5.5 Summary:

In this chapter a mmWave quadband antenna array is proposed. The array design is based on a multi-slotted structure. The proposed design has been manufactured using Rogers RT Duroid 5880 substrate of thickness 0.5 mm. The manufactured array has been tested and measured. The proposed mmWave antenna array is compact in size, has a very simple design and is able to resonate at four distinct frequency bands with centre frequencies of 30.58 GHz, 34.5 GHz, 38.3 GHz, and 49.3 GHz. In addition, the proposed mmWave antenna array has high measured gains of 7.98 dBi, 8.43 dBi, 9.93 dBi, and 9.87 dBi at 30.58 GHz, 34.5 GHz, 38.3 GHz, and 49.3 GHz. The compact simple design and quadband resonance capability with high gain render the proposed antenna array suitable to be effectively used in future standalone 5G mmWave applications.

CHAPTER 06

CONCLUSION AND FUTURE WORK

6.1 Conclusion:

Smart and intelligent antenna designs for current 4G, and future 5G communication systems have been presented in this dissertation. The antenna structures proposed and presented are based on intelligent design techniques like reconfigurability, MIMO and array approach. Table 6.1 presents a summarized comparison of the three developed antennas.

Table 6.1 Summarized Comparison of Presented Antennas

Antenna Design No.	Design Technique Adopted	Antenna Design Basic Shape	Operating Frequency Bands	Gains Achieved at Operating Frequencies	Major Application
Antenna Design 1	Reconfigurability	Circular Loop	3.42 GHz and 8.02 GHz (PIN diodes OFF state), 2.21 GHz, 4.85 GHz, and 10.19 GHz (PIN diodes ON state)	3.03 dBi at 3.42 GHz, and 3.37 dBi at 8.02 GHz (PIN diodes OFF state), 3.06 dBi at 2.21 GHz, 2.81 dBi at 4.85 GHz, and 2.92 dBi at 10.19 GHz (PIN diodes ON state)	Current 4G and in-deployment non-standalone 5G communication services
Antenna Design 2	MIMO	L and I shaped slotted patch	2.5 GHz, 3.7 GHz, 4.3 GHz, and 5.5 GHz	3.49 dBi at 2.5 GHz, 2.97 dBi at 3.7 GHz, 2.93 dBi at 4.3 GHz, and 2.54 dBi at 5.5 GHz	Current 4G and in-deployment non-standalone 5G communication services
Antenna Design 3	Array	Patch consisting of rectangular slots	30.58 GHz, 34.5 GHz, 38.3 GHz, and 49.3 GHz	7.98 dBi at 30.58 GHz, 8.43 dBi at 34.5 GHz, 9.93 dBi at 38.3 GHz, and 9.87 dBi at 49.3 GHz	Future standalone mmWave 5G communication services

Antenna design 1 consists of a reconfigurable antenna that offers frequency and bandwidth switching using PIN diodes. The antenna design is based on a circular loop structure. The proposed reconfigurable antenna resonates at 3.42 GHz and 8.02 GHz in PIN diodes 'OFF' state whereas the antenna is able to resonate at 2.21 GHz, 4.85 GHz and 10.19 GHz in PIN diodes 'ON' state. The antenna can find applications in current 4G and in-deployment non-standalone 5G communication systems. The detailed structure and results of 'Antenna Design 1' have been discussed in Chapter 3. Antenna design 2 consists of a two element MIMO antenna that offers multiband resonance with high isolation and decreased mutual coupling. The antenna design utilizes L and I shaped slots. The proposed MIMO antenna resonates at 2.5 GHz, 3.7 GHz, 4.3 GHz, and 5.5 GHz. The antenna owing to its results and performance can find suitable applications in current 4G and in-deployment non-standalone 5G communication systems. The detailed structure and results of 'Antenna Design 2' have been presented in Chapter 4. Antenna design 3 consists of a multi-slotted array antenna structure. The antenna design utilizes several rectangular slots for multiband resonance. The proposed array antenna is able to resonate at mmWave frequencies of 30.58 GHz, 34.5 GHz, 38.3 GHz, and 49.3 GHz. The mmWave antenna array can find effective applications in future standalone mmWave based 5G communication systems. The detailed structure and results of 'Antenna Design 3' have been discussed in Chapter 5. Overall, the three antenna structures presented have been intelligently designed using smart antenna design techniques like reconfigurability, MIMO and array-based approach. These intelligent and smart antenna designs can effectively find applications in modern 4G and 5G communication systems.

6.2 Future Work:

The antenna designs presented in this thesis have been developed primarily for 4G/ 5G communication devices. The developed antenna designs can be utilized in current 4G/ 5G as well as future 5G applications. Some recommendations as described, may be employed on the developed antenna designs for future work.

‘Antenna Design 1’ and ‘Antenna Design 2’ can be altered in shape and size to resonate at certain other sub 6 GHz frequency bands in order to accommodate different applications like WiFi, cognitive radio platforms, access points etc. Massive MIMO technology may also be explored for ‘Antenna Design 1’ and ‘Antenna Design 2’. ‘Antenna Design 3’ may be evolved to resonate at frequency bands targeting satellite communications along with the mmWave frequency bands. Research related to this particular approach (termed 6G) can be used in antenna development for modern 6G communication devices. ‘Antenna Design 3’ can also be evolved into a frequency reconfigurable antenna.

REFERENCES

- [1] T. L. Singal, *Wireless Communications*, Tata McGraw-Hill Education, 2010.
- [2] W. Stallings and C. Beard, *Wireless Communication Networks and Systems*, Pearson, 2016.
- [3] T. Seymour and A. Shaheen, "History of Wireless Communication," in *Review of Business Information Systems (RBIS)*, vol. 15, no. 2, pp. 37- 42, 2011, doi: 10.19030/rbis.v15i2.4202.
- [4] NASA, "Radio Spectrum," NASA, 11 August 2021. [Online]. Available: https://www.nasa.gov/directorates/heo/scan/spectrum/radio_spectrum/. [Accessed 4 January 2022].
- [5] RUTGERS School of Engineering, "Wireless Information Network Laboratory," 10 February 2021. [Online]. Available: <https://www.winlab.rutgers.edu/>. [Accessed 4 January 2022].
- [6] Tutorials Point, "History of Mobile Communication," [Online]. Available: https://www.tutorialspoint.com/umts/umts_history_of_mobile_communication.htm. [Accessed 5 January 2022].
- [7] A. Osseiran, J. F. Monserrat and P. Marsch, *5G Mobile and Wireless Communications Technology*, Cambridge University Press, June 2016, doi: 10.1017/CBO9781316417744.
- [8] A. Umar, *Mobile Computing and Wireless Communications: Applications, Networks, Platforms, Architectures, and Security*, nge solutions, 2004.

- [9] T. Halonen, J. Romero and J. Melero, GSM, GPRS and EDGE Performance: Evolution towards 3G/UMTS, Second ed., John Wiley & Sons, Ltd, 2003. doi: 10.1002/0470866969.
- [10] A. R. Mishra, Fundamentals of Network Planning and Optimisation 2G/3G/4G: Evolution to 5G, Second ed., John Wiley & Sons Ltd, 2018.
- [11] Net Informations, "1G Vs. 2G Vs. 3G Vs. 4G Vs. 5G," [Online]. Available: <http://net-informations.com/q/diff/generations.html>. [Accessed 6 January 2022].
- [12] Qualcomm, "New 3GPP effort on NR in Unlicensed Spectrum expands 5G to new areas," 2 December 2016. [Online]. Available: <https://www.qualcomm.com/documents/5g-spectrum-sharing>. [Accessed 10 March 2020].
- [13] "IEEE Standard Definitions of Terms for Antennas," in *IEEE Std 145-1983*, vol., no., pp.1-31, 22 June 1983, doi: 10.1109/IEEESTD.1983.82386.
- [14] C. A. Balanis, Antenna Theory: Analysis and Design, Fourth ed., New York: John Wiley & Sons, February 2016.
- [15] J. C. Maxwell, A Treatise on Electricity and Magnetism, London, UK: Oxford University Press, 1873.
- [16] S. Silver, Microwave Antenna Theory and Design, IET, 1984.
- [17] P. E. Mayes, "Frequency-independent antennas and broad-band derivatives thereof," in *Proceedings of the IEEE*, vol. 80, no. 1, pp. 103-112, Jan. 1992, doi: 10.1109/5.119570.
- [18] D. M. Pozar, "Microstrip antennas," in *Proceedings of the IEEE*, vol. 80, no. 1, pp. 79-91, Jan. 1992, doi: 10.1109/5.119568.
- [19] C. A. Balanis, "Antenna theory: a review," in *Proceedings of the IEEE*, vol. 80, no. 1, pp. 7-23, Jan. 1992, doi: 10.1109/5.119564.

- [20] L. V. Blake, *Antennas*, New York: John Wiley & Sons, 1966.
- [21] QUALCOMM, "What can we do with 5G NR Spectrum Sharing that isn't possible today?," 13 December 2017. [Online]. Available: <https://www.qualcomm.com/media/documents/files/new-3gpp-effort-on-nr-in-unlicensed-spectrum-expands-5g-to-new-areas.pdf>. [Accessed 10 March 2020].
- [22] NIVIUK, "NR frequency band," [Online]. Available: http://niviuk.free.fr/nr_band.php. [Accessed 11 March 2020].
- [23] P. M. Paul, K. Kandasamy and M. Sharawi, "SRR loaded slot antenna for multiband applications," 2017 IEEE International Symposium on Antennas and Propagation & USNC/URSI National Radio Science Meeting, 2017, pp. 2529-2530, doi: 10.1109/APUSNCURSINRSM.2017.8073307.
- [24] C. Huang, Y. Jiao, Z. Weng and X. Li, "A planar multiband antenna based on CRLH-TL ZOR for 4G compact mobile terminal applications," 2018 International Workshop on Antenna Technology (iWAT), 2018, pp. 1-3, doi: 10.1109/IWAT.2018.8379200.
- [25] N. I. M. Elamin and T. A. Rahman, "2-Element slot meander patch antenna system for LTE-WLAN customer premise equipment," 2015 IEEE-APS Topical Conference on Antennas and Propagation in Wireless Communications (APWC), 2015, pp. 993-996, doi: 10.1109/APWC.2015.7300191.
- [26] T. Cai, G. Wang and J. Liang, "Analysis and Design of Novel 2-D Transmission-Line Metamaterial and Its Application to Compact Dual-Band Antenna," in *IEEE Antennas and Wireless Propagation Letters*, vol. 13, pp. 555-558, 2014, doi: 10.1109/LAWP.2014.2312313.
- [27] B. Zong, G. Wang, C. Zhou and Y. Wang, "Compact Low-Profile Dual-Band Patch Antenna Using Novel TL-MTM Structures," in *IEEE Antennas and Wireless Propagation Letters*, vol. 14, pp. 567-570, 2015, doi: 10.1109/LAWP.2014.2372093.

- [28] A. Boukarkar, X. Q. Lin, Y. Jiang and Y. Q. Yu, "Miniaturized Single-Feed Multiband Patch Antennas," in *IEEE Transactions on Antennas and Propagation*, vol. 65, no. 2, pp. 850-854, Feb. 2017, doi: 10.1109/TAP.2016.2632620.
- [29] Huawei Technologies Co. Ltd., "5G Spectrum Public Policy Position," Huawei Technologies, Shenzhen, China, 2017.
- [30] L. Tao, J. Xu, H. Li, Y. Hao, S. Huang, M. Lei and K. Bi, "Bandwidth Enhancement of Microstrip Patch Antenna Using Complementary Rhombus Resonator," *Wireless Communications and Mobile Computing*, vol. 2018, 2018, doi: 10.1155/2018/6352181.
- [31] B. K. Kumar, P. V. V. Kishore and K. K. Naik, "Design of Rectangular Patch Antenna with X-slots for Wireless Communications," 2018 Second International Conference on Inventive Communication and Computational Technologies (ICICCT), 2018, pp. 1448-1451, doi: 10.1109/ICICCT.2018.8473111.
- [32] L. Sun, G. Zhang, B. Sun, W. Tang and J. Yuan, "A Single Patch Antenna With Broadside and Conical Radiation Patterns for 3G/4G Pattern Diversity," in *IEEE Antennas and Wireless Propagation Letters*, vol. 15, pp. 433-436, 2016, doi: 10.1109/LAWP.2015.2451132.
- [33] K. M. Mak, H. W. Lai and K. M. Luk, "A 5G Wideband Patch Antenna With Antisymmetric L-shaped Probe Feeds," in *IEEE Transactions on Antennas and Propagation*, vol. 66, no. 2, pp. 957-961, Feb. 2018, doi: 10.1109/TAP.2017.2776973.
- [34] W. Shi, Z. Qian and W. Ni, "Dual-Band Stacked Annular Slot/Patch Antenna for Omnidirectional Radiation," in *IEEE Antennas and Wireless Propagation Letters*, vol. 15, pp. 390-393, 2016, doi: 10.1109/LAWP.2015.2447280.
- [35] X. -Q. Zhu, Y. -X. Guo and W. Wu, "A Novel Dual-Band Antenna for Wireless Communication Applications," in *IEEE Antennas and Wireless Propagation Letters*, vol. 15, pp. 516-519, 2016, doi: 10.1109/LAWP.2015.2456039.

- [36] Y. He, K. Ma, N. Yan and H. Zhang, "Dual-Band Monopole Antenna Using Substrate-Integrated Suspended Line Technology for WLAN Application," in *IEEE Antennas and Wireless Propagation Letters*, vol. 16, pp. 2776-2779, 2017, doi: 10.1109/LAWP.2017.2745503.
- [37] S. Liu, W. Wu and D. -G. Fang, "Single-Feed Dual-Layer Dual-Band E-Shaped and U-Slot Patch Antenna for Wireless Communication Application," in *IEEE Antennas and Wireless Propagation Letters*, vol. 15, pp. 468-471, 2016, doi: 10.1109/LAWP.2015.2453329.
- [38] Y. L. Elo, F. Y. Zulkifli and E. T. Rahardjo, "Design of wideband microstrip antenna with parasitic element for 4G/LTE application," 2017 15th International Conference on Quality in Research (QiR) : International Symposium on Electrical and Computer Engineering, 2017, pp. 110-113, doi: 10.1109/QIR.2017.8168463.
- [39] A. A. Salih and M. S. Sharawi, "A Dual-Band Highly Miniaturized Patch Antenna," in *IEEE Antennas and Wireless Propagation Letters*, vol. 15, pp. 1783-1786, 2016, doi: 10.1109/LAWP.2016.2536678.
- [40] R. Goncalves, P. Pinho and N. B. Carvalho, "Compact, Frequency Reconfigurable, Printed Monopole Antenna," *International Journal of Antennas and Propagation*, vol. 2012, 2012, doi: 10.1155/2012/602780.
- [41] M. A. Aris, M. T. AH, N. H. Abd Rahman, N. Ramli and I. Pasya, "Frequency reconfigurable aperture-coupled microstrip patch antenna using periodic Defected Ground Structures," 2015 IEEE Conference on Antenna Measurements & Applications (CAMA), 2015, pp. 1-4, doi: 10.1109/CAMA.2015.7428153.
- [42] H. Zhang, Y. Jiao and R. Wang, "Dual-band frequency-reconfigurable antenna with meandered-line-based metasurfaces," 2017 Sixth Asia-Pacific Conference on Antennas and Propagation (APCAP), 2017, pp. 1-3, doi: 10.1109/APCAP.2017.8420864.

- [43] P. Saikia and B. Basu, "CPW Fed Frequency Reconfigurable Dual Band Antenna Using PIN Diode," 2018 Second International Conference on Electronics, Communication and Aerospace Technology (ICECA), 2018, pp. 1485-1488, doi: 10.1109/ICECA.2018.8474702.
- [44] T. Sabapathy, M. A. Bashah, M. Jusoh, P. J. Soh and M. R. Kamarudin, "Frequency reconfigurable rectangular antenna with T-slotted feed line," 2016 International Conference on Radar, Antenna, Microwave, Electronics, and Telecommunications (ICRAMET), 2016, pp. 81-84, doi: 10.1109/ICRAMET.2016.7849587.
- [45] S. Danesh, S. K. A. Rahim, M. Abedian and M. R. Hamid, "A Compact Frequency-Reconfigurable Dielectric Resonator Antenna for LTE/WWAN and WLAN Applications," in IEEE Antennas and Wireless Propagation Letters, vol. 14, pp. 486-489, 2015, doi: 10.1109/LAWP.2014.2369411.
- [46] A. E. Zahran, M. A. Abdalla and M. H. Abd El-Azeem, "Single/dual band reconfigurable metamaterial dipole loaded antenna for wireless applications," 2016 IEEE International Symposium on Antennas and Propagation (APSURSI), 2016, pp. 457-458, doi: 10.1109/APS.2016.7695937.
- [47] A. Mansoul and H. Kimouche, "A simple frequency reconfigurable microstrip patch antenna for wireless communication," 2013 8th International Workshop on Systems, Signal Processing and their Applications (WoSSPA), 2013, pp. 306-309, doi: 10.1109/WoSSPA.2013.6602381.
- [48] L. Yang, B. Cheng, Y. Zhu and Y. Li, "Compact antenna with frequency reconfigurability for GPS/LTE/WWAN mobile handset applications," in International Journal of Antennas and Propagation, vol. 2016, 2016, doi: 10.1155/2016/3976936.

- [49] M. M. Morsy, "A Compact Dual-Band CPW-Fed MIMO Antenna for Indoor Applications," *International Journal of Antennas and Propagation*, vol. 2019, 2019, doi: 10.1155/2019/4732905.
- [50] N. Pouyanfar, C. Ghobadi, J. Nourainia, K. Pedram and M. Majidzadeh, "A Compact Multi-Band MIMO Antenna with High Isolation for C and X Bands Using Defected Ground Structure," *Radioengineering*, vol. 27, no. 3, 2018, doi: 10.13164/re.2018.0686.
- [51] C. Luo, J. Hong and M. Amin, "Mutual Coupling Reduction for Dual-Band MIMO Antenna with Simple Structure," *Radioengineering*, vol. 26, no. 1, 2017, doi: 10.13164/re.2017.0051.
- [52] J. Deng, J. Li, L. Zhao and L. Guo, "A Dual-Band Inverted-F MIMO Antenna With Enhanced Isolation for WLAN Applications," in *IEEE Antennas and Wireless Propagation Letters*, vol. 16, pp. 2270-2273, 2017, doi: 10.1109/LAWP.2017.2713986.
- [53] S. Soltani, P. Lotfi and R. D. Murch, "A Dual-Band Multiport MIMO Slot Antenna for WLAN Applications," in *IEEE Antennas and Wireless Propagation Letters*, vol. 16, pp. 529-532, 2017, doi: 10.1109/LAWP.2016.2587732.
- [54] Z. Niu, H. Zhang, Q. Chen and T. Zhong, "Isolation Enhancement in Closely Coupled Dual-Band MIMO Patch Antennas," in *IEEE Antennas and Wireless Propagation Letters*, vol. 18, no. 8, pp. 1686-1690, Aug. 2019, doi: 10.1109/LAWP.2019.2928230.
- [55] Y. Zhao, J. Fu, K. Zhang, Q. Wu and X. Yin, "A Compact Multiband Planar MIMO Antenna with High Isolation," 2018 IEEE International Symposium on Antennas and Propagation & USNC/URSI National Radio Science Meeting, 2018, pp. 31-32, doi: 10.1109/APUSNCURSINRSM.2018.8609260.
- [56] Y. Rahayu and M. I. Hidayat, "Design of 28/38 GHz Dual-Band Triangular-Shaped Slot Microstrip Antenna Array for 5G Applications," 2018 2nd International Conference on

Telematics and Future Generation Networks (TAFGEN), 2018, pp. 93-97, doi: 10.1109/TAFGEN.2018.8580487.

- [57] M. Ur-Rehman et al., "A Wearable Antenna for mmWave IoT Applications," 2018 IEEE International Symposium on Antennas and Propagation & USNC/URSI National Radio Science Meeting, 2018, pp. 1211-1212, doi: 10.1109/APUSNCURSINRSM.2018.8608233.
- [58] S. Lee, S. Kim and J. Choi, "Dual-Band Dual-Polarized Proximity Fed Patch Antenna for 28 GHz/39 GHz 5G Millimeter-Wave Communications," 2019 13th European Conference on Antennas and Propagation (EuCAP), 2019, pp. 1-5.
- [59] Z. Lodro, N. Shah, E. Mahar, S. B. Tirmizi and M. Lodro, "mmWave Novel Multiband Microstrip Patch Antenna Design for 5G Communication," 2019 2nd International Conference on Computing, Mathematics and Engineering Technologies (iCoMET), 2019, pp. 1-4, doi: 10.1109/ICOMET.2019.8673447.
- [60] J. Choi, J. Park, W. Hwang and W. Hong, "mmWave Double Cavity-Backed Slot Antenna featuring Electrically Small and Low-Profile," 2019 IEEE International Symposium on Antennas and Propagation and USNC-URSI Radio Science Meeting, 2019, pp. 269-270, doi: 10.1109/APUSNCURSINRSM.2019.8888530.
- [61] G. S. Karthikeya, M. P. Abegaonkar and S. K. Koul, "Low cost high gain triple band mmWave Sierpinski antenna loaded with uniplanar EBG for 5G applications," 2017 IEEE International Conference on Antenna Innovations & Modern Technologies for Ground, Aircraft and Satellite Applications (iAIM), 2017, pp. 1-5, doi: 10.1109/IAIM.2017.8402582.
- [62] V. Miraftab, Wenyao Zhai and M. Repeta, "A wideband low cost E-band SIW antenna array for high capacity mmWave radio," 2015 IEEE MTT-S International Microwave Symposium, 2015, pp. 1-3, doi: 10.1109/MWSYM.2015.7167055.

- [63] T. S. S. Apoorva and N. Kumar, "Design of mmWave Dual Band Antenna for 5G Wireless," 2019 IEEE International Conference on Advanced Networks and Telecommunications Systems (ANTS), 2019, pp. 1-4, doi: 10.1109/ANTS47819.2019.9118020.
- [64] I. Ndip, T. H. Le, O. Schwanitz and K. -D. Lang, "A comparative analysis of 5G mmWave antenna arrays on different substrate technologies," 2018 22nd International Microwave and Radar Conference (MIKON), 2018, pp. 222-225, doi: 10.23919/MIKON.2018.8405183.
- [65] D. El Nabaoui, A. Tajmouati, J. Zbitou, A. Errkik, H. Bennis and M. Latrach, "Multiband fractal CPW antenna for GPS, WiMAX and IMT applications," 2017 International Conference on Wireless Technologies, Embedded and Intelligent Systems (WITS), 2017, pp. 1-5, doi: 10.1109/WITS.2017.7934596.
- [66] V. -A. Nguyen, B. -Y. Park, S. -O. Park and G. Yoon, "A Planar Dipole for Multiband Antenna Systems With Self-Balanced Impedance," in *IEEE Antennas and Wireless Propagation Letters*, vol. 13, pp. 1632-1635, 2014, doi: 10.1109/LAWP.2014.2347952.
- [67] M. A. Aris, M. T. Ali, N. H. A. Rahman and N. Ramli, "Frequency reconfigurable aperture-coupled microstrip patch antenna using Defected Ground Structure," 2015 IEEE International RF and Microwave Conference (RFM), 2015, pp. 200-204, doi: 10.1109/RFM.2015.75877.
- [68] K. Jhamb, L. Li and K. Rambabu, "Frequency Adjustable Microstrip Annular Ring Patch Antenna with Multi-band Characteristics," *IET Microwaves, Antennas & Propagation*, vol. 5, no. 12, pp. 1471-1478, 2011, doi: 10.1049/iet-map.2010.0571.
- [69] J. T. Bernhard, "Reconfigurable Antennas," in *Synthesis Lectures on Antennas*, California, USA, Morgan and Claypool Publishers, 2007, doi: 10.2200/S00067ED1V01Y200707ANT004.

- [70] A. Grau, J. Romeu, M. Lee, S. Blanch, L. Jofre and F. De Flaviis, "A Dual-Linearly-Polarized MEMS-Reconfigurable Antenna for Narrowband MIMO Communication Systems," in *IEEE Transactions on Antennas and Propagation*, vol. 58, no. 1, pp. 4-17, Jan. 2010, doi: 10.1109/TAP.2009.2036197.
- [71] Y. Tawk, J. Costantine and C. G. Christodoulou, "A Varactor-Based Reconfigurable Filtenna," in *IEEE Antennas and Wireless Propagation Letters*, vol. 11, pp. 716-719, 2012, doi: 10.1109/LAWP.2012.2204850.
- [72] Symeon Nikolaou *et al.*, "Pattern and frequency reconfigurable annular slot antenna using PIN diodes," in *IEEE Transactions on Antennas and Propagation*, vol. 54, no. 2, pp. 439-448, Feb. 2006, doi: 10.1109/TAP.2005.863398.
- [73] D. V. Niture, P. A. Govind and S. P. Mahajan, "Frequency and polarisation reconfigurable square ring antenna for wireless application," *2016 IEEE Region 10 Conference (TENCON)*, 2016, pp. 1302-1306, doi: 10.1109/TENCON.2016.7848223.
- [74] P. T. Minh, T. T. Thao, N. T. Duc and V. Van Yem, "A novel multiband frequency reconfigurable PIFA antenna," *2016 International Conference on Advanced Technologies for Communications (ATC)*, 2016, pp. 7-12, doi: 10.1109/ATC.2016.7764832.
- [75] Y. Kim and J. Y. Young, "A high gain pattern reconfigurable antenna with simple structure," *2016 IEEE International Symposium on Antennas and Propagation (APSURSI)*, 2016, pp. 653-654, doi: 10.1109/APS.2016.7696035.
- [76] S. Chen, Q. Chu and N. Shinohara, "A bandwidth reconfigurable planar antenna for WLAN/WiMAX applications," *2016 Asia-Pacific Microwave Conference (APMC)*, 2016, pp. 1-3, doi: 10.1109/APMC.2016.7931467.

- [77] R. Hussain and M. S. Sharawi, "A Cognitive Radio Reconfigurable MIMO and Sensing Antenna System," in *IEEE Antennas and Wireless Propagation Letters*, vol. 14, pp. 257-260, 2015, doi: 10.1109/LAWP.2014.2361450.
- [78] H. Nachouane, A. Najid, A. Tribak and F. Riouch, "Reconfigurable and Tunable Filtenna for Cognitive LTE Femtocell Base Stations," *International Journal of Microwave Science and Technology*, vol. 2016, 2016, doi: 10.1155/2016/9460823.
- [79] A. Mehdipour, A. Sebak, C. W. Trueman and T. A. Denidni, "Compact Multiband Planar Antenna for 2.4/3.5/5.2/5.8-GHz Wireless Applications," in *IEEE Antennas and Wireless Propagation Letters*, vol. 11, pp. 144-147, 2012, doi: 10.1109/LAWP.2012.2185915.
- [80] X. Gao, H. Zhong, Z. Zhang, Z. Feng and M. F. Iskander, "Low-Profile Planar Tripolarization Antenna for WLAN Communications," in *IEEE Antennas and Wireless Propagation Letters*, vol. 9, pp. 83-86, 2010, doi: 10.1109/LAWP.2010.2043495.
- [81] Rong-Lin Li, V. F. Fusco and H. Nakano, "Circularly polarized open-loop antenna," in *IEEE Transactions on Antennas and Propagation*, vol. 51, no. 9, pp. 2475-2477, Sept. 2003, doi: 10.1109/TAP.2003.809845.
- [82] R. Li, B. Pan, J. Laskar and M. M. Tentzeris, "A Novel Low-Profile Broadband Dual-Frequency Planar Antenna for Wireless Handsets," in *IEEE Transactions on Antennas and Propagation*, vol. 56, no. 4, pp. 1155-1162, April 2008, doi: 10.1109/TAP.2008.919171.
- [83] W. Liu, C. Wu and Y. Dai, "Design of Triple-Frequency Microstrip-Fed Monopole Antenna Using Defected Ground Structure," in *IEEE Transactions on Antennas and Propagation*, vol. 59, no. 7, pp. 2457-2463, July 2011, doi: 10.1109/TAP.2011.2152315.

- [84] M. S. Khan, A. Capobianco, A. Iftikhar, S. Asif, B. Ijaz and B. D. Braaten, "A Frequency-Reconfigurable Series-Fed Microstrip Patch Array With Interconnecting CRLH Transmission Lines," in *IEEE Antennas and Wireless Propagation Letters*, vol. 15, pp. 242-245, 2016, doi: 10.1109/LAWP.2015.2439637.
- [85] SKYWORKS, "SMP1322 SERIES Low Resistance, Plastic Packaged PIN Diodes," [Online]. Available: <https://www.skyworksinc.com/en/Products/%20Diodes/SMP1322-Series>. [Accessed 3 July 2019].
- [86] Mini-Circuits, "ADCH-80A RF CHOKE/ SURF MOUNT RoHS5," 2017. [Online]. Available: <https://www.minicircuits.com/WebStore/dashboard.html?model=ADCH-80A>. [Accessed 3 July 2019].
- [87] Federal Communications Commission, "Advanced Wireless Services (AWS)," 22 March 2019. [Online]. Available: <https://www.fcc.gov/wireless/bureau-divisions/broadband-division/advanced-wireless-services-aws>. [Accessed 11 March 2020].
- [88] ASIA-PACIFIC TELECOMMUNITY, "APT Report on Frequency Usage of the Band 3400-3600 MHz," [Online]. Available: https://www.apr.int/sites/default/files/Upload-files/AWG/APT-AWG-REP-37-R1-APT_Report_on_3400-3600MHz.docx. [Accessed 11 March 2020].
- [89] J. Chambers, "Commercial X-Band: The Technical + Operational Advantages," *MilsatMagazine*, April 2013. [Online]. Available: <http://www.milsatmagazine.com/story.php?number=1530000863>. [Accessed 11 March 2020].
- [90] A. Haidine and S. E. Hassani, "LTE-a pro (4.5G) as pre-phase for 5G deployment: Closing the gap between technical requirements and network performance," 2016

International Conference on Advanced Communication Systems and Information Security (ACOSIS), 2016, pp. 1-7, doi: 10.1109/ACOSIS.2016.7843933.

- [91] M. M. Morsy, "A Compact Dual-Band CPW-Fed MIMO Antenna for Indoor Applications," *International Journal of Antennas and Propagation*, vol. 2019, 2019, doi: 10.1155/2019/4732905.
- [92] A. M. Soliman, D. M. Elsheakh, E. A. Abdallah and H. El-Hennawy, "Design of planar inverted-F antenna over uniplanar EBG structure for laptop mimo applications," *Microwave and Optical Technology Letters*, vol. 57, no. 2, pp. 277-285, 2015, doi: 10.1002/mop.28828.
- [93] C. M. Luo, J. S. Hong and M. Amin, "Mutual Coupling Reduction for Dual-Band MIMO Antenna with Simple Structure," *Radioengineering*, vol. 26, no. 1, pp. 51-56, 2017, doi: 10.13164/re.2017.0051.
- [94] W. Liao, C. Hsieh, B. Dai and B. Hsiao, "Inverted-F/Slot Integrated Dual-Band Four-Antenna System for WLAN Access Points," in *IEEE Antennas and Wireless Propagation Letters*, vol. 14, pp. 847-850, 2015, doi: 10.1109/LAWP.2014.2381362.
- [95] N. Pouyanfar, C. Ghobadi, J. Nourinia, K. Pedram and M. Majidzadeh, "A Compact Multi-Band MIMO Antenna With High Isolation for C and X Bands Using Defected Ground Structure," *Radioengineering*, vol. 27, no. 3, pp. 686-693, 2018, doi: 10.13164/re.2018.0686.
- [96] Z. Ren, A. Zhao and S. Wu, "MIMO Antenna With Compact Decoupled Antenna Pairs for 5G Mobile Terminals," in *IEEE Antennas and Wireless Propagation Letters*, vol. 18, no. 7, pp. 1367-1371, July 2019, doi: 10.1109/LAWP.2019.2916738.
- [97] F. B. Shiddanagouda, R. M. Vani and P. V. Hunagund, "Design and Analysis of Printed MIMO Antenna for Next Generation Wireless Applications," *2018 IEEE Indian*

- Conference on Antennas and Propagation (InCAP)*, 2018, pp. 1-4, doi: 10.1109/INCAP.2018.8770872.
- [98] Z. Ren, S. Wu and A. Zhao, "Triple Band MIMO Antenna System for 5G Mobile Terminals," *2019 International Workshop on Antenna Technology (iWAT)*, 2019, pp. 163-165, doi: 10.1109/IWAT.2019.8730605.
- [99] A. H. Jabire, H.-X. Zheng, A. Abdu, and Z. Song, "Characteristic Mode Analysis and Design of Wide Band MIMO Antenna Consisting of Metamaterial Unit Cell," *Electronics*, vol. 8, no. 1, p. 68, Jan. 2019, doi: 10.3390/electronics8010068.
- [100] K. Qian, G. Huang, J. Liang, B. Qian and T. Yuan, "An LTCC Interference Cancellation Device for Closely Spaced Antennas Decoupling," in *IEEE Access*, vol. 6, pp. 68255-68262, 2018, doi: 10.1109/ACCESS.2018.2879569.
- [101] E. Thakur, N. Jaglan and S. D. Gupta, "Design of compact triple band-notched UWB MIMO antenna with TVC-EBG structure," *Journal of Electromagnetic Waves and Applications*, vol. 34, no. 11, pp. 1601-1615, 2020, doi: 10.1080/09205071.2020.1775136.
- [102] V. Ionescu, M. Hnatiuc and A. Topală, "Optimal design of mushroom-like EBG structures for antenna mutual coupling reduction in 2.4 GHz ISM band," *2015 E-Health and Bioengineering Conference (EHB)*, 2015, pp. 1-4, doi: 10.1109/EHB.2015.7391559.
- [103] M. Farahani, J. Pourahmadazar, M. Akbari, M. Nedil, A. R. Sebak and T. A. Denidni, "Mutual Coupling Reduction in Millimeter-Wave MIMO Antenna Array Using a Metamaterial Polarization-Rotator Wall," in *IEEE Antennas and Wireless Propagation Letters*, vol. 16, pp. 2324-2327, 2017, doi: 10.1109/LAWP.2017.2717404.
- [104] Z. Li, Z. Du, M. Takahashi, K. Saito and K. Ito, "Reducing Mutual Coupling of MIMO Antennas With Parasitic Elements for Mobile Terminals," in *IEEE Transactions on*

- Antennas and Propagation*, vol. 60, no. 2, pp. 473-481, Feb. 2012, doi: 10.1109/TAP.2011.2173432.
- [105] X. Shi, M. Zhang, S. Xu, D. Liu, H. Wen and J. Wang, "Dual-band 8-element MIMO antenna with short neutral line for 5G mobile handset," *2017 11th European Conference on Antennas and Propagation (EUCAP)*, 2017, pp. 3140-3142, doi: 10.23919/EuCAP.2017.7928046.
- [106] S. Zhang and G. F. Pedersen, "Mutual Coupling Reduction for UWB MIMO Antennas With a Wideband Neutralization Line," in *IEEE Antennas and Wireless Propagation Letters*, vol. 15, pp. 166-169, 2016, doi: 10.1109/LAWP.2015.2435992.
- [107] S.-C. Chen, J.-Y. Sze and K.-J. Chuang, "Isolation enhancement of small-size WLAN MIMO antenna array for laptop computer application," *Journal of Electromagnetic Waves and Applications*, vol. 31, no. 3, pp. 323-334, 2017, doi: 10.1080/09205071.2016.1277958.
- [108] I. Gil and R. Fernández-García, "Study of metamaterial resonators for decoupling of a MIMO-PIFA system," *2016 International Symposium on Electromagnetic Compatibility - EMC EUROPE*, 2016, pp. 552-556, doi: 10.1109/EMCEurope.2016.7739172.
- [109] R. Garg, P. Bhartia, I. J. Bahl and A. Ittipiboon, *Microstrip Antenna Design Handbook*, New York (USA): Artech House, 2001.
- [110] C.-F. Yang, M. Cheung, C.-Y. Huang and J.-S. Sun, "Print a Compact Single- and Quad-Band Slot Antenna on Ceramic Substrate," *Journal of Electromagnetic Waves and Applications*, vol. 24, no. 13, pp. 1697-1707, 2010, doi: 10.1163/156939310792486593.
- [111] A. K. Gautam, L. Kumar, B. K. Kanaujia and K. Rambabu, "Design of Compact F-Shaped Slot Triple-Band Antenna for WLAN/WiMAX Applications," in *IEEE*

- Transactions on Antennas and Propagation*, vol. 64, no. 3, pp. 1101-1105, March 2016, doi: 10.1109/TAP.2015.2513099.
- [112] J. Bao, Q. Huang, X. Wang and X. Shi, "Compact Multiband Slot Antenna for WLAN/WiMAX Operations," *International Journal of Antennas and Propagation*, vol. 2014, 2014, doi: 10.1155/2014/806875.
- [113] X. Yang, Y. Z. Yin, W. Hu and S. L. Zuo, "Low-Profile, Small Circularly Polarized Inverted-L Antenna With Double-Folded Arms," in *IEEE Antennas and Wireless Propagation Letters*, vol. 9, pp. 767-770, 2010, doi: 10.1109/LAWP.2010.2063011.
- [114] I. M. Rafiqul, A. A. Zahirul, M. F. A. J. Khan and S. Alkaraki, " Design of Microstrip Patch Antenna Using Slotted Partial Ground And Addition Of Stairs And Stubs For UWB Application," *Journal of Selected Areas in Telecommunications (JSAT)*, 2012.
- [115] Laird Connectivity, "Simplifying MIMO Antenna Installations With The FlexMIMO Antenna," July 2019. [Online]. Available: https://connectivity-staging.s3.us-east-2.amazonaws.com/2019-07/072019%20-%20MIMO%20Application%20Brief_0.pdf. [Accessed 25 June 2020].
- [116] S. Blanch, J. Romeu and I. Corbella, "Exact representation of antenna system diversity performance from input parameter description," *Electronics Letters*, vol. 39, no. 9, pp. 705-707, 2003, doi: 10.1049/el:20030495.
- [117] R. G. Vaughan and J. B. Andersen, "Antenna diversity in mobile communications," in *IEEE Transactions on Vehicular Technology*, vol. 36, no. 4, pp. 149-172, Nov. 1987, doi: 10.1109/T-VT.1987.24115.
- [118] M. Khalid, S. I. Naqvi, N. Hussain, M. Rehman, Fawad, S. S. Mirjavadi, M. J. Khan and Y. Amin, "4-Port MIMO Antenna with Defected Ground Structure for 5G Millimeter Wave Applications," *Electronics*, vol. 9, no. 1, 2020, doi: 10.3390/electronics9010071.

- [119] R. Chandel, A. K. Gautam and K. Rambabu, "Tapered Fed Compact UWB MIMO-Diversity Antenna With Dual Band-Notched Characteristics," in *IEEE Transactions on Antennas and Propagation*, vol. 66, no. 4, pp. 1677-1684, April 2018, doi: 10.1109/TAP.2018.2803134.
- [120] K. Rosengren and P.-S. Kildal, "Radiation efficiency, correlation, diversity gain and capacity of a six-monopole antenna array for a MIMO system: theory, simulation and measurement in reverberation chamber," *IEE Proceedings - Microwaves, Antennas and Propagation*, vol. 152, no. 1, pp. 7-16, 2005, doi: 10.1049/ip-map:20045031.
- [121] QUALCOMM, "Spectrum for 4G and 5G," [Online]. Available: <https://www.qualcomm.com/media/documents/files/spectrum-for-4g-and-5g.pdf/>. [Accessed 25 June 2020].
- [122] ElectronicsNotes, "WiMAX Frequencies and Spectrum Allocations," Adrio Communications Ltd, [Online]. Available: <https://www.electronics-notes.com/articles/connectivity/wimax/frequencies-spectrum-bands.php/>. [Accessed 26 June 2020].
- [123] CableFree, "WLAN Frequency Bands & Channels," Wireless Excellence Ltd, [Online]. Available: <https://www.cablefree.net/wirelesstechnology/wireless-lan/wlan-frequency-bands-channels/>. [Accessed 21 June 2020].
- [124] Federal Communications Commission (USA), "FCC ID Database," [Online]. Available: <https://fccid.io/frequency-explorer.php?lower=4227&upper=4460/>. [Accessed 21 June 2020].
- [125] 3GPP, "About 3GPP," [Online]. Available: <https://www.3gpp.org/about-3gpp>. [Accessed 10 October 2020].
- [126] M. I. Magray, Y. -C. Hsu and J. -H. Tarng, "All Metallic CPW-Fed Corner Bent Orthogonal Pattern Diversity Antenna Module for mmWave 5G Smartphones," *2020*

- IEEE Asia-Pacific Microwave Conference (APMC)*, 2020, pp. 142-144, doi: 10.1109/APMC47863.2020.9331575.
- [127] Z. Lodro, N. Shah, E. Mahar, S. B. Tirmizi and M. Lodro, "mmWave Novel Multiband Microstrip Patch Antenna Design for 5G Communication," *2019 2nd International Conference on Computing, Mathematics and Engineering Technologies (iCoMET)*, 2019, pp. 1-4, doi: 10.1109/ICOMET.2019.8673447.
- [128] A. Firdausi and M. Alaydrus, "Designing multiband multilayered microstrip antenna for mmWave applications," *2016 International Conference on Radar, Antenna, Microwave, Electronics, and Telecommunications (ICRAMET)*, 2016, pp. 99-102, doi: 10.1109/ICRAMET.2016.7849591.
- [129] A. Qayyum, A. H. Khan, S. Uddin, O. Ahmad, J. S. Khan and S. Bashir, "A Novel mmWave Defected Ground Structure Based Microstrip Antenna for 5G Cellular Applications," *2020 First International Conference of Smart Systems and Emerging Technologies (SMARTTECH)*, 2020, pp. 28-31, doi: 10.1109/SMARTTECH49988.2020.00023.
- [130] H. A. Diawuo and Y. -B. Jung, "Broadband Proximity-Coupled Microstrip Planar Antenna Array for 5G Cellular Applications," in *IEEE Antennas and Wireless Propagation Letters*, vol. 17, no. 7, pp. 1286-1290, July 2018, doi: 10.1109/LAWP.2018.2842242.
- [131] B. T. Mohamed, H. Ammor and M. Himdi, "Design of Parallel-series Microstrip Patch Antenna Array at mmWave, for future 5G applications," *2019 7th Mediterranean Congress of Telecommunications (CMT)*, 2019, pp. 1-4, doi: 10.1109/CMT.2019.8931371.
- [132] M. Khalily, R. Tafazolli, P. Xiao and A. A. Kishk, "Broadband mm-Wave Microstrip Array Antenna With Improved Radiation Characteristics for Different 5G

- Applications," in *IEEE Transactions on Antennas and Propagation*, vol. 66, no. 9, pp. 4641-4647, Sept. 2018, doi: 10.1109/TAP.2018.2845451.
- [133] A. Farahbakhsh, D. Zarifi and A. U. Zaman, "A mmWave Wideband Slot Array Antenna Based on Ridge Gap Waveguide With 30% Bandwidth," in *IEEE Transactions on Antennas and Propagation*, vol. 66, no. 2, pp. 1008-1013, Feb. 2018, doi: 10.1109/TAP.2017.2782263.
- [134] H. Ozpinar, S. Aksimsek and N. T. Tokan, "A Novel Compact, Broadband, High Gain Millimeter-Wave Antenna for 5G Beam Steering Applications," in *IEEE Transactions on Vehicular Technology*, vol. 69, no. 3, pp. 2389-2397, March 2020, doi: 10.1109/TVT.2020.2966009.
- [135] G. Kim and S. Kim, "Design and Analysis of Dual Polarized Broadband Microstrip Patch Antenna for 5G mmWave Antenna Module on FR4 Substrate," in *IEEE Access*, vol. 9, pp. 64306-64316, 2021, doi: 10.1109/ACCESS.2021.3075495.
- [136] M. M. Kamal, S. Yang, X.-c. Ren, A. Altaf, S. H. Kiani, M. R. Anjum, A. Iqbal, M. Asif and S. I. Saeed, "Infinity Shell Shaped MIMO Antenna Array for mm-Wave 5G Applications," *Electronics*, vol. 10, no. 2, 2021, doi: 10.3390/electronics10020165.
- [137] H. Chen, Y. Shao, Y. Zhang, C. Zhang and Z. Zhang, "A Low-Profile Broadband Circularly Polarized mmWave Antenna With Special-Shaped Ring Slot," in *IEEE Antennas and Wireless Propagation Letters*, vol. 18, no. 7, pp. 1492-1496, July 2019, doi: 10.1109/LAWP.2019.2920875.